Impact of supermassive black holes on galaxy clusters

Paola Rebusco

München 2007

Impact of supermassive black holes on galaxy clusters

DISSERTATION

der Fakultät für Physik der Ludwigs-Maximilians-Universität München
zur Erlangung des Grades
Doktor der Naturwissenschaften
Dr. rer. nat.

vorgelegt von

Paola Rebusco aus Brescia, Italien

München, den 2 Februar 2007

Erstgutachter : Prof. Dr. Rashid Sunyaev
Zweitgutachter : Prof. Dr. Andreas Burkert
Tag der mündlichen Prüfung : 4 Mai 2007

A nonna Pia.

Contents

List of Figures

List of Tables

Zusammenfassung

Diese semi-analytische Arbeit untersucht das Feedback von supermassiven schwarzen Löchern auf Galaxienhaufen. Insbesondere konzentrieren wir uns auf die Entwicklung diagnostischer Instrumente, um die charakteristischen Geschwindigkeiten und räumlichen Skalen des heissen Intracluster Mediums (ICM) zu bestimmen. In sogenannten "cool core" Haufen wird angenommen, dass die Dynamik des ICM von der Aktivität des zentralen schwarzen Lochs bestimmt wird. Die Methoden, die wir hier entwickelt haben, zusammen mit existenten und zukünftigen Beobachtungen, können helfen, das "cooling flow problem" zu lösen (siehe Sektion 1.3) und die Wechselwirkung zwischen Active Galactic Nuclei (AGN) und Gas in kleineren Systemen (bis hinunter zu Galaxien) zu verstehen.

Galaxienhaufen sind die grössten gravitativ gebundenen Systeme im Universum: sie bestehen aus hunderten bis tausenden von Galaxien, die sich im tiefen Gravitationspotential der dunklen Materie bewegen. Das gesamte Volumen des Haufens ist mit heissem (Temperatur $\sim 10^7 - 10^8$ K), dünnen (Elektronendichte $10^{-4} - 10^{-1}$ cm^{-3}) Gas gefüllt. Bei solch hohen Temperaturen sind selbst schwere Elemente (z.B. Silizium, Schwefel, Eisen) stark ionisiert, bis hin zu Wasserstoff-ähnlichen Ionen, und emittieren in Linien mit Energien um die $0.7 - 8$ keV. Mit Hilfe von Röntgenbeobachtungen kann man die wichtigsten Gaseigenschaften messen: Temperatur, Dichte und Häuftigkeit der schweren Elemente.

Ein beachtlicher Teil der Haufen ("cool core clusters" genannt) zeigt besondere Eigenschaften in ihren Zentren: die Gastemperatur fällt nach innen hin ab, während die Gasdichte ansteigt. Die Kühlzeit des Gases im Zentrum in solchen Haufen ist viel kürzer als das Alter des Haufens und ohne externe Heizquelle muss das Gas unter die Röntgentemperatur sinken. Allerdings belegen Beobachtungen, dass die Temperatur nur auf $1-2$ keV fällt. Eine plausible Erklärung dieses Problems ist, dass das zentrale supermassive schwarze Loch grosse Mengen mechanischer Energie im ICM deponiert, die die Strahlungsverluste ausgleichen. Eine direkte Folge dieser Hypothese ist, dass das heisse Gas nicht ruht sondern kontinuierlich in Bewegung versetzt wird.

Dieselbe Klasse von Haufen mit kühlem Kern wird ausserdem charakterisiert durch eine Häuftigkeitsverteilung von Metallen mit einem zentralen Maximum (gewöhnlicherweise mit der He-ähnlichen Eisen-56 Linie gemessen). Die zugespitzte Häuftigkeitsverteilung ist wahrscheinlich auf die Sterne einer massiven Galaxie zurückzuführen, die sich stets im Zentrum dieser Haufen

befindet. Jedoch sind die Häuftigkeitsverteilungen deulich breiter als die Lichtprofile der zentralen Galaxie. Das legt nahe, dass Gasbewegungen die Metalle von der Galaxie wegbewegen. Wir betrachten diesen Prozess in einer Diffusionsnäherung und können so aus Röntgenbeobachtungen die charakteristischen Geschwindigkeiten und räumlichen Skalen in unseren Galaxienhaufen und Gruppen ableiten (Kapitel 2 und 3). Die Parameters dieses semi-analytischen Modells werden mit numerischen Simulationen von AGN/Gas-Wechselwirkungen im Haufenzentren verglichen.

In Kapitel 5 diskutieren wir den Einfluss von Gasbewegungen auf die Breite der stärksten Emissionslinien in Röntgenbereich. Da die charakteristischen thermischen Geschwindigkeiten der schweren Ionen (z.B. Eisen) viel kleiner sind als die Schall Geschwindigkeit des Gases, hängt die Linienbreite sensibel von der Gasgeschwindigkeit ab. Wir zeigen, dass sowohl die absolute Linienbreite als auch ihre Abhängigkeit von der projizierten Entfernung vom Haufenzentrum wertvolle Diagnostik für Gasbewegungen bieten. Solche Messungen werden bald mit dem Start von Röntgen-Mikrokalorimetern ins All möglich werden.

Diese Arbeit ist in Zusammenarbeit mit E. Churazov, R. Sunyaev, H.Böhringer, M.Brüggen, W. Forman und E. Roediger. gen, W. Forman und E. Roediger gemacht worden.

Summary

In the semi-analytical work presented here the feedback from supermassive black holes on galaxy clusters is investigated. In particular we aim at providing simple diagnostics tools to constrain the characteristic velocities and spatial scales of the hot Intra Cluster Medium (ICM) motions. In the so-called "cold core" clusters these motions are believed to be driven by the activity of a central black hole. The methods developed here, together with present-day and future observations, are designed to help to solve the puzzle of cooling flow clusters (see section 1.3) and understand better the AGN/gas interaction in smaller systems (down to individual galaxies).

Clusters of galaxies are the largest gravitationally bound systems in the Universe: they are composed of hundreds to thousands of galaxies, moving in a deep potential well set by the dominating dark matter. The whole volume of clusters is filled with hot (temperature $\sim 10^7 - 10^8$ K) and rarefied (electron density $10^{-4} - 10^{-1} \text{cm}^{-3}$) gas. In such a high-temperature regime

even heavy elements (e.g. silicon, sulfur, iron etc.) are highly ionized up to [H]- or [He]-like ions and they emit in bright lines with energies from ~ 0.7 to ~ 8 keV. Using X-ray observations one can reliable measure all the major gas properties: the temperature, density and abundance of heavy elements.

A significant fraction of clusters (called "cool core" clusters) show distinct signatures in the central region: the gas temperature drops inward, while the gas density increases. The central gas radiative cooling time in such clusters is much shorter than the age of the cluster and without any external source of energy the gas would cool well below X-ray temperatures. However observations suggest that the gas temperature drops only to 1-2 keV. One plausible explanation of this problem is that the activity of a central supermassive black hole deposits large amounts of mechanical energy into the cluster gas and that this balances the gas radiative losses. A direct implication of this hypothesis is that the hot gas is not at rest, but it is continuously stirred by the AGN activity.

The same class of cool core clusters is characterized by a centrally peaked distribution of the heavy elements abundance (usually measured using the He-like iron 6.7 keV line). The peaked abundance profiles are likely associated with the metals ejection by the stars of very massive elliptical galaxies, that are always present at the centers of these clusters. However the observed abundance distributions are significantly broader than the central galaxy light profiles, suggesting that some gas motions are spreading the metals ejected from the galaxy. We treat this process in a diffusion approximation to derive, from the X-ray observations, constraints on the characteristic velocities and spatial scales of the gas motions for a sample of cool core clusters and groups (Chapters 2 and 3). The parameters derived from a simple semi-analytic model are then compared with the results of numerical simulations of the AGN/gas interaction in the cluster core (Chapter 4).
In Chapter 5 we discuss the impact of the gas motions on the width of the strongest X-ray emission lines. Since the characteristic thermal velocities of heavy ions (e.g. iron) are much smaller than the sound speed of the gas, the width of the lines sensitively depends on the presence of gas motions. We show that both the absolute value of the linewidth and its dependence on the projected distance from the cluster center provide valuable diagnostics of the gas motions. Such measurements will soon become possible with the launch of X-ray micro-calorimeters in space.

This work has been done in collaboration with E.Churazov, R.Sunyaev, H.Böhringer, M.Brüggen, W.Forman and E.Roediger.

1

The physical context

1.1 Clusters of galaxies

It was one hundred years ago when clusters of galaxies were first studied in detail (Wolf 1906), although they had been noted long before.
Clusters of galaxies are the largest gravitationally bound systems in the Universe. At optical wavelengths they appear as over-densities of galaxies with respect to the field average density: hundreds to thousands of galaxies moving in a common gravitational potential well make a cluster (a smaller assembly is defined a galaxy group). The typical masses of clusters of galaxies are $\sim 10^{13} - 10^{15} M_\odot$ ($\sim 10^{43} - 10^{45}$ kg) and their sizes are of the order of $1 - 4$ Mpc ($\sim 10^{22} - 10^{23}$ m). The right panel in Figure 1.1 shows an optical image of the Perseus cluster, a nearby (at a distance of ~ 78 Mpc $\sim 2.4 \times 10^{24}$ m) rich cluster.

A cluster is said to be rich when it contains many galaxies. How many, it depends on the criteria used to define the richness and on the method used to determine whether a galaxy belongs to a cluster or to its background. Hence there are different catalogues of clusters, whose membership is based on the richness, which is the measure of the number of associated galaxies (e.g. Abell 1958, Zwicky et al. 1961-1968).
Optical surveys led also to morphological classifications of clusters, based on the properties of the member galaxies and on their spatial distribution (e.g. Abell 1965, 1975, Zwicky et al. 1961-1968, Bautz & Morgan 1970, Rood
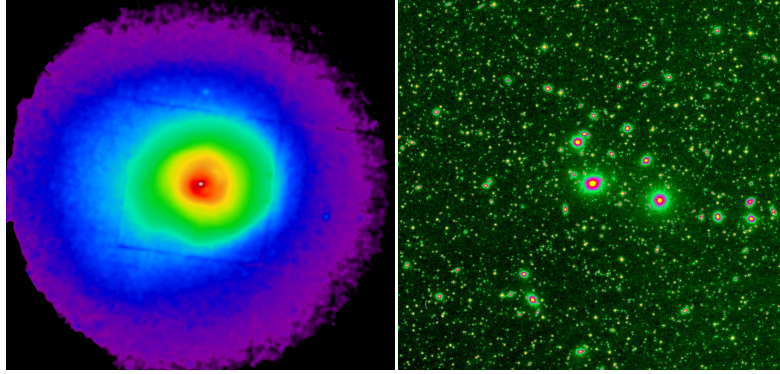
Figure 1.1: Left: X-ray image of the Perseus cluster (XMM-Newton satellite, $\sim 600 \times 600$ kpc, Churazov et al. 2003); Right: optical image of the Perseus cluster (Digitized Sky Survey, same field of view as the X-ray image).
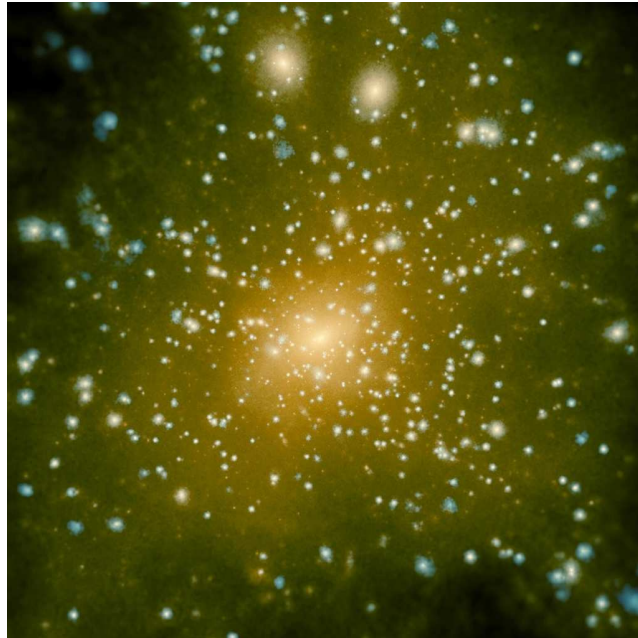
Figure 1.2: Dark matter substructure in a rich galaxy cluster (simulation by Volker Springel, $\sim 4 \times 4$ Mpc).

& Sastry 1971). According to the Abell classification, a regular cluster is spherical and centrally condensed, while an irregular cluster is asymmetric and less compact (e.g. the Virgo cluster).

Galaxy clusters form through gravitational collapse, driven by dark matter,

that is their main component ($\sim 80\%$ of the total mass). In the hierarchical scenario more massive objects form at later times: clusters of galaxies are originated by the gravitational merger of smaller systems, such as groups and subclusters.

The existence of dark matter is indicated in clusters and groups of galaxies by their high mass-to-light ratio. One can estimate the cluster total mass by assuming that the member galaxies have become dynamically relaxed and that they are in an equilibrium configuration: hence the virial theorem can be used ($U = -2\ K$, where U and K are the potential and the kinetic energies respectively) to obtain the virial mass (once the radial velocity dispersion σ_r^2 has been measured). The observed optical luminosity of the galaxies was found to correspond to a mass that is much lower than the total cluster mass, pointing at the presence of a large quantity of matter not visible as stars (i.e. in the optical). X-ray emitting gas constitutes a portion of this "missing mass", but most of it is "dark" and it remains unexplained. The formation of the dark matter haloes and the clustering of galaxies are highly nonlinear phenomena. They can be studied for example through numerical simulations (e.g. Springel et al. 2006): billions of cold dark matter particles (they are assumed to be elementary particles that interact only gravitationally) are created and followed starting $400,000$ years after the Big Bang (see Figure 1.2).

The galaxies in clusters are embedded in a deep potential well of dark matter, but the space between them is not empty: a hot gas (the so-called intracluster medium, ICM) fills it. The ICM is about 15% of the total cluster mass. Felten et al. (1966) first suggested that both if the ICM was ejected by the galaxies in the cluster and if it fell into the cluster, then its particle velocity would be similar to the velocity of the galaxies in the cluster. Indeed in the first case it would keep the same energy as the matter in the galaxy, in the second case it would be anyway under the effect of the same gravitational potential as the member galaxies. Hence the characteristic temperature of the gas reflects the depth of the gravitational well: $3/2\ k\ T_{gas} \sim 3/2\ m_p\ \sigma_r^2$. Substituting the actual values, one gets:

$$T_{gas} \simeq 7 \times 10^7 \left(\frac{\sigma_r}{1000\ \mathrm{km/s}} \right)^2 \mathrm{K}. \qquad (1.1)$$

The observed gas has a temperature of $\sim 10^7 - 10^8$ K, that corresponds to a total mass of $\sim 10^{15}\ M_\odot$.

1.2 Galaxy clusters in X-rays

An important discovery was done in 1965, when X-ray the instruments aboard an Aerobee rocket detected an X-ray source, M87 in the Virgo cluster (Byram et al.1966). Successive X-ray missions (*Uhuru, HEAO-1 A-2, Einstein, ROSAT*) revealed that the sources of X-ray emission are extended and that they have a typical luminosity of $\sim 10^{37}$J s^{-1} $\sim 10^{44}$erg s^{-1}. The left panel in Figure 1.1 shows an X-ray image of the Perseus cluster taken with the *XMM Newton* satellite.

Already the first X-ray observations indicated that the emission associated with galaxy clusters comes from an optically thin plasma with atomic density of about $10^{-10} - 10^{-8}$ m^{-3}=$10^{-4} - 10^{-2}$ cm^{-3} (e.g. Felten et al. 1966; Catura et al. 1972). The ICM was found to be composed mainly of hydrogen ($\sim 75\%$) and helium ($\sim 24\%$), but heavy elements are present as well. Indeed oxygen, magnesium, silicon, sulfur, argon, calcium, iron and nickel are released from the galaxies into the medium and their presence is detected in strong emission lines in the X-ray range (see Figure 1.2).

Many basic properties of the X-ray spectra are well explained and reproduced by theoretical models: there is general agreement in considering that the X-ray radiation is primarily due to thermal bremsstrahlung emission of diffuse hot plasma; the number density of ions in the ICM is consistent with collisional ionization equilibrium. In the collisional ionization equilibrium the ions radiative and dielectric recombinations and the collisional ionization balance each other. Few spectral models (like *MEKAL* - Mewe et al. 1985, Kaastra 1992, Liedahl et al. 1995 - and *APEC* -Smith et al. 2001) are used to predict the emission of such optically thin, collisional plasmas.

The shape of the X-ray continuum is used to derive the temperature or the range of temperatures for the gas in the cluster. This and the observed flux determine the gas density (see Figure 1.4), because the bremsstrahlung emissivity (the radiated energy per unit time, frequency and volume) is proportional to the product of the ion density (n_i) and the electron density (n_e):

$$\epsilon_{brems} = \frac{2^5 \ \pi \ e^6}{3 \ m_e \ c^3} \left(\frac{2 \ \pi}{3 \ m_e \ k} \right)^{1/2} Z^2 \ n_e \ n_i \ g_{ff} \times T_{gas}^{-1/2} \exp \left(-\frac{h \ \nu}{k \ T_{gas}} \right), \quad (1.2)$$

where Z is the ion charge and $g_{ff} = g_{ff}(Z, T_g, \nu)$ is the Gaunt factor. The most robust evidence in support of the thermal model is the detection of the strong X-ray emission lines: models involving Inverse Compton emission or the combined contribution of many compact X-ray sources would have problems
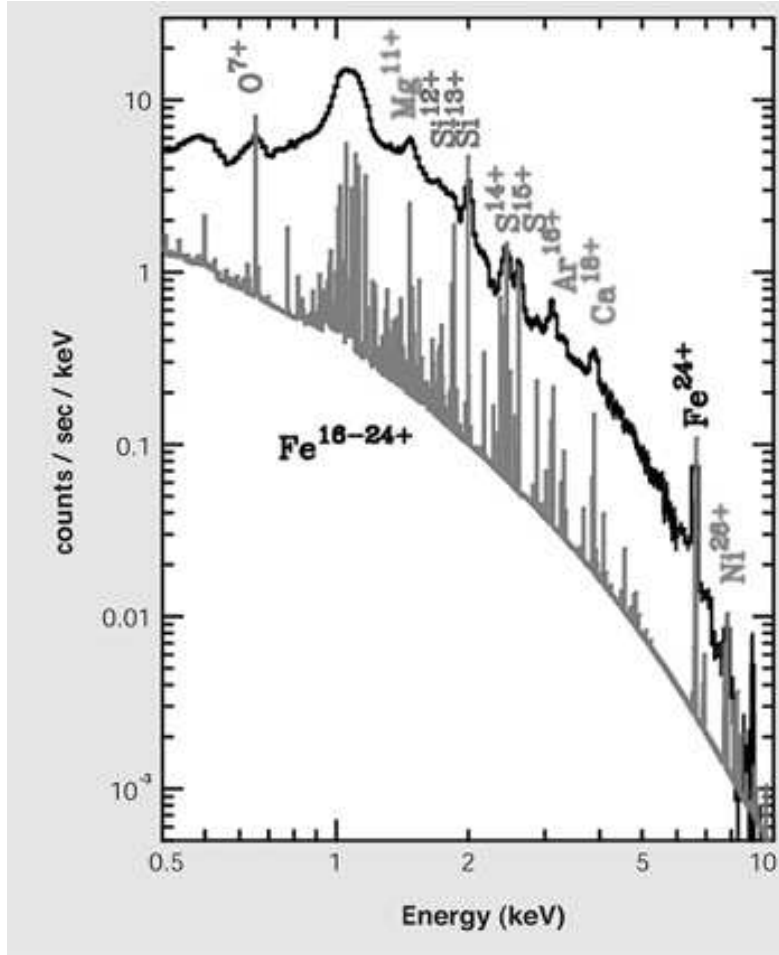
Figure 1.3: X-ray spectrum of the Virgo galaxy cluster observed by the XMM-Newton satellite. The horizontal axis shows the X-ray energy, while the vertical axis represents the distribution of the number of photons at each energy. The upper plot is the spectrum actually measured by the detector; the lower one is the intrinsic spectrum. The bright emission lines from oxygen (O), magnesium (Mg), silicon (Si), sulfur (S), argon (Ar), calcium (Ca), iron (Fe) and nickel (Ni) are clearly detected above the X-ray continuum (credit: Kyoko Matsushita).

in explaining the complex of observed emission lines, which on the other hand are naturally produced in the bremsstrahlung picture (e.g. Sarazin 1988).

A strong line emission due to highly ionized iron (a blend of lines from iron ions) was first detected in the spectrum of Perseus cluster by Mitchell et al. (1976, using *Ariel* 5). This so-called 7 kev complex is present in all the
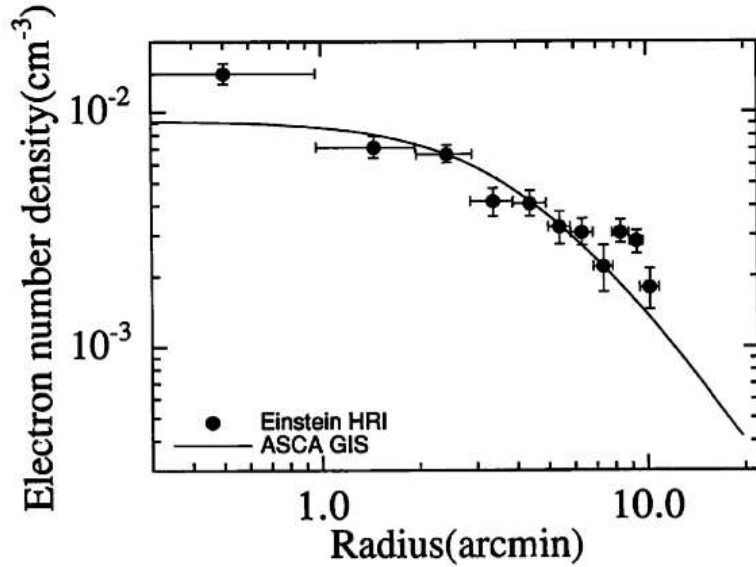
Figure 1.4: Ophiuchus cluster. Gas density radial profile from the Einstein HRI and the ASCA data; the solid line is the best-fit β-model (Matsuzawa et al, 1996).

observed clusters. Lower energy lines, corresponding to elements lighter than iron, were identified as well (see Figure 1.3). The emission of a collisionally excited line is proportional to the ion abundance, which can then be obtained from spectroscopic analysis. Early observations constrained the abundances of heavy elements in the ICM to be about one third of the solar value and roughly constant with radius. The advent of the high resolution *Chandra* and *XMM-Newton* satellites showed that in a large family of clusters (the cool core clusters) the iron abundance is not constant, but it increases towards the center, up to solar abundances (see section 1.3).

X-ray observations are also extensively used to reconstruct the cluster potential, by assuming hydrostatic equilibrium. The sound crossing time (the time required for a sound wave to cross the cluster) is given by:

$$t_{sound}(r) = \frac{r}{c_s(r)} \sim 7 \times 10^8 \text{yr} \left(\frac{T_{gas}}{10^8 \text{K}}\right)^{-1/2} \left(\frac{r}{\text{Mpc}}\right), \qquad (1.3)$$

where c_s is the sound speed in the intracluster gas, T_{gas} the gas temperature and r the distance from the centre. This time is short compared to the

8

probable age of the cluster (which is few to ten Gyr), hence it is reasonable to assume that the gas distribution is in hydrostatic equilibrium. The intracluster medium is generally considered to be locally homogeneous and spherically symmetric. The hydrostatic approximation permits to derive the total cluster mass from X-ray observables. Indeed:

$$\frac{1}{\rho_{gas}} \frac{dP}{dr} = -G \frac{M_{tot}}{r^2} \ . \tag{1.4}$$

One can use the ideal gas law to express the gas pressure P in terms of the gas density ρ_{gas}, temperature T_{gas} and mean molecular mass μ and finally:

$$M_{tot} = -\frac{k \ T \ r}{\mu \ m_p \ G} \left(\frac{\partial \ln \rho_{gas}}{\partial \ln r} + \frac{\partial \ln T_{gas}}{\partial \ln r} \right) \ . \tag{1.5}$$

Isothermal models assume a constant temperature distribution and a Gaussian radial velocity distribution of the galaxies in the cluster. King (1962) demonstrated that a good approximation to the inner parts of a self-gravitating isothermal sphere is given by:

$$\rho_{gal}(r) = \rho_{gal}(0) \left[1 + \left(\frac{r}{r_c} \right)^2 \right]^{-\frac{3}{2}}, \tag{1.6}$$

where r_c is the core radius (determined from optical observations). This result is know as analytic King model for the spatial density of galaxies ρ_{gal}. A finite cutoff radius of ρ_{gal} has to be introduced in order to avoid a divergence of the total number of galaxies at large radii. For constant temperature one can rewrite equation 1.4 by introducing the cluster potential ϕ:

$$\frac{\partial \ln \rho_{gas}}{\partial r} = -\frac{\mu \ m_p}{k \ T_{gas}} \frac{d\phi}{dr}. \tag{1.7}$$

For an isotropic velocity dispersion of the galaxies, the galaxy density ρ_{gal} is also given by equation 1.7, just by replacing $kT_{gas}/\mu m_p$ with the square of the galaxy velocity dispersion, σ_r^2. Therefore

$$\rho_{gas} \propto \rho_{gal}^{\frac{\mu m_p \sigma_r^2}{kT_{gas}}} \ . \tag{1.8}$$

The parameter $\beta = \frac{\mu m_p \sigma_r^2}{kT_{gas}}$ is the ratio of the galaxy-to-gas velocity dispersion (i.e. the specific energy of the dark matter particles to the gas kinetic energy). The gas density profile known as the β-model (Cavaliere & Fusco-Femiano

1976) is obtained by substituting the King approximation (equation 1.6) into $\rho_{gas} \propto \rho_{gal}^{\beta}$:

$$\rho_{gas}(r) = \rho_{gas}(0) \left[1 + \left(\frac{r}{r_c} \right)^2 \right]^{-\frac{3}{2}\beta}. \qquad (1.9)$$

While none of the previous assumptions is fully justified, this model has the advantage that the gas distribution as well as the integrals required to compare the model with observations can be solved analytically. This popular model is a useful guideline to study the cluster emissivity and it fits very well most of the data (e.g. see Figure 1.4).

The gas general properties are well established, but some issues are not yet resolved: the characteristics and the effect of magnetic fields, the role of cosmic rays, and the nature of turbulent motions are nowadays still subject of vivid debate.

1.3 The cooling flow problem

A significant fraction of clusters, the cooling core clusters, are more dynamically relaxed and show distinct signatures within the inner ~ 100 kpc (see Figure 1.5): the gas temperature drops inward by a factor of three or more (e.g. Canizares et al 1979, Mushotzky et al 1981, Lea et al 1982), the gas density n_{gas} steepens (this is attested by the sharply peaked X-ray surface brightness distribution, $I_X \propto n_{gas}^2$) and the radiative cooling time t_{cool} due to the emission of the observed X-rays falls considerably below the age of the cluster (down to about $10^7 - 10^8$ yr). Lea et al.(1973) first found (with the *Uhuru* satellite) that the cooling time in the core of some clusters is close to the Hubble time (the age of the Universe). Even shorter cooling times have been measured later in most bright clusters, groups and large elliptical galaxies (e.g. Stewart et al 1984, Nulsen et al 1984, Edge & Stewart 1991a,b, Mulchaey et al 1993).

A simple homogeneous cooling flow model, based on the early measurements, was suggested independently by different theoreticians: Cowie & Binney (1977), Fabian & Nulsen (1977), Mathews & Bregman (1978). In a homogeneous model the gas is assumed to have a single temperature and density at each radius. The gas cooling time can be written as the gas thermal energy per volume divided by the energy lost per volume:

$$t_{cool} = \frac{3/2 \; n_{gas} \; k \; T_{gas}}{n_{gas}^2 \Lambda(T_{gas})}, \qquad (1.10)$$

where Λ is the gas cooling function. In the core the density is so high that the radiative cooling time drops below the age of the cluster ($t_{cool} \sim n_{gas}^{-1}$). In order to maintain the pressure to support the weight of the overlying warmer gas, a subsonic inflow develops (for a review on cooling flows see Fabian 1994). In spherical symmetry the hydrodynamic equation of conservation of mass is:

$$\dot{M} = 4\pi r^2 \rho_{gas} v, \qquad (1.11)$$

where $v = r/t_{cool}$ is the inflow velocity. An order of magnitude estimate of $\dot{M}$ can be done by dividing the observed X-ray luminosity of the cooling flow region by the enthalpy of a particle $\dot{M} \sim L_{cool}/(5/2\ n_{gas}\ k\ T_{gas})$: in some clusters it reaches ~ 1000 M$_\odot$/yr. Neglecting the temperature dependance one can write $v \sim r/n_{gas}$ and substitute it into equation 1.11. In a homogeneous cooling flow $\dot{M} \sim \rho_{gas}^2\ r^3 = const$. Hence ρ_{gas} is proportional to $r^{-3/2}$ and the surface brightness profile $I_x \sim n_{gas}^2 r$ is proportional to r^{-2}. In these first models (Fabian & Nulsen 1977, Mathews & Bregman 1978) the gas remains hot until it reaches the very core (~ 1 kpc). Then Field's thermal instability (Field 1965) is invoked to create overdense inhomogeneities. Such blobs would decouple from the flow when their specific cooling time is faster than the flow free-fall time and they would eventually form clouds, filaments or stars. The fragmentation of the optical thin clouds in the isobaric and isochoric regimes were studied e.g.by Burkert & Lin (2000). If a fair fraction of the cooling flow mass ($\dot{M}$) goes into star formation, then the central galaxy in a cooling flow cluster should have a very blue color.

The Solid State Spectrometer (SSS) on the *Einstein* Observatory supported the existence of cooling flows in the core of the Perseus and Virgo Clusters (Canizares et al. 1979, 1982, Mushotzky et al. 1981) by detecting low ionization X-ray lines, such as OVIII, FeXVII, SXV, SiXIII, characteristic of a gas at few 10^6 K. This idealized picture was broadly in agreement with the observations, but it did not match the details.

The first problem was that the X-ray surface brightness profiles was not as peaked as expected in a homogeneous flow model (Fabian et al. 1984, Stewart et al. 1984a,b). Such observations implied that the mass flow scales linearly with the radius $\dot{M} \sim r$ instead of being constant (e.g. Peres et al. 1998).

Therefore an inhomogeneous cooling flow model, such that the ICM can consist of a range of densities and temperatures all in pressure equilibrium, was proposed (Nulsen 1986, White & Sarazin 1987, 1988). In these models the growth of thermal instability is required to have a multitemperature gas at any radius. However Cowie et al. (1980) pointed out that overdense blobs would move inward until they would reach and merge with the regions of gas at the same entropy. This would suppress the instability. Malagoli et al. (1987) and
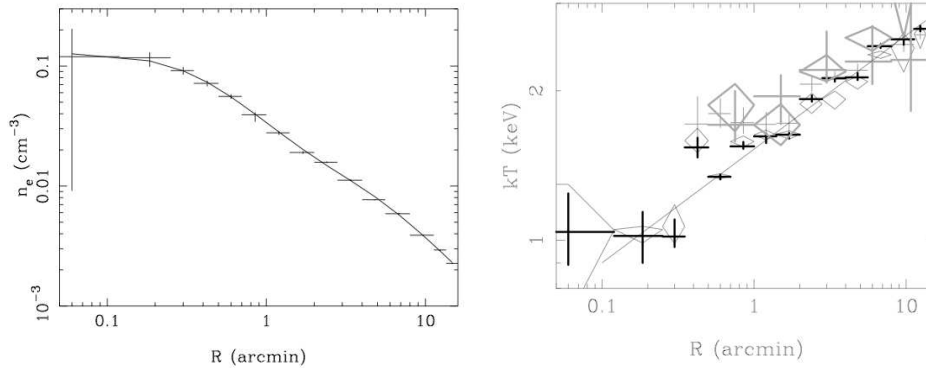
Figure 1.5: Observations of the cD galaxy M87, in the Virgo Cluster (data taken with the X-ray satellite XMM-Newton). Left panel: deprojected gas density profile; the solid line is the best fit to the data, with a double-β profile (in the innermost region the density is steeper and a single β-profile would not take this into account). Right panel: deprojected radial profile of the temperature; the different symbols correspond to different energy bands, while the solid line is the best linear fit for the MEKAL model using the whole energy band (Matsushita et al 2002).

Balbus (1988) analyzed thermal instabilities in a Eulerian and Lagrangian approach respectively: the conclusions of both studies is that thermal instability alone cannot be responsible for the drop out from the cooling flow at large radii. Lowenstein (1990) included the effect of magnetic fields: for a given domain in the wavenumber perturbation of density, buoyancy and conduction are suppressed. This enhances the growth of thermal instabilities. However the restrictions to the initial perturbation are such that any growth of the instability is weak cluster-wide, and it is possible only in localized filaments. Note that magnetic fields were required already in the model by Nulsen (1986) to hold overdense clumps together.

The second issue is that the mass deposition rates $\dot{M}$ inferred from the cooling flow models are of the order of few 100 to 1000 $M_\odot\mathrm{yr}^{-1}$. Optical observations show that the central galaxies are not as blue (i.e. forming stars in recent times) as expected from so high cooling rates (e.g. Allen 1995), nor significant sinks of cold gas clouds have been detected (O'Dea 1994). Moreover *ASCA* and *XMM-Newton* X-ray observations limit $\dot{M}$ to a factor of 10 to 100 times lower (e.g. Allen et al. 2001, Tamura et al. 2001).

The third problem is that the shape of the soft X-ray spectrum is not consistent with a simple cooling flow . Undeniably the high spatial resolution imaging of the *Chandra* satellite and the high spectral resolution of the *XMM-*

Newton Reflection Grating Spectrometer (RGS) opened a new era. Indeed the RGS spectra disproved the previous low-ionization lines detection of the *Einstein* SSS. Although it would seem that cooling has taken place, the new spectra indicated no evidence for strong mass cooling rates of gas to below temperatures of 1-2 keV (see Figure 1.6). For this reason Böhringer (2001) and Molendi & Pizzolato (2001) proposed to substitute the term "cooling flow" clusters with that of "cool core" clusters.

The possible solutions to the cooling flow problem that have been discussed so far can be divided into two categories: those foreseeing that the gas does cool, but it escapes detection and those invoking a source of heating.

In the first case different explanations have been proposed. It has been suggested that the low energy X-ray emission is photoelectrically absorbed by clouds of cold gas (e.g. Ferland et al. 2002). Another explanation is that the gas below 1-2 keV may have become dense enough to separate from the cooling flow and mix with surrounding colder gas associated with optical filaments or molecular clouds (Begelman & Fabian 1990, Fabian et al. 2002). Fabian et al. (2001) suggested a bimodal metallicity distribution to explain the absence of soft X-ray lines. These models have not been yet thoroughly tested: the missing X-ray luminosity could emerge in the ultraviolet, optical and infrared bands or in high resolution X-ray spectroscopy. However the fate of up to 10^{12-13} M$_\odot$ of gas accumulated during the cluster life ($\sim 10^{10}$ years) is still not explained by these models.

A class of models that assume that there is a heating mechanism which balances the gas radiative cooling in the cluster cores, seems to be more likely. In these models the net mass deposition is small compared to the straightforward estimates $\dot{M} \sim \frac{L_x}{5/2kT}\mu m_p$. Since the cooling flow problem exists in a broad class of objects ranging from individual elliptical galaxies to the most massive clusters, the heating mechanism must be able to operate at vastly different scales. The heating mechanism must be quasi-continuous (on the time scales much longer than the cooling time) and self-tuning to the properties of a given object.

Many suggestions have been made: heat conduction from the outer cluster atmosphere to the core (e.g. Norman & Meiksin 1996, Zakamska & Narayan 2003, Voigt & Fabian 2004), heating by a central radio source (e.g. Pedlar et al. 1990, Churazov et al. 2001, 2002, Böhringer et al., 2002), cosmic ray heating (e.g. Colefrancesco et al. 2004, Oh 2004, Chandran 2005), heating by galaxy motions (e.g. El-Zant et al. 2004, Kim et al. 2005), dark matter interactions (e.g. Qin & Wu 2001, Chuzhoy & Nusser 2006), viscous heating (Brüggen & Ruszkowski 2005), turbulent motions (e.g. Churazov et al. 2002,
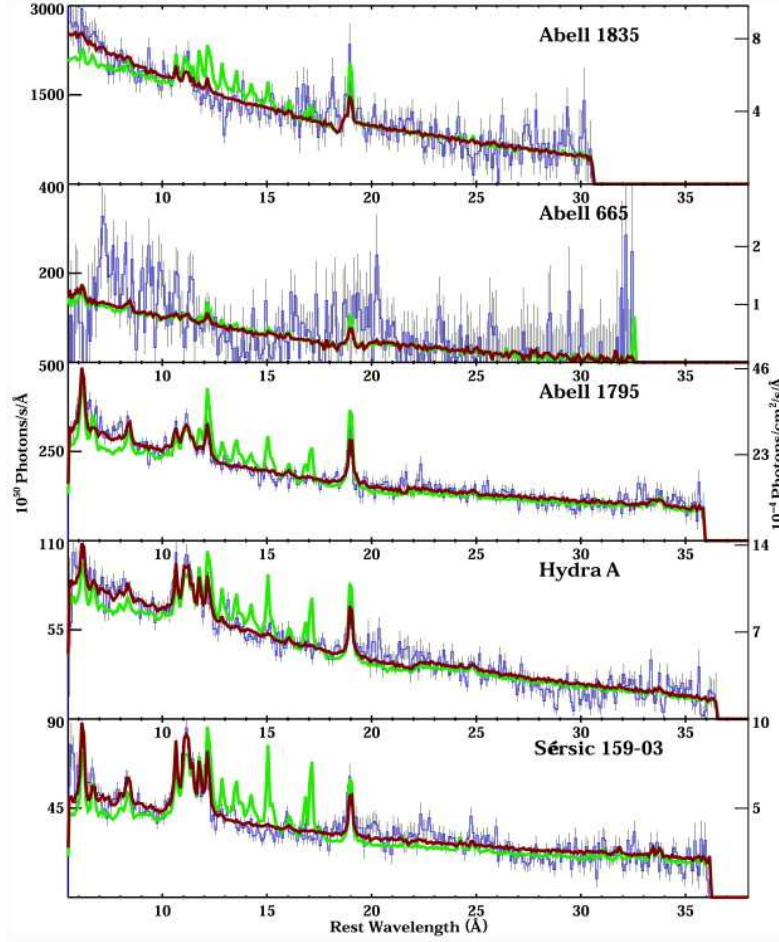
Figure 1.6: RGS spectra vs cooling flow models for a sample of massive clusters (Peterson et al. 2003). Comparison of the data (blue), the standard cooling-flow model (green) and an empirical best fit model where the emission from a simple cooling flow is allowed to be adjusted in given temperature ranges (red). The emission lines between 10 and 13 Å indicate the presence of cool gas (at $1-3$ keV). However in all spectra there is a severe overprediction of emission lines from gas at the lowest temperatures (the lack of lines between 13 and 18 Å is evident) .

Fabian et al. 2003, Fujita et al. 2004). In this thesis we concentrate on the model which assumes that a central radio source is responsible for the generation of gas motions in the core and that the mechanical energy of the gas motion is the source of energy for the cooling gas.

14

1.4 Gas motions induced by AGN feedback

Rosat and *Chandra* X-ray images of the Perseus clusters (see Figure 1.7) clearly show X-ray dim regions coincident with the location of radio bright regions (Böhringer et al. 1993, Fabian et al. 2000). These radio bright regions are the radio lobes associated with the nucleus (supemassive black hole) of the central galaxy of the Perseus cluster (NGC 1275). The same kind of structures are observed in many other cooling flows. It was already well known that elliptical galaxies in the cluster centers very often have a radio bright nucleus (Burns 1990). Now with *Chandra* and *XMM-Newton* it is clear that a strong interaction between the radio plasma and the thermal gas is happening in essentially all the cool core clusters or groups (e.g. Fabian et al. 2006, Forman et al. 2006).

It is believed that supermassive black holes are present in all (or almost all) galaxies and that their masses are correlated with the properties of the host galaxies. Supermassive black holes are a very attractive solution as a source of energy for gas heating, since they can provide large amounts of energy, extracted from the gravitational energy of accreting matter. The Eddington luminosity for a 10^9 $M_\odot$ black hole is of the order of 10^{47} erg s^{-1}. This energy is more than enough to offset the gas cooling losses in the most strong cooling flows, even if one considers a moderate efficiency of the heating mechanisms. Moreover a self-tuning of the energy release is possible through the modulation of the accretion rate onto the black hole (e.g. Nulsen 2004, Böhringer et al. 2004b, Chandran 2005).

The simplest model, currently intensively discussed in the literature, assumes that an outflow of relativistic plasma from the supermassive black hole plays a central role in transferring the energy to the thermal gas. Cavities, shocks, ripples in the distribution of the thermal gas are now observed in many clusters with cool cores, clearly showing that the mechanical interaction of the radio plasma with the thermal gas is strong and that the gas is disturbed by the activity of the nucleus. Furthermore, bubbles of relativistic plasma, created by the supermassive black hole, move through the thermal gas, driven by the buoyancy force. During their motion these bubbles stir the gas and generate turbulent motions (unless the viscosity of the thermal gas is high). It is believed that much of the gas heating is happening not through the shocks, but through the dissipation of the turbulent motions induced by the bubbles. The central part of this thesis is to evaluate the parameters of these motions.

1.5 Gas mixing by turbulent motions

It is known that clusters with cool cores, apart from having a sharp X-ray brightness profile and a drop in the temperature at the center, have also strongly peaked abundance profiles (the relative concentrations of iron and hydrogen) centered at the brightest cluster galaxy (e.g. Fukazawa et al. 1994, 2000, Matsumoto et al. 1996, Ikebe et al. 1999, De Grandi & Molendi 2001). These peaked profiles are likely produced by the stars of the central galaxy over a period of few Gyr (Böhringer et al., 2004). However the observed abundance profiles are shallower than one would expect from the light distribution of the central galaxies. A natural explanation may be that some mechanism is mixing the iron produced by the central galaxy with the thermal cluster gas and effectively transports the iron outwards. This idea can be visualized through the "cappuccino paradigm", where the hot ICM is the milk foam (Figure 1.8, first panel) and the moka (stellar winds and supernovae explosions) injects coffee (iron) at the center of the system (second panel). Without mixing the iron (coffee) would concentrate in the core, but if there is a mixing mechanism (the tea-spoon, third panel), then the final profile is broader (fourth panel).

In the context of cool core clusters we can assume that stochastic gas motions (induced by a central AGN) are responsible for mixing the iron through the large gas masses. Modern X-ray telescopes can measure the radial distribution of iron in the cluster cores rather accurately (e.g. Fukazawa et al. 2000, Irwin & Bregman 2001, De Grandi & Molendi 2001, Schmidt et al. 2002, Matsushita et al. 2002, Churazov et al. 2003, Böhringer et al., 2004, De Grandi et al. 2004). We therefore should be able to use the observed abundance profile to constrain the characteristics of the gas motions averaged over the cluster history: a strong turbulence would delete any abundance peak, while a very weak turbulence would not distribute the iron sufficiently.

An additional useful assumption is that the dissipation of the turbulent gas motions is compensating the gas cooling losses. The combination of this assumption with the constraints coming from the abundance profiles, significantly narrows the allowed range of the turbulence parameters.

1.6 Turbulent broadening of the emission lines

A more direct probe of the gas motions may be obtained by measuring the width of the emission lines (see chapter 4). For lines of heavy ions (especially for iron) the turbulent broadening can easily exceed the pure thermal broadening (see figure 1.10). Hence iron ions are important tracers of turbulent
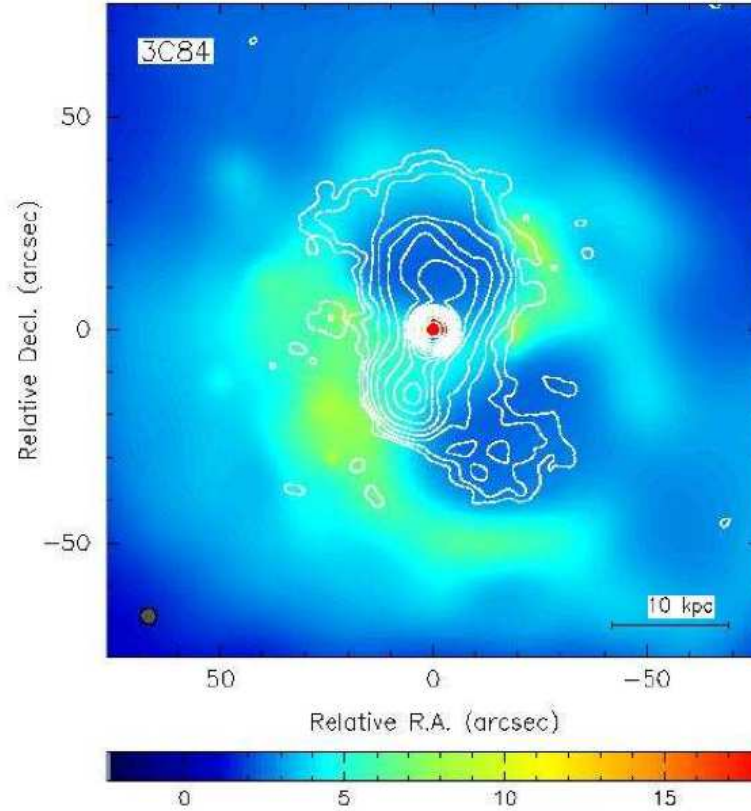
Figure 1.7: Adaptatively-smoothed $0.5 - 7$ keV Chandra X-ray map of the center of the Perseus cluster; the radio (1.4 GHz) contours are superposed (Fabian et al. 2000). Holes in the X-ray surface brightness coincide with some radio lobes, pointing at strong mechanical interaction between the thermal and the radio plasmas.

velocity fields in cluster cores. However the existing telescopes cannot measure the broadening even for the most promising He-like iron line at 6.7 keV. The Japanese-American X-ray satellite *Suzaku* (see Figure 1.9) was the first satellite that carried a new type of X-ray micro-calorimeter (XRS), capable of doing such measurements. Unfortunately XRS failed shortly after launch before any cluster observations were performed. It is clear, however, that micro-calorimeters with the resolution of few eV in the X-ray range will soon be in orbit (e.g. *XEUS* and *Constellation X*). It is therefore timely to study the effect of the turbulence induced by AGNs in the cluster gas on the shape of the brightest emission lines (chapter 4).

Figure 1.8: The "cappuccino paradigm" (see Section 1.5).
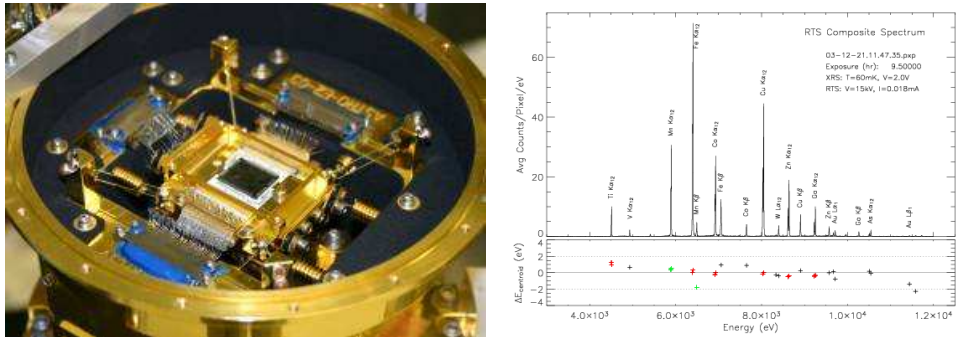
Figure 1.9: Left: the X-ray spectrometer mounted on the X-ray Suzaku. Right: calibration spectrum of XRS-2; the expected energy resolution was of about 6.5 eV at the energy of 6 keV (http://heasarc.gsfc.nasa.gov).

1.7 Structure of the thesis

The thesis is composed by three published papers (chapters 2, 3 and 4) and one which is close to submission at the time of writing (chapter 5). Chapters 2 and 3 discuss the impact of gas motions on the cluster iron abundance profiles and how the observed profiles can be used to constrain the features of turbulence in the core of galaxy clusters and groups. This semi-analytical work is accompanied by the numerical simulations done by Elke Roediger and Marcus Brüggen (chapter 4): the turbulent diffusion coefficient which was estimated from X-ray observations is compared to the one expected from diffusion due to simulated buoyant bubbles in the ICM.

Chapter 5 argues about the possibility to use the shape of the emission lines to determine the velocity fields of the detected gas motions. The last chapter condenses our findings to a general picture.

Units and physical parameters that are usually adopted in Astrophysics can be found in the Appendix.
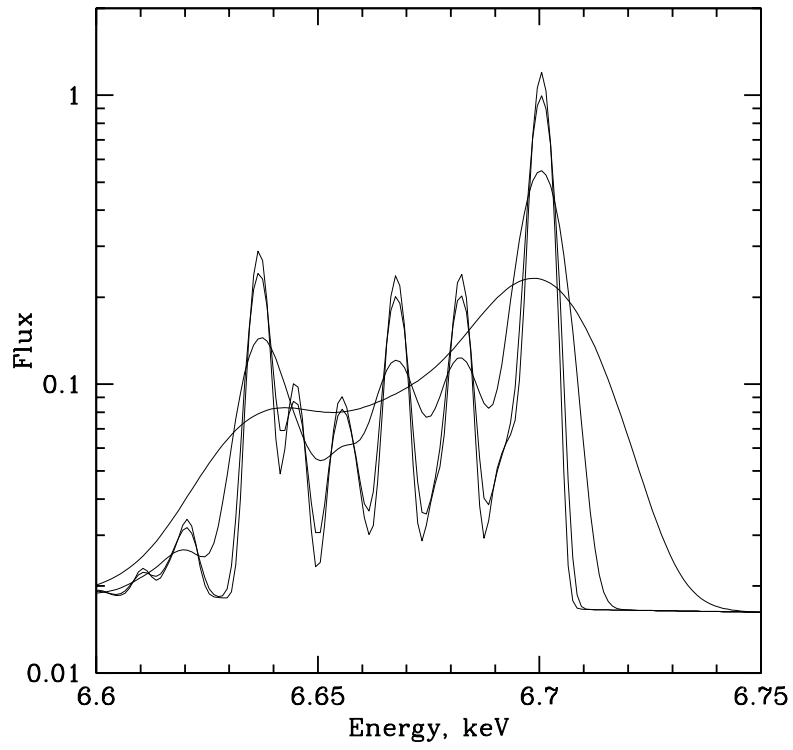
Figure 1.10: 6.7 keV line complex for a $T =4$ keV plasma. The spectra correspond to the thermal broadening and turbulent broadenings with v_{turb}=0, 100, 300 and 900 km/s. For comparison the sound speed in a 4 keV plasma is $\sim$1000 km/s.

Bibliography

[1] Abell G.O. 1958, ApJS, 3, 211

[2] Abell G.O. 1965, ARA&A, 3, 1

[3] Abell G.O. 1975, in Stars and Stellar Systems IX: Galaxies and the Universe, edited by A. Sandage, M. Sandage & J. Kristian, p. 601 (University of Chicago, Chicago)

[4] Allen S.W. 1995, MNRAS, 276, 947

[5] Allen S. W., Fabian A. C., Johnstone R. M., Arnaud K. A., Nulsen P. E. J. 2001, MNRAS, 322, 589

[6] Balbus S.A. 1988, ApJ, 328, 395

[7] Bautz L.P., Morgan W.W. 1970, ApJ, 162, L149

[8] Begelman M.C., Fabian A.C. 1990, MNRAS, 1244, 26

[9] Byram E.T., Chubb T.A., Friedman H. 1966, Science, 152, 66

[2] Böhringer H., Voges W., Fabian A.C., Edge A.C., Neumann D.M. 1993, MNRAS, 264, L25

[11] Böhringer H. 2001, AGM, 18, 122

[12] Böhringer H., Matsushita K., Churazov E., Ikebe Y., Chen Y. 2002, A&A, 382, 804

[14] Böhringer H., Matsushita K., Churazov E., Finoguenov A., Ikebe Y. 2004, A&A, 416, L21

[14] Böhringer H., Matsushita K., Churazov E., Finoguenov A. 2004b, Proceedings of The Riddle of Cooling Flows in Galaxies and Clusters of Galaxies, Eds. T. Reiprich, J. Kempner, and N. Soker, http://www.astro.virginia.edu/coolflow

[15] Brüggen M., Ruszkowski M. 2005, astro-ph/0512148

[16] Burkert A., Lin D.N.C. 2000, ApJ, 537, 270

[17] Burns, J.O. 1990, ApJ, 99, 14

[18] Canizares C.R. et al. 1979, ApJ , 234, L33

[19] Canizares C.R., Clark G.W., Jernigan J.G., Markert T.H. 1982, ApJ, 262, 33

[20] Catura R.C., Fisher P.G., Johnson M.M., Meyerott A.J. 1972, ApJ, 177, L1

[21] Cavaliere A., Fusco-Femiano R. 1976, A&A, 49, 137

[22] Chandran B.D.G., 2005, ApJ, 632, 809

[11] Churazov E., Brüggen M., Kaiser C. R., Böhringer H., Forman W., 2001, ApJ, 554, 261

[24] Churazov E., Sunyaev R., Forman W., Böhringer H. 2002, MNRAS, 332, 729

[25] Churazov E.,Forman W., Jones C., Böhringer H., 2003, ApJ, 590, 225

[26] Chuzhoy L., Nusser A. 2006, ApJ, 645, 950

[27] Colafrancesco et al. 2004, A&A, 413, 441

[28] Cowie L.L., Binney J. 1977, ApJ, 215, 723

[29] Cowie L.L., Fabian A.C., Nulsen P.E.J. 1980, MNRAS, 191, 399

[18] De Grandi S., Molendi S., 2001, ApJ, 551, 153

[19] De Grandi, S.,Ettori, S., Longhetti, M., Molendi, S.,2004, A&A, 419, 7

[9] Edge A.C., Stewart G.C. 1991a, MNRAS, 252, 414

[33] Edge A.C., Stewart G.C. 1991b, MNRAS, 252, 428

[34] El Zant A.A. et al. 2004, MNRAS, 354, 169

[35] Fabian A.C., Nulsen P.E.J. 1977, MNRAS, 180, 479

[36] Fabian A.C., Nulsen P.E.J., Canizares C.R. 1984, Nature, 310, 733

[10] Fabian A.C. 1994, ARA&A, 32, 277

[38] Fabian A.C. et al. 2000, MNRAS, 318, L65

22

[39] Fabian A.C., Mushotzky R.F., Nulsen P.E.J., Peterson J.R. 2001, MN-RAS, 321, L20

[40] Fabian A.C. et al. 2002, MNRAS, 332, L50

[41] Fabian A. C., Sanders J.S., Allen S.W., Crawford C.S., Iwasawa K., Johnstone R.M., Schmidt R.W. 2003, MNRAS, 344, L43

[42] Fabian A.C. et al. 2006, MNRAS, 366, 417

[43] Felten J.E., Gould R.J., Stein W.A., Woolf N.J. 1966, ApJ, 146, 955

[44] Ferland G.J., Fabian A.C., Johnstone R.M. 2002, MNRAS, 333, 876

[45] Field G.B. 1965, ApJ, 142, 531

[16] Forman et al. 2006, astro-ph/0604583

[47] Fujita Y., Matsumoto T., Wada K. 2004, ApJ Lett., 612, L9

[27] Fukazawa Y., Ohashi T., Fabian A. C., Canizares C. R., Ikebe Y., Makishima K., Mushotzky R. F., Yamashita K., 1994, PASJ, 46, L55

[28] Fukazawa Y., Makishima K., Tamura T., Nakazawa K., Ezawa H., Ikebe Y., Kikuchi K., Ohashi T., 2000, MNRAS, 313, 21

[55] Ikebe Y. et al., 1999, ApJ, 525, 581

[32] Irwin J. A., Bregman J. N., 2001, ApJ, 546, 150

[52] Kaastra J. S. 1992, An X-Ray Spectral Code for Optically Thin Plasmas. Internal SRON-Leiden Report

[53] Kim W.T., El Zant A.A., Amr A.E., Kamionkowski M. 2005, ApJ, 632, 157

[54] King I.R. 1962, AJ, 74, 804

[55] Lea S.M., Silk J., Kellogg E., Murray S. 1973, ApJ, 184, L105

[56] Lea S.M., Mushotzky R.F., Holt S.S. 1982, ApJ, 262, 24

[57] Liedahl D.A., Osterheld A.L., Goldstein W.H. 1995, ApJ , 438, L115

[58] Loewenstein M. 1990, ApJ, 349, 471

[59] Malagoli A., Rosner R., Bodo G. 1987, ApJ, 319, 632

[60] Markevitch M. et al. 2000, ApJ, 541, 542

[61] Mathews W.G., Bregman J.N. 1978, ApJ, 224, 308

[37] Matsumoto H., Koyama K., Awaki H., Tomida H., Tsuru T., Mushotzky R., Hatsukade I., 1996, PASJ, 48, 201

[63] Matsushita K., Belsole E., Finoguenov A., Böhringer H. 2002, A&A, 386, 77

[64] Matsuzawa H., Matsuoka M., Ikebe Y., Mihara T., Yamashita K. 1996, PASJ, 48, 565

[65] Mewe R., Gronenschild E. H.B.M., van den Oord G.H.J. 1985, A&AS, 62, 197

[66] Mitchell R.J., Culhane J.L., Davidson P.J., Ives J.C. 1976, MNRAS, 127, 29

[67] Molendi S., Pizzolato F. 2001, ApJ, 560, 194

[27] Mulchaey J.S., Davis D.S., Mushotzky R.F., Burstein D. 1993, ApJ, 404, L9

[69] Mushotzky R.F., Holt S.S., Smith B.W., Boldt E.A., Serlemitsos P.J. 1981, ApJ Lett., 244, L47

[70] Norman C., Meiksin A. 1996, ApJ, 468, 97

[28] Nulsen P.E.J., Stewart G.C., Fabian A.C. 1984, MNRAS, 208, 185

[72] Nulsen P.E.J. 1986, MNRAS, 221, 377

[73] Nulsen P.E.J. 2004, Proceedings of The Riddle of Cooling Flows in Galaxies and Clusters of Galaxies, Eds. T. Reiprich, J. Kempner, and N. Soker, http://www.astro.virginia.edu/coolflow

[74] O'Dea C. et al. 1994, ApJ, 422, 467

[75] Oh S.P. 2004, MNRAS, 353, 468

[76] Pedlar A. et al. 1990, MNRAS, 246, 477

[78] Peres C.B., Fabian A.C., Edge A.C., Allen S.W., Johnstone R.M., White D.A. 1998, MNRAS, 298, 416

[78] Peterson J.R., Kahn S.M., Paerels F.B.S. 2003, ApJ, 590, 207

[79] Qin B., Wu X. 2001, PRL, 87, 1301

[80] Rood H.J., Sastry G.N. 1971, PASP, 83, 313

[81] Sarazin C. L. 1988, X-ray emissions from clusters of galaxies (Cambridge Astrophysics Series)

[47] Schmidt, R.W., Fabian, A.C., Sanders, J.S., 2002, MNRAS, 337, 71

[83] Smith R. K., Brickhouse N. S., Liedahl D. A., Raymond J. C. 2001, ApJ, 556, L91

[84] Springel V., Frenk C.S., White S.D.M. 2006, Nature, 440, 1137

[41] Stewart G.C., Fabian A.C., Jones C., Forman W. 1984, ApJ, 285, 1

[86] Tamura et al. 2001, A&A 365, L87

[87] Voigt L.M., Fabian A.C. 2004, MNRAS, 347, 1130

[88] White R.E. III, Sarazin C.L. 1987, ApJ, 318, 612

[89] White R.E. III, Sarazin C.L. 1988, ApJ, 385, 688

[90] Wolf M. 1906, Astron. Nachr., 170, 211

[91] Zakamska N.L., Narayan R. 2003, ApJ, 582, 162

[92] Zwicky F., Herzog E., Wild P., Karpowicz M., Kowal C.T. 1961-1968, Catalogues of Galaxies and Clusters of Galaxies, Vol. 1-6 (Caltech, Pasadena)

2

Impact of stochastic gas motions on galaxy cluster abundance profiles

P.Rebusco, E.Churazov, H.Böhringer & W.Forman

Abstract

The impact of stochastic gas motions on the metal distribution in cluster core is evaluated. Peaked abundance profiles are a characteristic feature of clusters with cool cores and abundance peaks are likely associated with the brightest cluster galaxies (BCGs) which dwell in cluster cores. The width of the abundance peaks is however significantly broader than the BCG light distribution, suggesting that some gas motions are transporting metals originating from within the BCG. Assuming that this process can be treated as diffusive and using the brightest X-ray cluster A426 (Perseus) as an example, we estimate that a diffusion coefficient of the order of 2×10^{29} cm^2 s^{-1} is needed to explain the width of the observed abundance profiles. Much lower (higher) diffusion coefficients would result in too peaked (too shallow) profiles. Such diffusion could be produced by stochastic gas motions and our analysis provides constraints on the product of their characteristic velocity and their spatial coherence scale. We speculate that the activity of the supermassive black hole of the BCG is driving the stochastic gas motions in cluster cores. When combined with the assumption that the dissipation of the same motions is a key gas heating mechanism, one can estimate both the velocity and the spatial scale of such a diffusive processes.

Keywords: clusters: individual: Perseus - cooling flows

2.1 Introduction

Heavy metals are observed through X-ray spectroscopy of the hot gas in galaxy clusters through the emission lines of highly ionized Ca, Si, S, Fe and other elements. These elements are produced in stars and subsequently injected into the intracluster medium (ICM). On average, the metallicity of the cluster ICM is $\sim 1/3$ of the solar value and it does not seem to vary significantly at least up to a redshift of ~ 1 (e.g. Mushotzky & Loewenstein 1997, Tozzi et al. 2003). This lack of evolution and the relative abundances of the different elements suggest an early enrichment of the ICM by type II supernovae (e.g. Finoguenov et al. 2002). With the high spatial and energy resolution of ASCA, Beppo-Sax, Chandra and XMM-Newton, the radial distribution of metals has been recently mapped for a large sample of nearby clusters (e.g. Fukazawa et al. 2000, Irwin & Bregman 2001, De Grandi & Molendi 2001, Schmidt, Fabian & Sanders 2002, Matsushita et al. 2002, Churazov et al. 2003, De Grandi et al. 2004). Clusters can be divided into two groups, depending on their X-ray properties (Jones & Forman 1984): clusters with cool cores (having a peaked surface brightness profile and a cool core centered at the BCG) and clusters without cool cores (having more or less a flat surface brightness profile in the core and no clear evidence for a cool region near the center). These two groups are traditionally called cooling flow and non-cooling flow clusters (Fabian 1994). The spatial distribution of metals for these two groups is also markedly different: clusters without cool cores have a more or less uniform distribution, while clusters with cool core have strongly peaked abundance profiles (sometimes exceeding the solar abundance) centered at the BCG (e.g. Fukazawa et al. 1994, 2000, Matsumoto et al. 1996, De Grandi & Molendi 2001). Moreover the relative abundances of different elements in the central peaks of cool core clusters suggests that type Ia supernovae have played a significant role in the enrichment process (e.g. Finoguenov et al. 2002, see also Renzini et al. 1993). It is very likely (e.g. Böhringer et al. 2004, De Grandi et al. 2004) that these central abundance peaks are produced predominantly by the stars of the brightest cluster galaxy after the cluster was assembled. If so, then the distribution of the metals should reflect the distribution of the stars (i.e. light) of the BCG and the differences in the light and metal distributions can be used as a proxy for processes which transport and mix the metals of the ICM. Indeed in the best studied cases such as M87, Centaurus or Perseus (Matsushita et al. 2003, 2004, Churazov et al. 2003) the metal distribution in the central abundance peaks is broader than the BCG light distribution, implying that injected metals diffuse to larger radii.

Another characteristic property of cool core clusters is a short gas cooling

time – a factor of 10 to 100 shorter than the Hubble time. Recent X-ray observations (e.g. Peterson et al. 2003, Matsushita et al. 2002, Kaastra et al. 2004) however suggest that the gas does not cool below temperatures of 1-3 keV and an external source of energy is needed to compensate for the gas cooling losses. A number of potential sources of energy have been considered - among them thermal conduction (e.g. Narayan & Medvedev 2001, Voigt & Fabian 2004) or gas motions of different origin. One of the latter family of models utilizes outflows of relativistic plasma, driven by the central super massive black hole (AGN), which interact with the ICM (e.g. Churazov et al. 2001, 2002). The details of the outflow/gas interactions are not yet understood completely and the assumptions on the character of the induced gas motion vary from being almost pure radial (e.g. Fabian et al. 2003) to mostly stochastic (e.g. Churazov et al. 2002). The observed peaked abundance profiles provide a possibility to evaluate the velocities and the spatial scales of these motions. The same motions may affect the thermal balance of the gas in the core by viscous dissipation or by tubulent transport of heat from larger radii (Cho et al., 2003, Kim & Narayan 2003, Voigt & Fabian 2004). The relative importance of both mechanisms is compared in Dennis & Chandran (2004).

In this paper we focus on the impact of stochastic gas motions of arbitrary origin on the transport of metals from the BCG through the ICM in cool core clusters. We adopt here a simple assumption that a diffusion approximation can crudely characterize this transport process. Using the brightest X-ray cluster, Perseus (A426), as an example we estimate parameters of the stochastic motions which are broadly consistent with the data.

The structure of the paper is the following. In section 2.2 the basic input data and the ingredients of the model are described. In section 2.3 the evolution of the abundance profiles is analyzed for various assumptions on the diffusion coefficient. The results are discussed in section 2.4. The last section summarizes our findings.

We adopt a Hubble constant of $H_0 = 70\ km\ s^{-1}\ Mpc^{-1}$, $\Omega_M = 0.3$ and $\Omega_\Lambda = 0.7$, which places the Perseus cluster at 78 Mpc for a redshift of 0.018.

2.2 The model

In this section the basic input parameters of the model are described.

2.2.1 A426 density, temperature and abundance profiles

The electron density n_e and the temperature T_e profiles used here are based on the deprojected XMM-Newton data (Churazov et al. 2003, 2004) which

are also in broad agreement with the ASCA (Allen & Fabian 1998), Beppo-Sax (De Grandi & Molendi 2001, 2002) and Chandra (Schmidt et al. 2002, Sanders et al. 2004) data. Namely:

$$n_e = \frac{4.6 \times 10^{-2}}{[1 + (\frac{r}{57})^2]^{1.8}} + \frac{4.8 \times 10^{-3}}{[1 + (\frac{r}{200})^2]^{0.87}} \quad \text{cm}^{-3} \tag{2.1}$$

and

$$T_e = 7 \times \frac{[1 + (\frac{r}{71})^3]}{[2.3 + (\frac{r}{71})^3]} \quad \text{keV}, \tag{2.2}$$

where r is measured in kpc. The hydrogen number density is assumed to be related to the electron number density as $n_H = n_e/1.2$.

For the abundance profile $a(r)$ (Fig.2.1) we use the deprojected profile obtained from XMM-Newton data (Churazov et al. 2003). The normalization was reduced by $\sim$15% percent to match better the most recent deep Chandra observations of the Perseus core (Schmidt et al. 2002, Sanders et al. 2004). Namely:

$$a(r) = 0.3 \times \frac{2.2 + (r/80)^3}{1 + (r/80)^3} a_\odot, \tag{2.3}$$

where r is in kpc, and $a_\odot$ is the solar abundance (Anders & Grevesse 1989). The functional form used neglects completely the central "abundance hole" observed in the Perseus cluster (Schmidt et al. 2002, Churazov et al. 2003, Sanders et al. 2004) or in M87 (Böhringer et al. 2001, Matsushita et al. 2003). The nature of the abundance hole is unclear and it might be related to "visual" effects (like the presence of a nonthermal component in the X-ray continuum emission or resonant scattering, see however Churazov et al. 2004, Gastaldello & Molendi, 2004 for arguments against resonant scattering) rather than to a real decrease of the metal abundance in the very core. The solid line in (Fig.2.1) is the iron abundance profile from which a constant value of $\sim$0.3 was subtracted. We assume below that the central abundance excess is primarily due to the metal ejection from the central galaxy. The total iron mass in the central excess is of the order of 1.3×10^9 $M_\odot$ (or $\sim 5 \times 10^8$ $M_\odot$ within the central 100 kpc). Compared to Böhringer et al. (2004) the lower overall abundance normalization and the larger value of the subtracted constant lead to somewhat lower masses attributed to the excess.

For comparison we show in Fig.2.1 the expected iron abundance (thin solid line) due to the ejection of metals from the galaxies, assuming a SNIa rate of 0.35 SNU, $k = 1.4$ (see Section 2.2.3 for definitions) and a cluster age of 8 Gyr. The expected profile was calculated assuming that the ejected metal
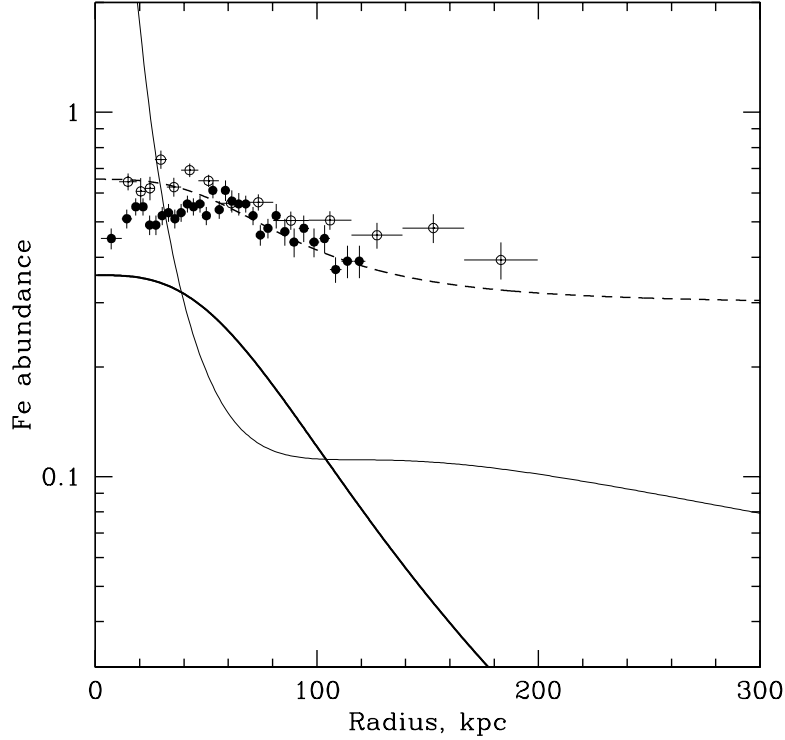
Figure 2.1: Comparison of the observed and the expected iron abundance profiles for the Perseus cluster. Solid circles correspond to the Chandra measurements of projected abundance profile (from Schmidt et al. 2002), while open circles correspond to the XMM-Newton deprojected profile (from Churazov et al. 2003). The dashed line shows the abundance profile adopted in this paper. This profile ignores the central abundance decrement observed in Perseus and several other cooling flow clusters. The thick solid line shows the same profile where a constant value of ~ 0.3 is subtracted. We assume below that this central abundance excess (thick solid line) is primarily due to the metal ejection of the central galaxy. For comparison we show the expected iron abundance (thin solid line) due to the ejection of metals from the galaxies, assuming a SNIa rate of 0.35 SNU, $k = 1.4$ (see the text for definitions) and a cluster age of 8 Gyr. The expected profile was calculated assuming that the ejected metal distribution follows the optical light. The expected abundance profile is much more peaked than the observed profile (due to the contribution of the central galaxy) suggesting that some mechanism is needed to spread the metals.

distribution follows the optical light. The expected abundance profile is much more peaked than the observed profile (due to the contribution of the central galaxy) suggesting that some mechanism is needed to spread the metals.

2.2.2 The central galaxy: NGC 1275

The light distribution of the central elliptical galaxy is described here by a simple Hernquist profile (Hernquist 1990). The effective radius $r_e = 15.3$ kpc and the total blue luminosity 2.8×10^{11} $L\odot$ are taken from Schombert (1987, 1988). While the actual light profile of NGC1275 is more complicated than a single Hernquist profile, this is an acceptable approximation for the purpose of this study. In Fig.2.2 the light distribution of the central galaxy is compared with the light distribution due to all the other cluster galaxies excluding NGC1275. The central galaxy dominates up to a distance of $\sim$ 100 kpc and in subsequent calculations we assume (unless explicitly stated otherwise) that the central excess of metals is produced by the central galaxy alone.

2.2.3 Iron and gas injection rates

The bulk of the cluster gas is enriched at early times of cluster formation by a large number of type II supernovae. The central abundance excess is believed to be formed at later times and the main contributors are likely to be the type Ia supernovae and the stellar mass loss associated with the central galaxy (Matsushita et al. 2003, Böhringer et al. 2004, De Grandi et al. 2004). Both channels inject gas enriched with heavy elements, in particular - iron, into the ICM. We use here similar rates of iron injection by SNIa (eq. 2.4) and stellar mass loss (eq. 2.5) as in Böhringer et al. (2004):

$$\left(\frac{dM_{Fe}}{dt}\right)_{SNIa} = SR \times 10^{-12} \left(\frac{L_B}{L_\odot^B}\right) \eta_{Fe} \tag{2.4}$$

$$= R(t) \, 0.105 \times 10^{-12} \left(\frac{L_B}{L_\odot^B}\right) M_\odot \; yr^{-1},$$

$$\left(\frac{dM_{Fe}}{dt}\right)_* = \gamma_{Fe} \times 2.5 \times 10^{-11} \left(\frac{t}{t_H}\right)^{-1.3} \tag{2.5}$$

$$\times \left(\frac{L_B}{L_\odot^B}\right) M_\odot \; yr^{-1},$$

where SR is the present SNIa rate in SNU (1 SNU - rate of supernova explosions, corresponding to one SN event per century per galaxy with a blue luminosity of 10^{10} $L_\odot^B$), $\eta_{Fe} = 0.7 M_\odot$ is the iron yield per SNIa, $\gamma_{Fe} = 2.8 \times 10^{-3}$
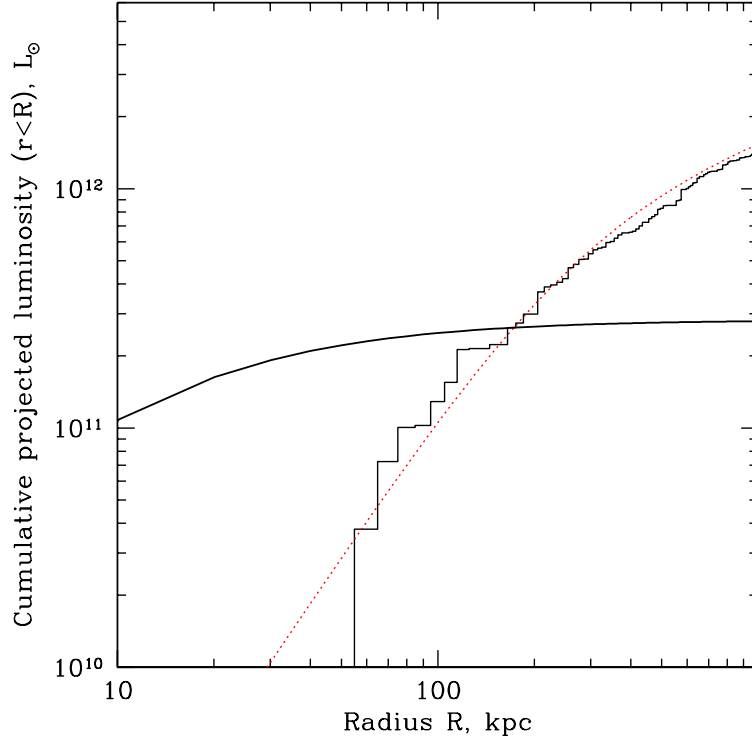
Figure 2.2: Cumulative projected light distribution of the central galaxy NGC1275 (thick solid line) and of all the other galaxies in the cluster excluding NGC1275 (histogram). The positions and the magnitudes of the galaxies are taken from Brunzendorf & Meusinger (1999). A simple King model fit to the light distribution (omitting NGC1275) is shown. The central galaxy dominates light up to a distance of $\sim$100 kpc.

is the mean iron mass fraction in the stellar winds of an evolved stellar population, t_H is the Hubble time. The expression for the stellar mass loss was adopted from Ciotti et al. (1991), assuming a galactic age of 10 Gyr. Along with heavy elements (iron) the stellar mass loss can make a substantial contribution of hydrogen to the ICM. This effect is important only in the central ~ 20 kpc and it was neglected in the subsequent calculations. We therefore assume that only heavy elements are injected to ICM by SNIa and stellar mass loss. The time dependent factor $R(t) = (t/t_H)^{(-k)}$ takes into account an increased SNIa rate in the past (Renzini et al. 1993), with the index k

34

ranging from 1.1 up to 2. A fiducial value for the present day SNIa rate of 0.15 SNU (Cappellaro, Evans, & Turatto 1999) was assumed. Thus the total iron injection rate within a given radius r can be written as

$$s(< r, t) = \left(\frac{dM_{Fe}}{dt}\right)_* + \left(\frac{dM_{Fe}}{dt}\right)_{SN} \propto \left(\frac{L_B(< r)}{L_\odot^B}\right) \qquad (2.6)$$

The total amount of iron produced by the central galaxy during its evolution from some initial time to the present is simply an integral of equation (3.4) over time. The total amount of iron in the central excess is set above (by our definition of the central excess, see Fig.2.1) to $\sim 1.3 \times 10^9 \ M_\odot$. Therefore, the parameters of the model (SR, k, t_{age}) are constrained by the observed total iron mass (see Fig.2.3).

For the subsequent analysis we have selected two combinations of these parameters: (0.35, 1.4, 8 Gyr) and (0.26, 2, 8 Gyr). With these choices of parameters one can readily predict the amount and the distribution of the metals ejected from the galaxies into the ICM as displayed in Fig.2.1. In this figure we show the observed iron abundance and the expected iron abundance, determined by comparing the amount of injected iron (by all the galaxies, including the BCG) with the present day gas density distribution. On large scales $\sim$30% of the observed amount of iron is provided by SNIa and stellar mass loss. The remaining $\sim$70% could be attributed to early enrichment by SNII. The central excess of iron generated by the central galaxy is much more peaked than the observed abundance profile. This is of course an expected result, given that the effective radius of the galaxy is $\sim$15 kpc, while the characteristic size of the abundance excess is much larger. The difference between the distribution of the ejected iron and the observed abundance profile suggests that some process is transporting the metals to larger radii. We assume below that this process can be treated in a diffusion approximation.

2.2.4 Diffusion of metals due to stochastic gas motions

We assume that the ICM at a given radius r is involved in stochastic motions with a characteristic size sufficiently smaller than r and that this motion mixes the ICM. We assume moreover that such motion with a characteristic velocity v and a characteristic coherence length l will lead to an effective diffusion coefficient of the order of $D \sim \frac{vl}{3}$. We further make the strong simplification that the gas density and temperature do not evolve with time, i.e. the gas entropy losses (due to radiation) and gains (due to the dissipation of the stochastic motions and to the mixing of the low entropy gas with the outer layers of higher entropy gas) cancel each other (e.g. Churazov et al., 2002). In this approximation the stochastic motions have a clear impact on
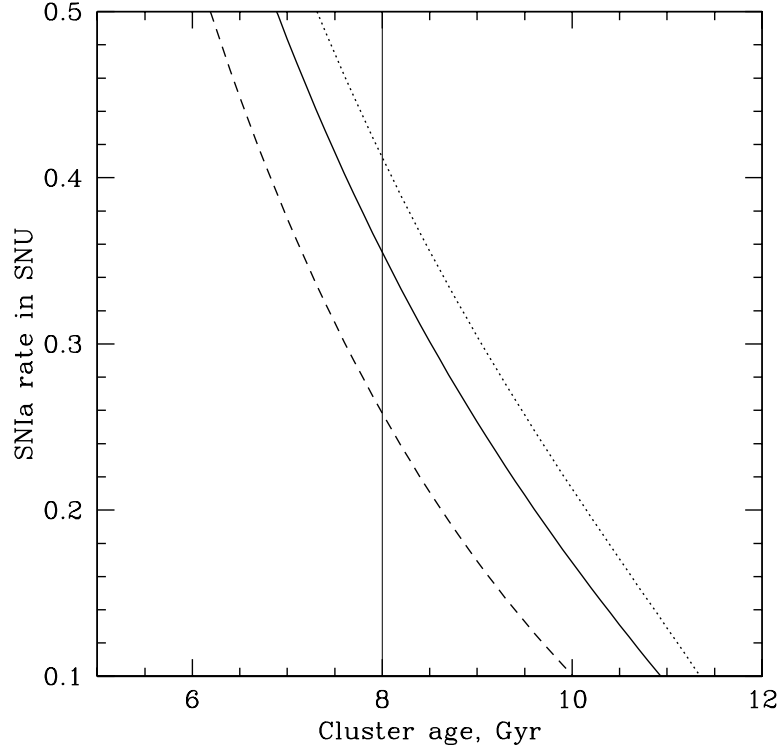
Figure 2.3: SNIa rate in SNU required to produce the excess amount of iron of $\sim 1.3 \times 10^9 \ M_\odot$ by the BCG with $L_B = 2.8 \times 10^{11} \ L_\odot$ according to 2.6. The solid line is for $k = 1.4$, the dotted one for $k = 1.1$, the dashed one for $k = 2$

the distribution of metals and this process can be considered in a diffusion approximation:

$$\frac{\partial na}{\partial t} = \nabla \cdot (Dn\nabla a) + S, \tag{2.7}$$

where $n = n(r)$ is the gas density, $a = a(r,t)$ is the iron abundance and $S = S(r,t)$ is the source term due to the iron injection from the central galaxy, D is the diffusion coefficient. Once the diffusion coefficient is specified, eq.2.7 can be readily integrated.

A rough estimate of the required diffusion coefficient can be obtained by comparing the characteristic time scales for diffusion and enrichment (Fig.2.4). In this figure the cumulative iron enrichment time - i.e. the ratio of the

36
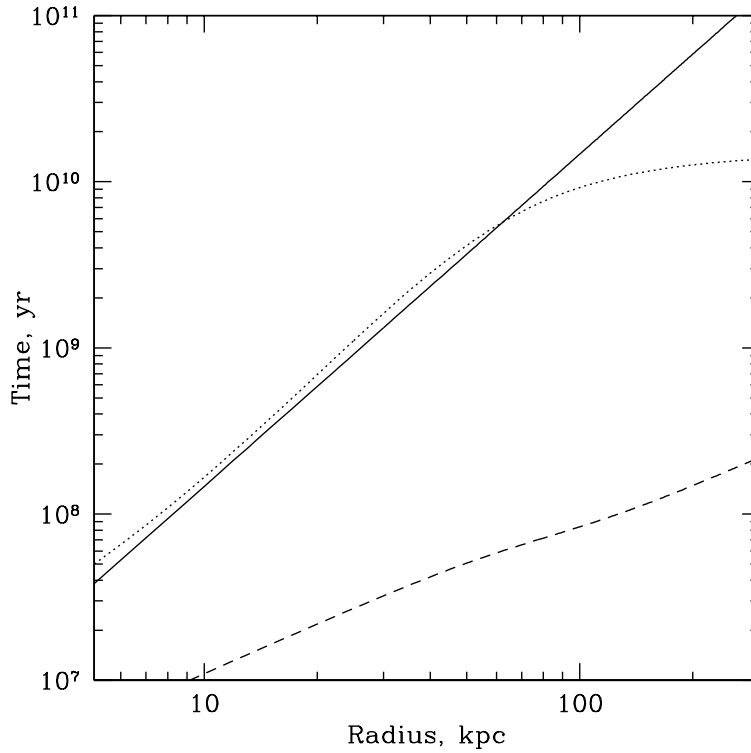
Figure 2.4: Diffusion time scale (solid line) estimated as $t_{\mathrm{diff}} \sim r^2/D$, where $D = 2 \times 10^{29}$ cm^2 s^{-1}. For comparison the cumulative enrichment time (ratio of the amount of metals in the abundance excess to the metal ejection rate by the central galaxy) is shown by the dotted line. The dashed line shows the sound crossing time.

observed amount of metals in the abundance excess within a given radius r is compared to the current injection rate of iron by the central galaxy within the same radius. The diffusion time was estimated as $t_{\mathrm{diff}} \sim r^2/D$, where the diffusion coefficient D is set to 2×10^{29} cm^2 s^{-1}. Fig.2.4 suggests that diffusion with coefficient $D \sim 2 \times 10^{29}$ cm^2 s^{-1} would significantly affect the metal distribution in the core.
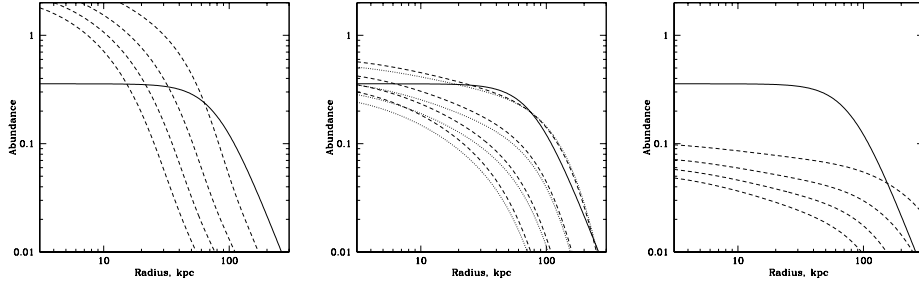
Figure 2.5: Time evolution of the abundance profiles for different diffusion coefficients $D = 2 \times 10^{28}, 2 \times 10^{29}, 2 \times 10^{30}$ cm^2 s^{-1} for the left, middle and right plots respectively. The thick solid line is the observed abundance peak, while the dashed lines show the abundance of metals produced by the central galaxy during 1,2,4 and 8 Gyr (from the bottom to the top)in the model with $k = 1.4$ and $SR = 0.35$. For comparison in the middle plot the dotted line shows the same evolution for $k = 2$ and $SR = 0.26$.

2.3 Results

2.3.1 Constant diffusion coefficient

In a more detailed modeling of the diffusion transport of metals in the ICM, we first consider the simplest case of a diffusion coefficient which is independent of both time and radius. Fig.2.5 shows the evolution of the abundance peak produced by the central galaxy after 1, 2, 4 and 8 Gyr for different values of the diffusion coefficient: $D = 2 \times 10^{28}, 2 \times 10^{29}, 2 \times 10^{30}$ cm^2 s^{-1} for the left, middle and right plots respectively. The thick line in all plots shows the observed abundance peak. It is clear that too small (or too large) diffusion coefficients produce too peaked (or too shallow) abundance profiles, while $D = 2 \times 10^{29}$ cm^2 s^{-1} is roughly consistent with the data. These calculations were done assuming $k = 1.4$ and $SR = 0.35$. The comparison with the alternative model with $k = 2$ and $SR = 0.26$ (dotted curves in the middle plot) shows that the differences in the shape of the final abundance excess are minor.

A similar characteristic value of the diffusion coefficient can be derived by comparing the characteristic size of the observed abundance excess and the excesses produced by ejection and diffusion in the model. Fig.2.6 shows the effective radius (the radius containing half of the ejected metals) as a function of the diffusion coefficient. For small diffusion coefficients the metal distribution is essentially set by the light distribution of the central galaxy. As the diffusion coefficient increases the effective radius also increases. This

38
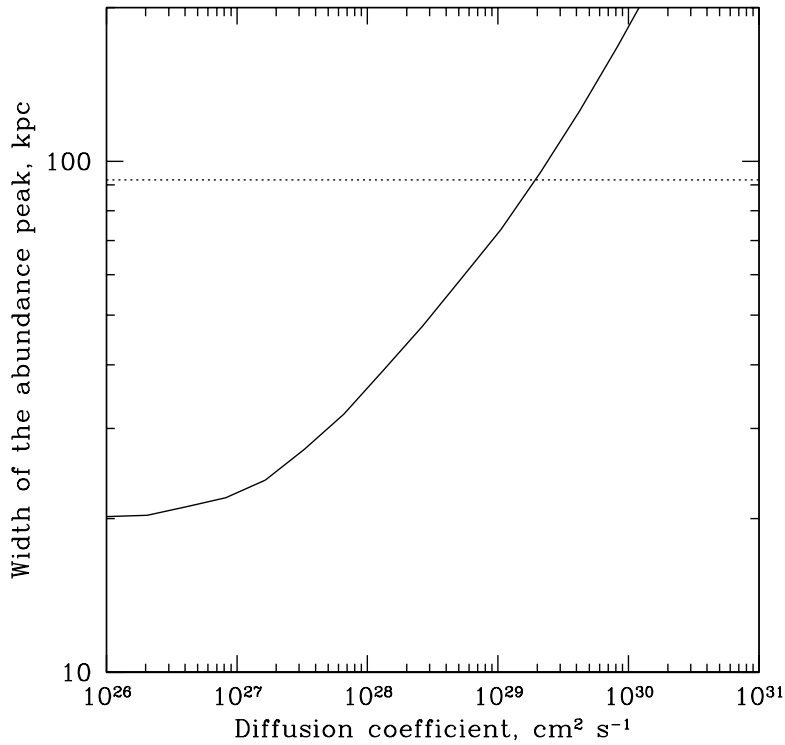
Figure 2.6: Width of the abundance peak distribution (radius containing half of the ejected iron) as a function of the diffusion coefficient for $k = 1.4$ and 8 Gyr cluster age. The dotted horizontal line shows the width of the observed abundance excess.

plot also suggests that $D \sim 2 \times 10^{29}$ cm^2 s^{-1} would provide a width of the metal distribution similar to the one observed in the abundance excess. One can further consider the present day evolution of the abundance profile, i.e. using the observed abundance peak as an initial condition, as shown in Fig.2.7. Again, too small (or too large) diffusion coefficients cause a quick steepening or flattening of the abundance peaks on time scales of Gyr. The evolution of the profile for the diffusion coefficient of the order of 2 10^{29} cm^2 s^{-1} is much more gradual.
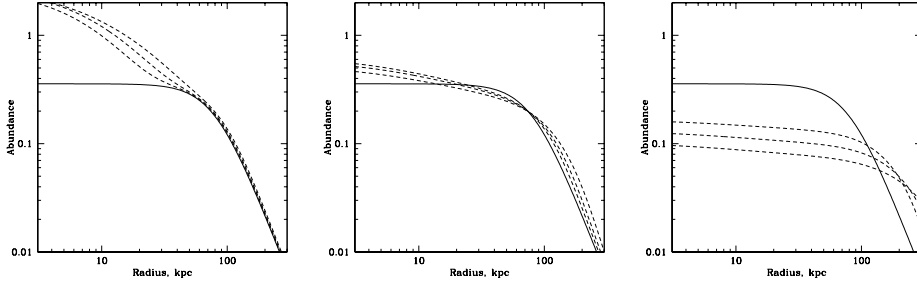
Figure 2.7: Time evolution of the abundance profiles starting from the observed abundance peak for different diffusion coefficients: $D = 2 \times 10^{28}, 2 \times 10^{29}, 2 \times 10^{30}$ cm^2 s^{-1} for the left, middle and right plots respectively. The initial profile is the observed abundance peak distribution and the evolution of the profile is shown after 1,2 and 4 Gyr (dashed curves from the bottom to the top) for the model with $k = 1.4$ and $SR = 0.36$. The thick solid line is the observed abundance peak. The calculations were done assuming metal injection rates according to eq.2.6, starting from $t = t_H$. Note that for the figures on the left(right) the profile quickly evolves to a peaked (shallow) distribution, while for the central plot ($D = 2 \times 10^{29}$ cm^2 s^{-1}) the evolution is very slow, approximately corresponding to a quasi-steady state.

2.3.2 Varying diffusion coefficient as a function of radius

In this section we estimate the impact of diffusion on the abundance peaks when the diffusion coefficient is a function of the radius. One natural motivation for such an assumption is the hypothesis that an AGN at the center of the BCG is driving the gas motions in the core. In this case one would expect these motions to fade away outside the cluster core, when the energy injected by the AGN into the ICM spreads over large masses of gas. Let us assume that a fraction f of the ICM volume at a given radius is involved in the stochastic motions with characteristic velocity v and spatial scale l. If the dissipation of the stochastic motions with the rate $\Gamma_{diss} \propto nv^3/l$ is the main source of energy which offsets the gas radiative losses $\Gamma_{cool} \propto n^2\Lambda(T)$, then $f\Gamma_{diss} \sim \Gamma_{cool}$ and therefore $f \propto n$ (if l and v do not vary strongly with the radius). The effective diffusion coefficient can then be written as $D \propto n$, i.e. D declines with the radius along with the density. This is of course an oversimplified scaling, but to see the influence of the diffusion coefficient changing with radius on the abundance profile, we parametrized it as $D = D_0 \left(n(r)/n(r_0) \right)^{\alpha}$, where $D_0 = 2 \times 10^{29}$ cm^2 s^{-1}, $r_0 = 50$ kpc. The resulting profiles for $\alpha = 1, 2, -1$ are shown in Fig.2.8. For declining diffusion coefficients, for larger values of α, the overall shape of the peak becomes more boxy than for a constant dif-
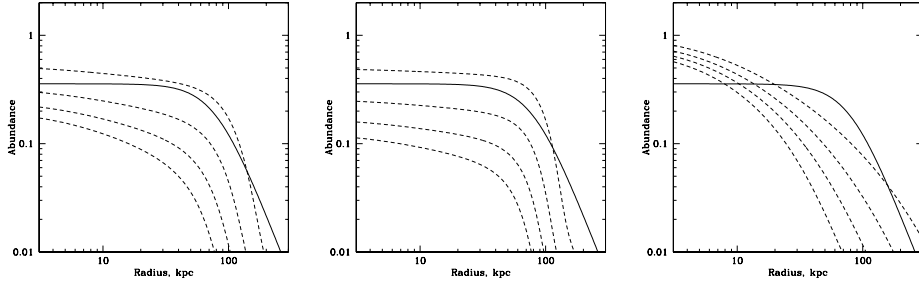
Figure 2.8: Time evolution of the abundance profiles for different radial dependence of the diffusion coefficient parametrized as $D = D_0\left(n(r)/n(r_0)\right)^{\alpha}$. $\alpha = 1, 2, -1$ for the left, middle and right plots respectively. $D_0 = 2 \times 10^{29}$ cm^2 s^{-1}, n is the gas density, $r_0 = 50$ kpc. The thick solid line is the observed abundance peak, while the dashed lines show the abundance of metals produced by the central galaxy during 1,2,4 and 8 Gyr (in the model with $k = 1.4$ and $SR = 0.35$). As α increases the distribution becomes more boxy, while for negative α the distribution is more steep than the observed one.

fusion coefficient (see Fig.2.8 middle panel). In fact the profile with $\alpha = 1$ is closer to the observed abundance peak than that with a constant diffusion coefficient. However, given the uncertainties of the adopted abundance peak and the oversimplified nature of the model, one cannot claim that a variable diffusion coefficient provides a significantly better description of the observed abundance peak.

The right plot in Fig.2.8 is calculated for $\alpha = -1$, i.e. diffusion coefficient rising with the radius (or with a decline of the density). This case represents the situation when the gas in the very center is more steady than in the outer layers. With our choice of D_0 and scaling radius r_0 the predicted profiles are too peaked compared to that observed. Of course with such simulations we cannot constrain the behavior of the diffusion coefficient at even larger radii where the stochastic motions produced by e.g. mergers may stir and mix the ICM. We can only conclude that within the core of the cluster diffusion coefficients declining with radius seem preferable compared to rising ones.

2.4 Discussion

2.4.1 Constraints on the velocities and spatial scales

Summarizing the results of the above section we conclude that the shape of the observed abundance peak produced by metal ejection from the central galaxy is consistent with the presence of a diffusive transport of iron with

effective diffusion coefficient of the order of $D_0 \sim 2 \times 10^{29}$ cm^2 s^{-1}. Under the assumption that the diffusion of iron is due to stochastic gas motions on much smaller spatial scales (smaller than the radius r), one can express the diffusion coefficient in the form $D \sim C_1 v l$, where C_1 is a dimensionless constant of the order of unity. Thus the value of D_0 estimated in the previous section can be considered as a measure of the product of the characteristic velocity v and the spatial scale l of the gas motions. On the other hand the gas heating rate due to the dissipation of the kinetic energy of the same motions also depends on the combination of v and l and can be written as $\Gamma_{diss} \sim C_2 \rho v^3 / l$, where ρ is the gas density and C_2 is a dimensionless constant. Assuming that the disspation of turbulent motions is the dominant source of heat and that the heating rate is equal to the gas cooling rate then $\Gamma_{diss} \sim \Gamma_{cool} = n^2 \Lambda(T)$. The cooling rate can be easily calculated from the observed gas temperature and density, thus providing another constraint on v and l. Therefore using D_0 and the cooling rate, one can estimate both v and l. The coefficients C_1 and C_2 (and the validity of the scaling itself) in the above expressions depend critically on the character of the gas motions, which is unknown. One can hope to derive an order of magnitude estimate using the simplest variants of turbulent flows. For this estimate we follow the definitions of Dennis & Chandran (2004) for v and l which lead to the following expressions for D and Γ_{diss}:

$$D \quad \sim \quad 0.11 v l \qquad (2.8)$$
$$\Gamma_{diss} \quad \sim \quad 0.4 \rho v^3 / l. \qquad (2.9)$$

Using the above definitions and choosing $r = 50$ kpc as a characteristic radius we set $D = 2 \times 10^{29}$ cm^2 s^{-1} and $\Gamma_{diss} = n^2 \Lambda(T)$ to balance cooling and dissipation. One can plot the resulting constraints in a v/l plot (see Fig.2.9). The thick solid line shows the combinations of v and l which give the same diffusion coefficient, while along the thick dotted line the dissipation rate is equal to the cooling rate at $r = 50$ kpc. The two pairs of solid and dotted lines show the effect of varying C_1 and C_2 by factor of $1/3$ and 3 each. The intersection of the two curves (bands) gives the locus of the combinations of l and v such that on one hand the diffusion coefficient is approximately equal to D_0 and on the other hand the dissipation rate is approximately equal to the cooling rate. In this figure l and v are the characteristic spatial scales and velocities of the stochastic gas motions (see Dennis & Chandran 2004 and references therein). This simplified model suggests that eddies with size of $\sim$10 kpc and velocities of the order of few hundred km/s can provide the appropriate iron diffusion and balance gas cooling losses at the same time. Such velocities and spatial scales seem reasonable for models where AGN driven outflows are present in
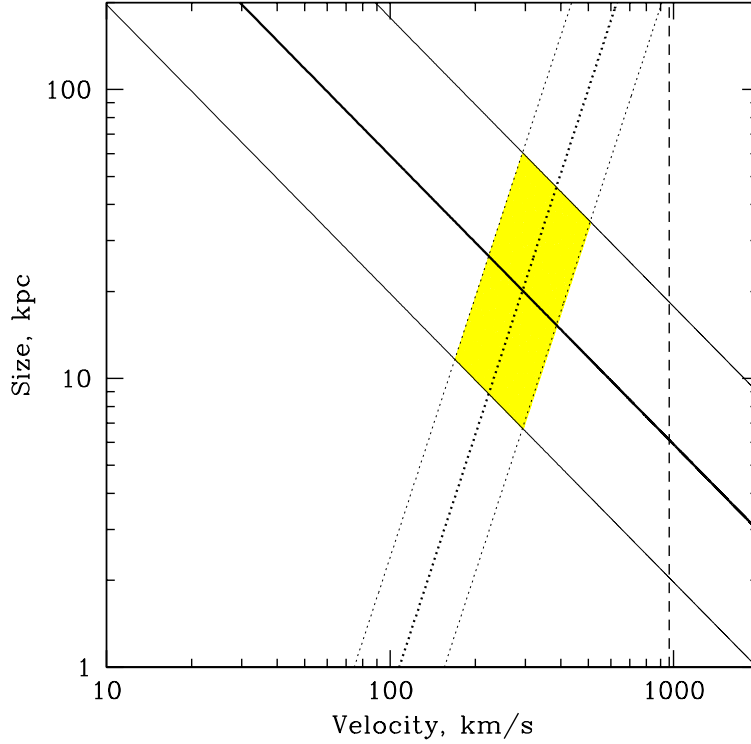
Figure 2.9: Range of the characteristic velocities v and spatial scales l of the gas motions which provide the necessary diffusion and dissipation rates. Along the thick solid line the diffusion coefficient $D = 0.11vl$ is constant and equal to 2×10^{29} cm^2 s^{-1}. Along the thick dotted line the dissipation/heating rate $\Gamma_{diss} = 0.4 \; \rho \; v^3/l$ is equal to the gas cooling rate $n^2\Lambda(T)$. At the intersection of these curves, $v \sim 300 \; km \; s^{-1}$ and $l \sim 20$ kpc, two conditions are satisfied: i) gas cooling is balanced by the dissipation and ii) the diffusion coefficient is of the right order. The thin solid and the dotted lines correspond to a variation of the coefficients in eqns. 2.8-2.9 by factors of 0.3 and 3. The vertical dashed line shows the sound velocity in the gas.

cool cluster cores. In these models the outflow generates motions of the gas on spatial scales of expanding and rising bubbles (10-15 kpc for the case of A426) and with velocities characteristic for outflows (a fraction of the sound speed or few hundred km/s for buoyantly rising bubbles). These gas motions eventually dissipate their energy through viscous heating and/or shocks. The latter mechanism of dissipation could occur almost without any mixing of metals - if

e.g. there are predominantly radial shock waves, while the former mechanism provides a closer link between heating and metal diffusion. While the estimates from Fig.2.9 are very crude, they are consistent with the assumption that the mixing/dissipation process plays an important role in clusters with cool cores. The presence of differential motions with velocities of the order of few hundred km/s is also consistent with the lack of spectral signatures of resonant scattering in the Perseus cluster (Churazov et al. 2004), although resonant scattering is sensitive to both isotropic (case with mixing of metals) and radial (no mixing) gas motions.

We stress again that the uncertainties in the expressions for the turbulent diffusion coefficient and for the dissipation rate (see eqns.2.8-2.9 are very large and that the numerical results (Fig.2.9) should be treated with caution. Moreover the actual transport of metals in a stratified cluster medium could be very complicated (e.g. Brueggen 2002), involving on one hand stages of efficient transport of metals entrained with the rising bubbles and on the other hand separation of the enriched clumps from the rising flow due to the entropy contrast. However the above analysis suggests that cool cores could be a long lived feature (at least few Gyr - judging from the amount of metals ejected by the BCG - see Böhringer et al. 2004, De Grandi et al. 2004), supported against the catastrophic cooling by the AGN activity. Of course AGN activity is not the only mechanism which can induce motions in the cluster core. The evidence for gas "sloshing" (Markevitch, Vikhlinin & Forman, 2003) is found in more than 2/3 of the cooling flow clusters and both mergers or AGN activity may be the cause. Fujita, Matsumoto & Wada (2004) argue that the turbulence in the core is caused by the bulk gas motions of the cluster gas. Depending on the characteristic spatial and velocity scales of the motions either direct dissipation or tubulent heat transport may affect the thermal state of the gas (Dennis & Chandran, 2004).

2.4.2 Alternative scenarios for the abundance peak formation.

The ejection of metals from the central BCG is not the only mechanism which could contribute to the formation of abundance peaks in cool core clusters. Given the uncertainties in the age of the system and in the rate of metal ejection by stars, one cannot exclude other sources of iron based on a simple comparison of the excess iron mass with the optical luminosity of the central galaxy. We briefly mention below the most obvious alternative channels of metal enrichment. One of the processes which could lead to an enhanced abundance of metals in the cluster core is gravitational settling (e.g. Fabian & Pringle 1977, Rephaeli 1978, Gilfanov & Sunyaev 1984, Chuzhoy & Nusser 2003, Chuzhoy & Loeb 2004). For clusters with cool cores the temperature

in the core is low (few keV) while the gas density is high. In such conditions the process of gravitational settling is rather slow and it is unlikely that it plays an important role in modifying the observed peaked iron distributions. More promising seems to be the stripping of metal enriched gas from smaller subclusters and groups which may have lower entropy than the bulk of the cluster ICM: group/subcluster gas may sink to the bottom of the potential well (e.g. Churazov et al. 2003), unless hydrodynamical instabilities mix it with the ICM before it reaches the cluster center. In a similar way, stripping the interstellar medium (ISM) of infalling spirals or elliptical galaxies (e.g. Böhringer et al. 1997, Toniazzo & Schindler, 2001) that spend a large part of their time in orbit at large radii can lead to a concentration of metals in the cluster center in comparison to the overall galaxy distribution. A closer inspection of the expected effect of the stripping of the bulk of the ISM from spirals at column densities of $10^{20} - 10^{21}$ cm^{-2} shows that this should occur at gas densities less than $n_e \sim 10^{-4}$ cm^{-3} for spiral galaxies falling in face on and at somewhat larger densities if the galaxies are inclined but little ISM should reach the inner part of the cluster with gas densities larger than $n_e \sim 10^{-3}$cm^{-3} (e.g. Cayatte et al. 1994, Böhringer et al. 1997). Thus most of the stripping enrichment of the ICM should happen outside a radius of 300 kpc and well outside the region considered here. Stripping should take place both in cooling flow and non-cooling flow clusters. And unless all non-cooling flow clusters have experienced a recent merger one would expect abundance gradients in both types of clusters. The good correlation of the BCG luminosity and the iron excess mass (e.g. De Grandi et al. 2004) seems to suggest that the above mentioned alternative mechanisms do not play a dominant role in the formation of the central abundance excess. Nevertheless it is not easy to discard these mechanisms completely. One can hope that with the launch of ASTRO-E it will be possible to derive new constraints on the character of the gas motions in the cool cores clusters, in particular on the amplitude and the characteristic spatial scales of the velocity perturbations in the cluster cores. The anticipated energy resolution of ASTRO-E spectrometer - FWHM$\sim$ 6-7 eV (see e.g. `http://heasarc.gsfc.nasa.gov/docs/astroe`) corresponds to velocities of $\sim$ 200 km/s for the 6.7 keV line. For comparison the width of the 6.7 keV line due to thermal motions of iron ions is $\sim$100 km/s (at a temperature of 3 keV). Therefore it is realistic to expect the detection of line broadening for characteristic stochastic velocities larger than $\sim$100 km/s. The position of the line can be measured with much higher accuracy and therefore the presence of large scale motions can be verified. Given the angular size of a single spectrometer pixel of $\sim 0.5'$, the spatial scales one can probe in Perseus are of order of 10 kpc. Thus Perseus observations with ASTRO-E will provide a decisive test of the models discussed above.

2.5 Conclusions

We show that the heavy metal abundance peak observed in the Perseus cluster is consistent with a diffusive spreading of metals, provided that the diffusion coefficient is of the order of 2×10^{29} cm^2 s^{-1}. Stochastic gas motions with characteristic velocities of the order of few hundred km/s and spatial scales of the order of 10 kpc can provide the diffusive transport of iron and simultaneously a dissipation rate comparable with the gas cooling rate. Such parameters seem to be broadly consistent with models where self-regulated AGN driven outflows are present in the cool cores clusters. ASTRO-E2 observations of Perseus should provide a clear test of the importance of turbulent mixing in cool cluster cores.

Bibliography

[1] Allen, S. W., Fabian, A. C., 1998, MNRAS, 297, L63

[2] Anders E., Grevesse N., 1989, Geochimica et Cosmochimica Acta, 53, 197

[3] Boehringer H., Neumann D. M., Schindler S., Huchra J. P., 1997, ApJ, 485, 439

[4] Böhringer, H., Belsole, E., Kennea, J., et al. 2001, A&A, 365, L18

[5] Böhringer H., Matsushita K., Churazov E., Finoguenov A., Ikebe Y., 2004, A&A, 416, 21

[6] Brüggen, M., 2002, ApJ, 571, L13

[7] Brunzendorf, J., Meusinger H., 1999, ApJS, 139, 141

[8] Cappellaro E., Evans R., Turatto M., 1999, A&A, 351, 459

[9] Cayatte V., Kotanyi C., Balkowski C., van Gorkom J. H., 1994, AJ, 107, 1003

[10] Cho J., Lazarian A., Honein A., Knaepen B., Kassinos S., Moin P., 2003, ApJ, 589, L77

[11] Churazov E., Brüggen M., Kaiser C. R., Böhringer H., Forman W., 2001, ApJ, 554, 261

[6] Churazov E., Sunyaev R., Forman W., Böhringer H., 2002, MNRAS, 332, 729

[13] Churazov, E.,Forman, W., Jones, C., Böringer, H., 2003, ApJ, 590, 225

[14] Churazov, E.,Forman, W., Jones, C., Sunyaev, R., Böringer, H. 2004, MNRAS, 347, 29

[15] Chuzhoy, L., Loeb, A., MNRAS, 349, L13

[16] Chuzhoy L., Nusser A., 2003, MNRAS, 342, L5

[17] Ciotti L.,D'Ercole A., Pellegrini S., Renzini A., 1991, ApJ 376 380

[18] De Grandi S., Molendi S., 2001, ApJ, 551, 153

[19] De Grandi, S.,Ettori, S., Longhetti, M., Molendi, S.,2004, A&A, 419, 7

[20] De Grandi S., Molendi S., 2002, ApJ 567 163

[21] Dennis, T., Chandran, B., 2005, ApJ, 622, 205

[22] Fabian, A.C., Pringle, J.E., 1977, MNRAS, 181, 5

[23] Fabian, A.,C. 1994, ARA&A, 32, 277

[24] Fabian A. C., Sanders J. S., Allen S. W., Crawford C. S., Iwasawa K.,
      Johnstone R. M., Schmidt R. W., Taylor G. B., 2003, MNRAS, 344, L43

[25] Finoguenov A., Matsushita K., Böhringer H., Ikebe Y., Arnaud M., 2002,
      A&A, 381, 21

[26] Fujita Y., Matsumoto T., Wada K., 2004, ApJ, 612, 9

[27] Fukazawa Y., Ohashi T., Fabian A. C., Canizares C. R., Ikebe Y., Mak-
      ishima K., Mushotzky R. F., Yamashita K., 1994, PASJ, 46, L55

[28] Fukazawa Y., Makishima K., Tamura T., Nakazawa K., Ezawa H., Ikebe
      Y., Kikuchi K., Ohashi T., 2000, MNRAS, 313, 21

[29] Gilfanov, M.R., Sunyaev, R.A.,1984, SvAL, 10, 137

[30] Gastaldello, F., Molendi, S., 2004, ApJ, 600, 670

[31] Hernquist L., 1990, ApJ, 356, 359

[32] Irwin J. A., Bregman J. N., 2001, ApJ, 546, 150

[33] Jones C., Forman W., 1984, ApJ, 276, 38

[34] Kaastra J. S., et al. 2004, A&A, 413, 415

[35] Kim, W., Narayan, R. 2003, ApJ, 596L, 139

[36] Markevitch M., Vikhlinin A., Forman W. R., Matter and Energy in Clus-
      ters of Galaxies, ASP Conference Proceedings, Vol. 301. Held 23-27 April
      2002 at National Central University, Chung-Li, Taiwan. Edited by Stuart
      Bowyer and Chorng-Yuan Hwang. San Francisco: Astronomical Society of
      the Pacific, 2003. ISBN: 1-58381-149-4, p.37

48

[37] Matsumoto H., Koyama K., Awaki H., Tomida H., Tsuru T., Mushotzky R., Hatsukade I., 1996, PASJ, 48, 201

[38] Matsushita, K., Belsole, E., Finoguenov, A., Böhringer, H., 2002, A&A, 386, 77

[39] Matsushita, K., Finoguenov, A., Böhringer, H., 2003, A&A, 401, 443

[40] Matsushita, K., Böhringer, H., Takahashi, I., Ikebe, Y., 2005, A&A, in press

[41] Mushotzky, R. F., Loewenstein, M., 1997, ApJ, 481, L63

[42] Narayan R., Medvedev M. V., 2001, ApJ, 562, L129

[43] Peterson J. R., Kahn S. M., Paerels F. B. S., Kaastra J. S., Tamura T., Bleeker J. A. M., Ferrigno C., Jernigan J. G., 2003, ApJ, 590, 207

[44] Renzini A., Ciotti L., D'Ercole A., Pellegrini S., 1993,ApJ, 419, 52

[45] Rephaeli, Y., 1978, ApJ, 225, 335

[46] Sanders J. S., Fabian A. C., Allen S. W., Schmidt R. W., 2004, MNRAS, 349, 952

[47] Schmidt, R.W., Fabian, A.C., Sanders, J.S., 2002, MNRAS, 337, 71

[48] Schombert J. M., 1987, ApJSS, 64, 643

[49] Schombert J. M., 1988, ApJ 328 475

[50] Toniazzo T., Schindler S., 2001, MNRAS, 325, 509

[51] Tozzi P., Rosati P., Ettori S., Borgani S., Mainieri V., Norman C. 2003, ApJ, 593, 705

[52] Voigt L. M., Fabian A. C. 2004, MNRAS, 347, 1130

3

Effect of turbulent diffusion on iron abundance profiles

P.Rebusco, E.Churazov, H.Böhringer & W.Forman

Abstract

We compare the observed peaked iron abundance profiles for a small sample of groups and clusters with the predictions of a simple model involving the metal ejection from the brightest galaxy and the subsequent diffusion of metals by stochastic gas motions. Extending the analysis of Rebusco et al. (2005) we found that for 5 out of 8 objects in the sample an effective diffusion coefficient of the order of 10^{29} cm^2 s^{-1} is needed. For AWM4, Centaurus and AWM7 the results are different suggesting substantial intermittence in the process of metal spreading across the cluster. There is no obvious dependence of the diffusion coefficient on the mass of the system.

We also estimated the characteristic velocities and the spatial scales of the gas motions needed to balance the cooling losses by the dissipation of the same gas motions. A comparison of the derived spatial scales and the sizes of observed radio bubbles inflated in the ICM by a central active galactic nucleus (AGN) suggests that the AGN/ICM interaction makes an important (if not a dominant) contribution to the gas motions in the cluster cores.

Keywords:clusters:individual-galaxies:abundances -turbulence- cooling flows-diffusion

3.1 Introduction

X-ray spectroscopy is widely used to determine the metallicity of the hot gas in galaxy clusters and groups. Using the high energy resolution of ASCA, *BeppoSAX*, *Chandra* and *XMM-Newton* the radial profiles of Fe, S, Si, Ca and other elements (e.g Buote et al. 2003b, Sanderson et al. 2003, Sun et al. 2003, Matsushita, Finoguenov & Böhringer 2002, Gastaldello& Molendi 2002, O'Sullivan et al. 2005, Fukazawa 1994, Tamura et al. 2001) have been derived for a sample of objects. Outside the cluster core regions the metallicity of the intracluster medium (ICM) is on average one-third of the solar one and it does not seem to evolve up to a redshift of about 1 (e.g Mushotzky & Loewenstein 1997, Tozzi et al. 2003). This suggests an early enrichment by Type II supernovae (SNII; e.g. Finoguenov et al. 2002). The metallicities in the core regions demonstrate much more diversity. For the so-called 'non-cooling flow' clusters the metallicity and the surface brightness do not vary strongly across the core region. For another group of so-called 'cooling flow' clusters, the metallicity and the surface brightness are both strongly peaked at the center. The clusters from the latter group always have a very bright galaxy (BG) dwelling in their centers, which makes these galaxies a prime candidate for producing the peaked abundance profiles. These peaked profiles were likely formed well after the cluster/group was assembled (e.g. Böhringer et al. 2004; De Grandi et al. 2004). The relative abundances of different elements indicate that Type Ia supernovae (SNIa) explosions and stellar winds within the BG have played a major role in the formation of the central abundance excesses (e.g. Renzini et al. 1993, Finoguenov et al. 2002). If the metals in the ICM are due to the galaxy stars then one would expect the abundance profiles to follow the BG light profile. However the observed metal profiles are much less steep than the light profiles, suggesting that there must be a mixing of the injected metals, a process which may help to diffuse them to larger radii (e.g.Churazov et al. 2003, Rebusco et al. 2005, Chandran 2005). Stochastic gas motions could provide such a mechanism of spreading metals through the ICM, provided that the characteristic velocities and the spatial scales are of the right order. Furthermore, the dissipation of the kinetic energy of the same gas motions could be an important source of energy for the rapidly cooling gas in the "cooling flow" clusters.

In Rebusco et al. 2005 we estimated the parameters (velocity and length scale) of stochastic gas motions in the core of Perseus cluster (A426) required to spread the metals ejected from the central galaxy. We found that a diffusion coefficient of the order of 2×10^{29} cm^2 s^{-1} is needed to explain the observed abundance profile and that for turbulent velocities of about 300 km s^{-1} and eddies sizes of about 20 kpc the dissipation of turbulent motions compensates

Name	kT	z
NGC 5044	1	0.0082
NGC 1550	1.37	0.0124
M87	2.2	0.0044
AWM4	2.3	0.0319
Centaurus	3.5	0.0107
AWM7	3.7	0.0176
A1795	6	0.0639
Perseus	6.3	0.0179

Table 3.1: The sample: (1) name of the cluster , (2) mean ICM temperature in keV, (3) redshift.

for the gas cooling losses. We now extend the same model to a small sample of clusters and groups. The sources we analyzed have mean temperatures which vary by a factor of ~ 6.

The structure of the paper is the following. In section 3.2 we describe the sample of clusters and groups; in section 3.3 the structure and the ingredients of the stochastic diffusion model are described. The results are discussed in section 3.4. The last section summarizes our findings.
We adopt a Hubble constant of $H_0 = 70$ km s^{-1} Mpc^{-1}, $\Omega_M = 0.3$ and $\Omega_\Lambda = 0.7$.

3.2 The Sample

We have selected a small sample of nearby "cooling flow" clusters and groups ($z < 0.07$) having a sufficiently detailed information on the abundance distributions in the core regions. To test for any obvious trend with the mass of the cluster, we selected the objects having the mean temperature ranging from 1 to 6 keV (see Table 3.1).

3.2.1 NGC 5044 Group

The NGC 5044 group of galaxies is relatively cool and loose. It is formed by a central luminous giant elliptical surrounded by about 160 galaxies, $\sim 80\%$ of which are dwarfs (Ferguson & Sandage 1990). There is evidence for multiple temperature gas components, that coexist within ~ 30 kpc. It is likely that the central heating is due to the presence of a central AGN (e.g. Buote et al. 2003). The X-ray emission is quite symmetric, indicating that there have not been recent strong mergers (David et al. 1994).

3.2.2 NGC 1550 Group

This luminous group is more relaxed than other bright low temperature ones (e.g. NGC 5044). The BG is a lenticular galaxy and it is almost isolated in the optical band (Garcia 1993).
Sun et al. (2003) suggest that NGC 1550 entropy profile shows signs of non-gravitational heating (e.g. a recent outburst). Moreover they point out the large role of the central galaxy in affecting the surrounding gas temperature. If this is the case, then the same nongravitational processes may help to distribute the metals within the group core.

3.2.3 M87 Galaxy

M87 is the dominant central galaxy in the Virgo Cluster. Because M87 is very close and bright it was used to study the role of SNIa and SNII in enriching the ICM (e.g. Gastaldello & Molendi 2002, Matsushita et al. 2003, Finoguenov et al. 2002).

There is clear dynamical evidence of the presence of a supermassive black hole in its core (e.g. Macchetto et al. 1997), with a one-sided jet (e.g. Schreier et al.1982, Owen et al. 1989, Sparks et al. 1996). At least two gas components with different temperatures are observed: the hotter component is almost symmetric around the central galaxy (Matsushita et al. 2002), while the cooler component forms extended structures correlated with the radio lobes. There are clear signs of an AGN/ICM interaction in this source both through the shocks and sound waves (Forman et al. 2005, 2006) and through mechanical entrainment of the cool gas by the bubbles of relativistic plasma (Churazov et al. 2001).

3.2.4 AWM4 Cluster

This poor relaxed cluster consists of 28 galaxies centered at the dominant elliptical NGC 6051 (Koranyi & Geller 2002). The cluster's stellar component is comparable with that of M87 and NGC 5044, but the iron abundance profile is flatter than in these sources and there is no evidence for multiphase gas (O'Sullivan et al. 2005). The density is not strongly peaked at the center and no strong temperature drop is seen. While it is not a prominent cooling flow cluster, it does contain a single cD galaxy and we include this cluster to see what will be the outcome of the analysis applied to this object.

The central galaxy hosts a powerful AGN (4C +24.36) which could be driving the gas motions in this cluster.
O'Sullivan et al. (2005) assert that in AWM4 there might be global motions

of the galaxies in the plane of the sky: these galaxy motions could contribute in spreading the metals.

3.2.5 Centaurus Cluster

Centaurus is the third nearest bright cluster (after Perseus and Virgo). The asymmetric X-ray structure around the central cD galaxy (NGC 4696) gives evidence for dynamical activity (e.g. Allen & Fabian 1994). This cluster is very interesting because it houses the most prominent abundance peak known (e.g. Fabian et al. 2005, Sanders & Fabian 2002, Ikebe et al. 1999). The analysis of the cool Hα filaments in its core indicates previous episodes of radio activity (Crawford et al. 2005). Fabian et al. 2005 and Graham et al. 2006 have recently calculated the effective diffusion coefficient in the picture of stochastic turbulence: we discuss our results in comparison to these earlier works in 3.4.2.

3.2.6 AWM7 Cluster

AWM7 is a poor bright cluster, part of the Perseus-Pisces super-cluster and centered about the dominant elliptical galaxy NGC 1129 (e.g. Neumann & Böhringer 1995). It is elliptically elongated in the east-west direction and it follows the general orientation of the Perseus-Pisces chain of galaxies (Neumann & Böhringer 1995). The 30 kpc shift of the X-ray peak from the optical peak indicates that AWM7 has a cD cluster in early stage of evolution (Furusho et al. 2003). The determination of the effective radius of NGC 1129 is quite controversial (see Table 3.2). This uncertainty does not affect our estimates, however.

3.2.7 A1795 Cluster

This compact and rich cluster is believed to being dynamically relaxed (e.g. Tamura et al.2001). On the other hand Ettori et al.(2002) suggest that the core has an unrelaxed nature, consistent with the detected motion of the central cD galaxy MCG +5-33-5 (Oegerle & Hill 1994, Fabian et al. 1994, Markevitch et al. 1998). There is a strong cooling flow in this cluster with a substantial temperature drop and a strong density peak in the core (e.g. Briel & Henry 1996, Allen et al. 2001).

3.2.8 Perseus Cluster

Perseus (A 426) is the brightest nearby X-ray cluster and it is one of the best-studied cases of cool core clusters, together with M87 and Centaurus. Its

central elliptical galaxy (NGC 1275) dominates in the optical light up to a distance of ~ 100 kpc. It hosts a moderately powerful radio source, 3C 84 (Pedlar et al. 1990). In the core region there is a complex substructure in the temperature and surface brightness distributions including depressions in surface brightness due to rising bubbles of relativistic plasma (Churazov et al., 2000, Fabian et al. 2000) and quasi-spherical ripples (Fabian et al. 2003a, 2006). Optical Hα filaments, whose origin is not well understood, seem to be drawn up by the rising bubbles (Fabian et al. 2003b, Hatch et al. 2005).

3.3 The model

The model is essentially the same used in Rebusco et al. (2005). For completeness we reproduce its main features below.

3.3.1 Diffusion of metals due to stochastic gas motions

We assume a static gas distribution in the gravitational potential of the cluster. The gas density and temperature distributions are known and assumed to be not evolving with time. We then suppose that the gas is involved in stochastic motions which do not affect the density and temperature distributions on time scales much longer than the time scales associated with the gas motions, but only spread the metals through the ICM. Due to such motions, the metals injected in the center of the cluster will be spread out off the center. We treat this process in the diffusion approximation:

$$\frac{\partial na}{\partial t} = \nabla \cdot (Dn\nabla a) + S, \tag{3.1}$$

where $n = n(r)$ is the gas density, $a = a(r,t)$ is the iron abundance and $S = S(r,t)$ is the source term due to the iron injection from the BG. D is the diffusion coefficient, of the order of $\sim \frac{vl}{3}$, with v being the characteristic velocity of the stochastic gas motions and l their characteristic length scale. Once the diffusion coefficient is specified, eq.3.1 can be integrated. In what follows we considered constant diffusion coefficients: the effect of having a diffusion coefficient as a function of radius is discussed in Rebusco et al. (2005).

3.3.2 Adopted light, gas density and metal abundance profiles

We list the parameters of the adopted profiles in Table 3.2: we used the existing analytical approximations (when available) or made our own fits to the original data (all the references used are given in the Table).

The light distribution of the central cD galaxies is modeled here by a simple Hernquist profile (Hernquist 1990): this is an acceptable approximation for the purpose of this study. For each source we compared the light distribution of the BG with the light distribution due to all the other gala

xies excluding the BG. The brightest galaxy dominates up to a distance of $\sim$ 100-150 kpc, hence in the calculations we assume (unless explicitly stated otherwise) that the central excess of metals is produced by the central galaxy alone.

The iron abundance profile is approximated with a simple β-profile: $a(r) = a(0) \left[1 + (r/r_a)^2\right]^{-b}$, where $a_\odot$ is the solar abundance (Anders & Grevesse 1989). The adopted functional form should work only in the central region, where the abundance excess is present. This form also neglects completely the central abundance "hole" observed in some sources (e.g. Schmidt et al. 2002, Böhringer et al. 2001). The nature of this abundance hole remains unexplained and it may be due to a not adequate modeling of the emission from the very central region rather than due to a real decrease of the metal abundance.

For the electron density profile we used a single β model again: $n_e(r) = n(0) \left[1 + (r/r_c)^2\right]^{-3/2\beta}$. The hydrogen number density is assumed to be related to the electron number density as $n_H = n_e/1.2$. In some cases (marked with an asterisk) a double β-profile is reported in the original papers: here we use the parameters of the component which provides the dominant contribution for the range of radii of interest. Only in the case of Centaurus the double profile have been used, because both the components are important. For Perseus cluster we adopted the same profiles as in Rebusco et al. (2005).

3.3.3 Iron enrichment

Much of the metals in the cluster ICM were produced at early times by SNII explosions. They are likely to be evenly distributed through the bulk of the ICM producing a uniformly enriched gas. The level of this uniform enrichment is uncertain - on average an iron abundance in the range 0.2–0.4 of the the solar value is reported. In the subsequent calculations we subtracted this "abundance basis" a_b in order to single out only the central abundance excess, which is believed to be formed later by the metal ejections from the BG alone (Matsushita et al. 2003, Böhringer et al. 2004, De Grandi et al. 2004). The assumed value of a_b is one of the main uncertainties in our model - for low values of a_b the central abundance excess becomes more extended and the mass of iron in the central excess grows substantially.

Ram-pressure stripping can also contribute to the enrichment of the ICM over a long period of cluster evolution. According to recent simulations (Do-

mainko et al. 2006) the cluster centers are enriched more strongly than the outer parts. It is not clear though how these results will be affected by the presence of cool and dense cores. Below we assume that ram pressure stripping produces broader abundance peaks than considered here and that the central abundance excess is solely due to the central galaxy.

We assume that the central abundance excess is due to the type Ia supernovae and the stellar mass loss by stars in the BG. Both channels inject gas enriched with heavy elements, in particular iron. Following Böhringer et al. (2004), the rates of iron injection by SNIa (eq. 3.2) and stellar mass loss (eq. 3.3) are:

$$
\left(\frac{dM_{Fe}}{dt}\right)_{SNIa} = SR \times 10^{-12} \left(\frac{L_B}{L_\odot^B}\right) \eta_{Fe} \tag{3.2}
$$

$$
= R(t)\,0.105 \times 10^{-12} \left(\frac{L_B}{L_\odot^B}\right) M_\odot\ yr^{-1},
$$

$$
\left(\frac{dM_{Fe}}{dt}\right)_* = \gamma_{Fe} \times 2.5 \times 10^{-11} \left(\frac{t}{t_H}\right)^{-1.3} \tag{3.3}
$$

$$
\times \left(\frac{L_B}{L_\odot^B}\right) M_\odot\ yr^{-1},
$$

where SR is the present SNIa rate in SNU (1 SNU - rate of supernova explosions, corresponding to one SN event per century per galaxy with a blue luminosity of $10^{10}\ L_\odot^B$), $\eta_{Fe} = 0.7 M_\odot$ is the iron yield per SNIa, $\gamma_{Fe} = 2.8 \times 10^{-3}$ is the mean iron mass fraction in the stellar winds of an evolved stellar population, t_H is the Hubble time. The expression for the stellar mass loss was adopted from Ciotti et al. (1991), assuming a galactic age of 10 Gyr. The stellar mass loss contribution to the hydrogen content of the ICM can be neglected, as its effect is important only in the central $\sim 10 - 20$ kpc (see Fig. 3.1). The time dependent factor $R(t) = (t/t_H)^{(-k)}$ takes into account an increased SNIa rate in the past (Renzini et al. 1993), with the index k ranging from 1.1 up to 2. We assume a fiducial value for the present day SNIa rate of 0.15 SNU (Cappellaro, Evans, & Turatto 1999). Hence the total iron injection rate within a given radius r can be written as

$$
s(<r,t) = \left(\frac{dM_{Fe}}{dt}\right)_* + \left(\frac{dM_{Fe}}{dt}\right)_{SN} \propto \left(\frac{L_B(<r)}{L_\odot^B}\right) \tag{3.4}
$$

The procedure of evaluating the diffusion coefficient in equation (3.1) was as follows. First the value of a_b was specified and subtracted from the observed abundance profile. The iron mass in the remaining abundance excess was then calculated and compared with the total amount of iron produced by

the central galaxy during its evolution from some initial time to the present (by integrating equation 3.4 over time). This provides the constraints on the parameters of the enrichment model (SR, k, t_{age}) (see Rebusco et al. 2005 for an extended discussion). For each source we explored different models, with $a_b \in [0.2, 0.4]$, $k \in [1.1, 2]$ $SR \in [0.07, 0.34]$ and $t_{age} \in [5, 10]$. In particular, we fixed $a_b = 0.2, 0.3$ and 0.4; then for each abundance basis we found a sample of enrichment parameters: e.g. by setting $k = 1.1, 2$ and $SR = 0.15, 0.3$, and calculating the t_{age} necessary to get the right amount of iron excess, then by fixing SR and t_{age} and calculating k, finally by calculating SR from four combinations of k and t_{age}. A representative set of these models is listed in Table 3.4.

Equation (3.1) was then integrated over time from $t_H - t_{age}$ till now starting from a zero initial abundance. The resulting profiles were visually compared with the observed abundance peaks and the diffusion coefficient was adjusted so that the predicted and observed profiles would agree reasonably well (see Fig.3.1). In this figure for each object in the sample the dashed line shows the expected iron abundance due to the ejection of metals from the galaxy if no mixing is present. In most cases such profiles are far too steep than the observed abundance excesses (shown with a solid line). The dotted line in Fig.3.1 shows the expected profiles calculated for the same parameters of iron injection model, but with the additional effect of diffusion. The actual values of the diffusion coefficient used in each case are listed in Table 3.3. Clearly allowing for metal mixing leads to a reasonable agreement between the observed and the predicted abundance profiles.

3.3.4 Cooling and heating

As shown above the observed and predicted abundance profiles can agree reasonably well if the metals are allowed to diffuse through the ICM. Assuming that the diffusion coefficient derived above is due to stochastic gas motions, one can cast it in a form $D \sim C_1 v l$, where C_1 is a dimensionless constant of the order of unity, v is the characteristic velocity of the gas motions and l their characteristic length scale. Thus the above analysis provides an estimate of the product of v and l for each object.

3.3.4.1 Dissipation of turbulent motions

Here we further assume that the dissipation of turbulent motions is the dominant source of energy for the rapidly cooling gas in the cluster cores. As in Rebusco et al. 2005 we suppose that the dissipation rate is simply equal to the gas cooling rate $\Gamma_{diss} \sim \Gamma_{cool}$. The gas heating rate due to the dissipation of

the kinetic energy can be written as $\Gamma_{diss} \sim C_2 \rho v^3 / l$, where ρ is the gas density and C_2 is a dimensionless constant, while the cooling rate $\Gamma_{cool} = n^2 \Lambda(T)$ can be estimated from the observed gas temperature and density at any given radius.

This requirement of the cooling and heating losses provides a second constraint on the combination of v and l. Thus fixing the diffusion coefficient and the heating rate one can easily estimate v and l, that we intend as the characteristic sizes and velocities of quasi-continua intermittent vortexes.

Below we use the expressions for D and Γ_{diss} from Dennis & Chandran (2005) (see references therein):

$$D = C_1 v l \sim 0.11 v l \tag{3.5}$$

$$\Gamma_{diss} = C_2 \rho v^3 / l \sim 0.4 \rho v^3 / l. \tag{3.6}$$

To evaluate the heating rate for each object from the sample we use the gas parameters near $r_0 = r_{cool}/2$ (where r_{cool} is the radius at which the cooling time is comparable with the Hubble time). We then used D from Table 3.3 and set $\Gamma_{diss} = n^2 \Lambda(T)$, evaluated at r_0.

This approach of choosing $r_0 = r_{cool}/2$ implies that the cooling rates used will not be drastically different from source to source (as it would happen if for instance one uses a fixed value of r_0 for all the objects in the sample). The resulting constraints are shown in Fig. 3.2. The thick dot-dashed line shows the combinations of v and l which give the same diffusion coefficient, while the thin dot-dashed lines show the effect of varying C_1 by factor of $1/3$ and 3. The effect of varying C_2 by factor of $1/3$ and 3 was estimated in Rebusco et al. (2005). Along the the dotted line the dissipation rate is equal to the cooling rate at $r_0 = r_{cool}/2$; the dot-short dashed line is for $r_0 = r_{cool}$ and the long dashed for $r_0 = r_{cool}/4$. The intersection of the two bands gives the locus of the combinations of l and v such that on one hand the diffusion coefficient is approximately equal to the required value (Table 3.3) and on the other hand the dissipation rate is approximately equal to the cooling rate at $r_{cool}/2$.

3.3.4.2 Turbulent mixing vs turbulent dissipation

Since cluster atmospheres are characterized by positive gradient of the specific entropy, stochastic motions should also lead to the heat flow into the central region (e.g. Dennis & Chandran, 2004). Following their work we estimate the rate of heating due to the turbulent transport of high-specific-entropy gas into low-specific-entropy regions:

$$\Gamma_{tt} = \nabla \cdot (D \rho T_{gas} \nabla e), \tag{3.7}$$

(a) NGC 5044   (b) NGC 1550   (c) M87

(d) AWM4   (e) Centaurus   (f) AWM7

(g) A1795   (h) Perseus
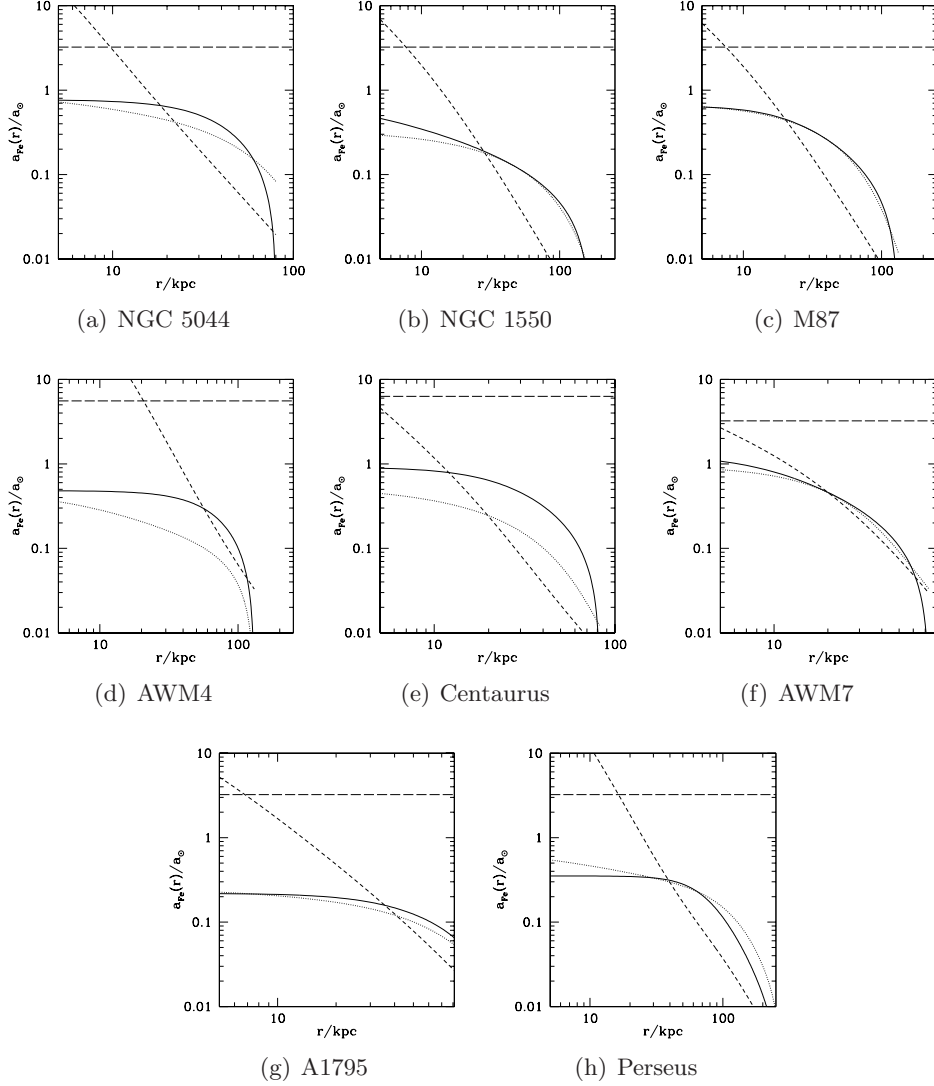
Figure 3.1: Comparison of the observed and the expected iron abundance profiles for each source: the set of enrichment parameters used are listed in Table 3.4. The solid line shows the abundance profile adopted in this paper, from which a constant value of a_b is subtracted. We assume that this central abundance excess is mainly due to the metal ejection of the central galaxy. For comparison we show the expected iron abundance (short dashed line) due to the ejection of metals from the galaxy. The expected profile was calculated assuming that the ejected metal distribution follows the optical light. In all the objects the expected abundance profile is much more peaked than the observed profile (due to the contribution of the central galaxy) suggesting that some mechanism is needed to spread the metals. The dotted line shows the profile derived with the same parameters of iron injection, but with the additional effect of diffusion. The long dashed line corresponds to the maximum abundance (it can be obtained from eq. 3.4), beyond which our approximation of neglecting the gas injection is not valid anymore.

62

(a) NGC 5044 (b) NGC 1550 (c) M87

(d) AWM4 (e) Centaurus (f) AWM7

(g) A1795 (h) Perseus
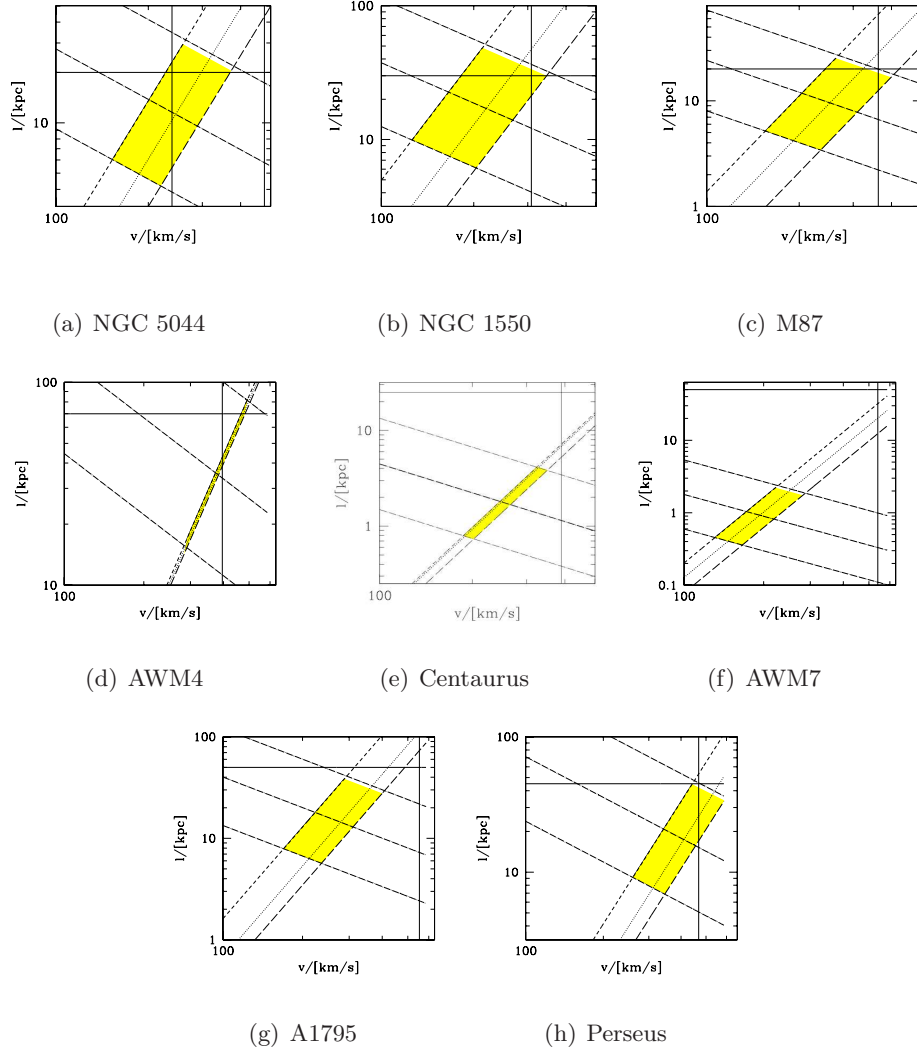
Figure 3.2: Range of the characteristic velocities v and spatial scales l of the gas motions which provide the necessary diffusion and dissipation rates. Along the thick dot-long dashed line the diffusion coefficient $D = C_1 vl$ is constant and equal to the values listed in Table 3.3, while the thin dot-long dashed lines show the effect of varying $C_1 = 0.11$ by factor of $1/3$ and 3. Along the the dotted line the dissipation rate is equal to the cooling rate at $r_0 = r_{cool}/2$; the dot-short dashed line is for $r_0 = r_{cool}$ and the long dashed for $r_0 = r_{cool}/4$. At the intersection of these bands, two conditions are satisfied: i) the gas cooling is balanced by the dissipation and ii) the diffusion coefficient is of the right order. The vertical solid lines show the sound speed in the gas c_s for $r = r_{cool}/2$ and half of it. In the plots where only one line is present, it corresponds to $c_s/2$.

Name	r_{eff}/kpc	$L_{TOT}/L_\odot^B$	r_a/kpc	$a(0)/a_\odot$	b	r_c/kpc	β	$n(0)10^{-3}/cm^3$
NGC 5044	10.05 [1]	4.510^{10} [1]	58.2 [2]	1.07	1.19	15 [3]	0.49	10.66
NGC 1550	9.1 [4]	3.510^{10} [5]	0.8 [4]	0.95	0.14	2.5 [4]	0.35	7
$M87^*$	7.8 [5]	5.310^{10}[21]	20 [7][8]	0.85	0.38	2 [6]	0.42	130
AWM4	20 [9]	5.510^{10} [10]	94	0.78 [11]	0.89	76 [3]	0.62	3.52
$Centaurus^*$	13 [9]	510^{10} [22]	25 [13]	1.31	0.48	7.7[14]	0.57	165
$AWM7^*$	42 [9] 16.6 [12]	1.410^{11} [15]	7.2 [16]	1.6	0.3	3.5 [17]	0.25	165
A1795	34[18]	210^{11}	2.7 [19]	0.51	0.21	17 [19][20]	0.4	50
Perseus	15	1.610^{11}	48	0.54	0.18	/	/	/

Table 3.2: Column (1) Name of the object (2)-(3) Effective radius and total blue luminosity of the central galaxy (4)-(5)-(6) Parameters of the iron abundance β-profile (7)-(8)-(9)Parameters of the gas density β-profile (see the text for the precise form). For the sources marked with ($*$) the best fit was a double β-model; here we report the parameters of the dominant one. References:[1]Buote et al. 2004[2]Buote et al. 2003[3] Sanderson et al. 2003[4] Sun et al. 2003[5] de Vaucouleurs et al. 1991 [6] Matsushita et al. 2002[7] Matsushita et al. 2003[8] Gastaldello & Molendi 2002[9] Schombert 1987[10] Finoguenov et al. 2001[11] O'Sullivan et al. 2005[12] Bacon et al. 1985 [13] Fukazawa 1994[14] Ikebe et al. 1999[15] Peletier et al. 1990[16] Furusho et al. 2003[17] Neumann & Böhringer 1995[18] Schombert 1988[19] Tamura et al. 2001[20] Ettori et al. 2002 [21] Arnaud et al. 1992[22] Laine et al. 2003.

where T_{gas} is the temperature and $e = C_V ln(c_s^2/\gamma\rho^{\gamma-1})$ is the specific entropy (adiabatic index $\gamma = 5/3$, specific heat at constant volume $C_V = 3k/2 \; n_H/\rho$).

First we consider the case of a diffusion coefficient independent of the radius. A typical example of Γ_{tt} radial dependence (NGC 5044), for the diffusion coefficients taken from Table 3.3, is shown in Fig. 3.3. While the heat flow is always towards the center, the volume heating rate Γ_{tt} is positive inside a certain radius and it becomes negative (i.e. cooling) in the outer regions. This is of course an expected result - for constant diffusion coefficient the heat flux $r^2 \, D \, \rho \, T_{gas} \frac{\partial e}{\partial r} \sim r \, \rho$ (see eq.3.7) and there is likely to be a radius near which this function is almost independent from the radius. As it is seen in Fig. 3.3 the turbulent transport (dotted line) calculated for $D = 9 \times 10^{28}$ cm^2 s^{-1} is an important source of heat in the innermost 10 kpc, but Γ_{tt} quickly declines with the radius. Obviously the diffusion coefficient has to increase with the radius if the turbulent heat transport Γ_{tt} balances the cooling over a broad range of radii. For comparison the heating rate due to the dissipation of turbulent motions Γ_{diss} (for the parameters taken from Table 3.3) is shown by the dashed line in Fig. 3.3. Note that the rate of dissipation is a very strong function of v and variations in v by a factor of 2 (for a fixed diffusion coefficient $\propto l \times v$) cause variations of Γ_{diss} by a factor of 16 (see Fig. 3.3).

Chandran (2005) considered convective motions in the cluster cores driven by the cosmic rays injected by a central AGN. In his two-fluid (thermal-plasma and cosmic-ray) mixing-length theory approach, the characteristic length and velocity scales are functions of the radius. Assuming that the turbulent heat transport is the dominant source of heat we calculated the diffusion coefficient $D_0(r)$ (needed to balance heating and cooling at every radius) by integrating the equation $\Gamma_{tt} = \Gamma_{cool}$ over the radius. The resulting diffusion coefficient linearly increases with the radius and it reaches the value of $D = 9 \times 10^{28}$cm^2 s^{-1} at $r \sim 5$ kpc. Such radially dependent diffusion coefficient produces progressively more and more efficient mixing with increasing distance and it leads to an abundance profile which drops to ~ 0.1 already at ~ 10 kpc (see Fig. 3.4).

We next assumed that $\Gamma_{diss} \approx \Gamma_{cool}$ at every radius and we calculated the quantity v^3/l as a function of the radius. We then considered several possibilities for the radial dependence of v and l and we derived the corresponding diffusion coefficients.

$$
\begin{aligned}
D_1(r) &= c_1 v l(r), & v &= \text{const} \\
D_2(r) &= c_1 v(r) l, & l &= \text{const} \\
D_3(r) &= c_1 v(r) l(r), & l(r) &= 0.3r.
\end{aligned}
\tag{3.8}
$$
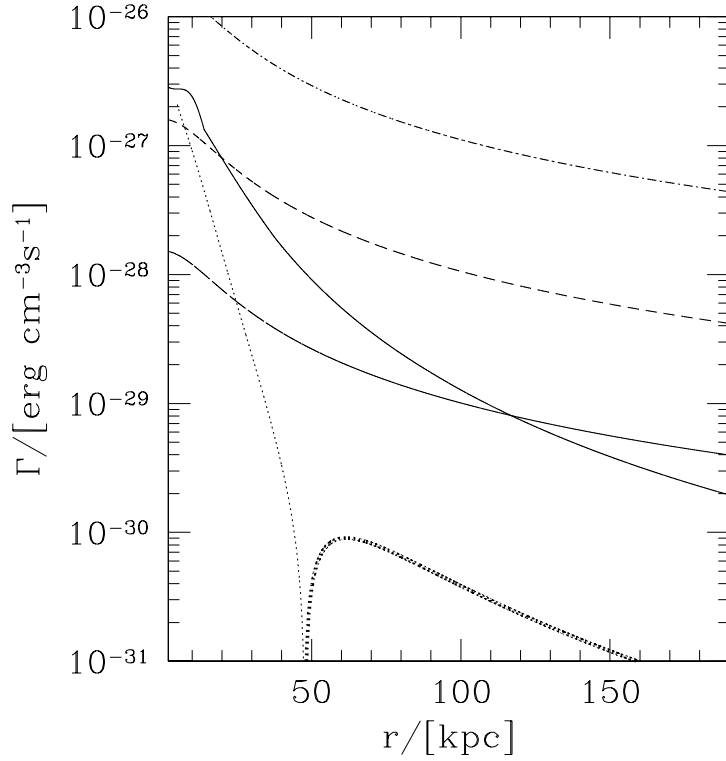
Figure 3.3: NGC 5044: the solid line shows the cooling rate as a function of radius; the dotted line is the heating rate Γ_{tt} evaluated for $D = 9 \times 10^{28} \mathrm{cm}^2\,\mathrm{s}^{-1}$: the thin line corresponds to the part where Γ_{tt} is positive, while the thick one is for $\Gamma_{tt} < 0$. The remaining lines represent the dissipation heating rate Γ_{diss} for the same D, but different velocity and length scales: $l = l_{ref} = 11$ kpc and $v = v_{ref} = 245$ km/s (short-dashed), $l = l_{ref}/1.8$ and $v = 1.8\,v_{ref}$ (dot-dashed), $l = 1.8\,l_{ref}$ and $v = v_{ref}/1.8$(dot-dashed). For the other sources, these plots show a similar qualitative behavior.

The choice of $l(r) \propto r$ for $D_3(r)$ is motivated by the work of Chandran (2005). For the first two models the constant v and l were fixed at the values taken from Table 3.3. The abundance profiles obtained by integrating equation 1 using these diffusion coefficients are shown in Fig. 3.4. The case of $D_2(r)$ (i.e. constant length scale l and variable velocity scale v) fits the observed profile the best, while the other versions of $D(r)$ yield profiles which strongly deviate from the observed one.

From these plots one can conclude that it is possible to construct a model with radially dependent velocity and length scales such that the abundance profiles are approximately reproduced and that the dissipation of turbulent

Figure 3.4: NGC 5044: in both plots the solid line represents the observed abundance profile from which the constant value $a_b = 0.3a_\odot$ is subtracted. The dotted line is for 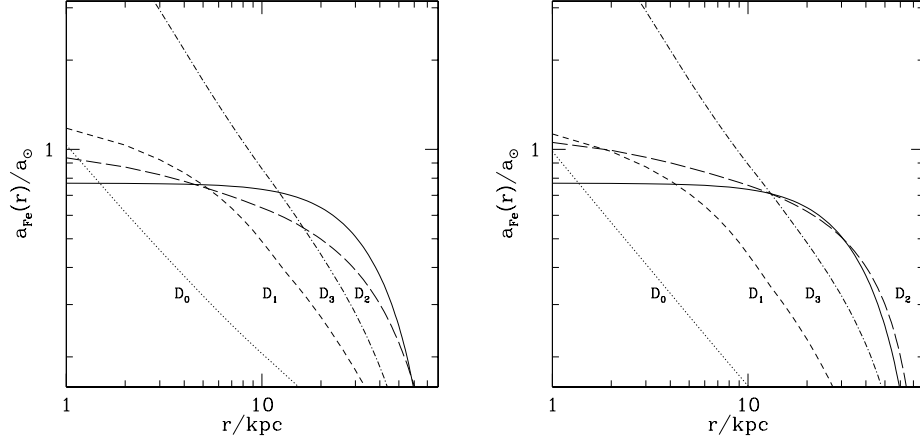$D = D_0(r)$, the short-dashed for $D = D_1(r)$, the long-dashed for $D = D_2(r)$ and the dotted-dashed for $D = D_3(r)$(see subsection 3.3.4.2 for an explanation): they show the expected abundances obtained according to equation 3.1, starting from a flat zero profile (left panel, $\tau_{age} = 5$ Gyr) and starting from the present-day profile (right panel, after 4 Gyr from now). For the other sources, these plots display a similar qualitative behavior.

motions compensates the gas cooling over a wide range of radii. In the simplest model of this type ($D_2(r)$ above) the length scale is independent of the radius and the velocity scale is a slowly decreasing function of the radius.

3.4 Results and their discussion

In Table 3.3 the estimated values of the diffusion coefficient D, the characteristic velocity v and the spatial length scale l are listed. The set of the parameters for the iron enrichment models (listed in Table 3.4, described in the Subsection 3.3.3) are chosen in order to get a reasonable approximation of the observed profiles (see Fig. 3.1): a factor of 3 smaller (or larger) diffusion coefficients produce too peaked (or too shallow) abundance profiles, inconsistent with the data.

For each source we made a consistency check evaluating the characteristic value of the diffusion coefficient by comparing the half mass radius of the observed central excess and the excesses produced by ejection and diffusion in the model. For small diffusion coefficients the metal distribution should follow the light distribution of the central galaxy (i.e. have the same effective

Name	$r_{cool}/2$ kpc	D cm^2 s^{-1}	l kpc	v km s^{-1}	v/c_s
NGC 5044	20	9×10^{28}	11	245	0.51
NGC 1550	30	1.2×10^{29}	17	219	0.35
M87	20	8×10^{28}	10	250	0.34
AWM4	70	4.5×10^{29}	35	378	0.45
Centaurus	25	2×10^{28}	2	250	0.30
AWM7	50	6×10^{27}	1	193	0.18
A1795	50	1.3×10^{29}	14	278	0.25
Perseus	45	2.4×10^{29}	17	410	0.44

Table 3.3: Estimate of the turbulence parameters for each source in our sample: name (1), half the cooling radius (2), diffusion coefficient (3), length scale (4) and velocity (5-6) of the gas motion.

radius), while for the increasing diffusion coefficient the effective radius should also increase. The values derived this way were consistent with those given in Table 3.3.

We then used the observed abundance peaks in each object as initial conditions and we calculated the subsequent evolution of the abundance profiles by fixing D at the value from Table 3.3. In each case 3 times smaller (or larger) diffusion coefficient causes a quick steepening (or flattening) of the abundance peaks on time scales of a Gyr, while for diffusion coefficients of the order of those listed in Table 3.3 the evolution is very slow on these time scales.

The diffusion coefficients listed in Table 3.3 are mostly of the order of 10^{29} cm^2 s^{-1}, apart from those obtained for AWM4, Centaurus and AWM7 (see next subsections). These values can be considered as an an upper limit on the effective diffusion coefficient set by the random gas motions, since other processes may contribute to spreading the metals through the ICM.

Note that our simple model predicts the abundance to be the highest in the center of the cluster. Thus the abundance "hole" observed in several well studied clusters (e.g. Böhringer et al. 2001, Schmidt et al. 2002) contradicts this conclusion. Potentially there are several explanations of the abundance hole. The simplest one supposes that the spectral models used for the abundance determination are not adequate for the central region, where a complicated mixture of different phases is present (e.g. Buote 2000). The resonant scattering and the diffusion of the line photons to larger radii is another possible explanation (e.g. Gilfanov et al. 1987, Molendi et al. 1998). However the model advocated here assumes that the gas in the center is not at rest, but it is involved in complex pattern of motions, which should reduce the effective optical depth (e.g. Churazov et al. 2004). Velocities of order the of few

hundred km/s should make most of the lines optically thin. Less straight-forward interpretations of the abundance hole are also possible, but they are beyond the scope of this paper. Future high energy resolution observations with micro-calorimeters should be able to resolve this question.

The sizes of the turbulent eddies obtained in this work are of the order of 10 kpc and the characteristic velocities of the order of few 100 km/s. In our model the velocity scale is determined from the combination of two quantities $D \sim vl$ and $\Gamma_{diss} \sim v^3/l$: $v \sim (D \, \Gamma_{diss})^{(1/4)}$. As a result the estimates of v come out very similar for all the objects, while l spans over a larger interval, compensating for all the peculiarities. We stress that these estimates have to be taken with caution, due to the simplicity of the model and the to uncertainties in the enrichment process.

3.4.1 AWM4

This object is not a cooling flow cluster, unlike the other objects in the sample. It does contain however a central bright galaxy (NGC 6051) which should enrich the ICM with metals in the same way as in cooling flow clusters. The enrichment will be even more efficient in AWM4 because the gas density is relatively small and even a modest amount of metals should produce a prominent abundance peak. As one can see from Table 3.3 the diffusion coefficient required to explain the lack of such abundance peak in AWM4 is larger than for any other objects in the sample. The length scale is also the largest in the sample. This can be easily understood since in this source a large value of the diffusion coefficient is needed along with a modest heating rate. As it is clear from eq.(3.5) and (3.6) this can be most naturally done by setting a large value of the gas motions spatial scale l.

If we would like to stay within the frames of our model then this is the object with the strongest level of gas mixing. There is a powerful radio source in NGC 6051 which clearly interacts with the ICM (e.g. O'Sullivan et al. 2005). It is not obvious however if the central AGN alone is responsible for the gas mixing and for the appearance of AWM4 as a non-cooling flow cluster. The alternative would be a recent merger followed by an intensive mixing of the ICM, but this case seems to be excluded by observations (O'Sullivan et al. 2005).

3.4.2 Centaurus

The Centaurus cluster has a central abundance peak which is difficult to reproduce with the enrichment model presented above. In order to produce such a large amount of iron in the central excess of this cluster, a long ac-

cumulation time (of the order of 10 Gyr) and a high SNIa explosion rate are necessary (see Table 3.3). With these parameters we get a diffusion coefficient of $\sim 1.5 \times 10^{28}$ cm^2 s^{-1}.

A previous estimate by Fabian et al. (2005) obtains that the diffusion coefficient in Centaurus is lower than 6×10^{28} cm^2 s^{-1}, consistently with our findings. Our result is also consistent (within the uncertainties of the profiles) with the value found by Graham et al. (2005). Since Graham et al. (2005) use higher blue luminosity for the central galaxy, their choice of enrichment parameters is less extreme than our. They also adopted higher value of the central abundance peak ($a_0 \sim 2a_\odot$), derived from fitting the spectra with a cooling flow model, while our lower central abundance ($a_0 \sim 1.3a_\odot$) is based on the two-temperature fits by Sanders & Fabian (2002). For their choice of parameters supersonic velocities are required to satisfy the equations (3.5) and (3.6). For lower luminosity (see Table 3.2), subsonic solutions are possible. However the results for Centaurus cluster remain quite controversial.

One plausible explanation of the extremely steep abundance gradient in Centaurus is the recent disturbance of the gas in the cluster core. "Cold fronts" are observed in many clusters with cool cores (e.g. Markevitch et al. 2000). These features are believed to form when the gas sloshing in the potential well brings layers of gas with different entropies in close contact: in a similar fashion layers of gas with different abundances can form a transient feature characterized by a steep abundance gradient. In the frame of the model discussed here any steep abundance gradient translates into strong limits on the diffusion coefficient.

3.4.3 AWM7

Taking the results of our analysis at face value, this cluster does not require strong stochastic motions to match the observed and predicted abundance profiles. There is also no evidence for a strong radio source in it(e.g. Furusho et al. 2003). From this point of view it is tempting to conclude that AWM7 is now passively cooling and that the activity of the central AGN is only about to start (in another cooling time $\sim 7 \times 10^8$ years). Then our estimate of the velocity and the length scale based on the assumption of a balance of the gas cooling would overestimate the combination v^3/l and underestimate l. Note however that Furusho et al. (2003) reported an unusual substructure in the metal distribution in the AWM7 core, which is at odds with the assumption that gas motions are almost absent in this cluster. Given that in several clusters an abundance hole is observed it is possible that the substructure in AWM7 has a similar nature.

3.4.4 Radio bubbles and stochastic gas motions

Vazza et al. (2006) simulated non-cooling flow clusters, finding that the energy due to turbulent bulk motions scales with the mass of the cluster: similar calculations had been done by Bryan & Norman (1998). In these simulations the turbulence is a result of the cluster formation, while in the core of CF clusters one can expect that the AGN is playing a dominant role in driving the turbulence: as a consequence the mass scaling of the two processes may be different.

Allen et al. (2006) found recently a tight correlation between the estimates of the Bondi accretion rate on to the central black hole and the jet power (estimated from the observed expanding bubbles) in X-ray luminous elliptical galaxies (similar calculations have been previously done by Di Matteo et al. 2001, Churazov et al. 2002 for M87 and by Taylor et al. 2006 for NGC 4696). At the same time the comparison of the jet powers and the cooling rates (e.g. Bîrzan et al. 2005) also shows a reasonable agreement. These results suggest that the amount of energy provided by jets (in the from of bubbles of relativistic plasma) is regulated by the gas properties in such a way that the gas cooling is approximately compensated. One can compare the rough estimates of the turbulence length scales (of the order of few - few tens kpc , see Table 3.3) with the observed sizes of radio bubbles in cluster cores (e.g. Dunn & Fabian 2004, Dunn, Fabian & Taylor 2005, Churazov et al. 2001). Broadly the numbers are of the same order. E.g. the observed radio bubbles sizes in M87 vary from ~ 1 to ~ 10 kpc (depending if one refers to the inner lobes or to the torus-like eastern or the outer southern cavities). In the Perseus, A1795 and Centaurus clusters the observed bubbles sizes also fall in the range few - few tens kpc. The characteristic velocities of the bubbles motions are of the order of $\sim 0.5c_s$ and they are also broadly consistent with the values listed in Table 3.3. From this point of view the observed bubbles seem to have all the necessary characteristics required to drive the gas motions needed to spread the metals.

3.5 Conclusions

We show that the iron abundance profiles observed in a small sample of nearby clusters and groups with cool core are consistent with the assumption that metals are spreading through the ICM with effective diffusion coefficients of the order of 10^{29}cm^2 s^{-1}. This value does not show any obvious trend with the mass or the ICM temperature of the system.

For characteristic velocities of the order of 300 km/s and length scales of the order of 10 kpc, the dissipation of the gas motions would approximately

balance the gas cooling. When observations are available, our estimates of the turbulent length scales are consistent with the observed buoyant bubbles size, pointing at the central supermassive black hole as the likely origin of the core gas motions.

Two objects in our sample require very different diffusion coefficients: for AWM7 very small level of gas mixing is needed, while for AWM4 the mixing has to be very intense. It is possible that these two objects hint to the intermittence of the gas mixing and that they represent two different episodes of the cluster evolution: AWM7 is only weakly disturbed now (but it will likely be disturbed soon by the onset of AGN activity), while AWM4 has been already mixed recently. O'Sullivan et al. 2005, using the analogy with M87 (where an abundance gradient is present in spite of clear signs of a radio jets interaction with the ICM) suggested that it is unlikely that AGN activity is responsible for the absence of the abundance peak in AWM4. One cannot however completely exclude the possibility that in the past there was a period of truly violent AGN activity in AWM4, which not only removed the central abundance peak, but also destroyed the whole cooling flow.

Acknowledgments

Name	$a_b/a_\odot$	$M_{Fe}/M_\odot \times 10^8$	r_m/kpc	k	SR/SNU	t_{age}/Gyr	$D/[cm^2/s] \times 10^{28}$
NGC 5044	0.2	1.5	42	1.1	0.26	8	12.2*
	# 0.3	0.5	36	1.1	0.15	5	8.7
	0.4	0.8	31	2	0.06	8	9
NGC 1550	# 0.3	0.8	67	1.1	0.15	7.6	12.6*
M87	# 0.2	0.9	46	1.1	0.15	6.2	8.3
	0.3	0.8	29	1.1	0.24	5	8.8
AWM4	# 0.2	7.2	83	2	0.33	10	45
	0.3	3.8	64	1.1	0.34	10	37.5
	0.4	1.9	55	2	0.30	6.4	25*
Centaurus	# 0.3	6.0	47	2	0.33	10	2*
	0.4	3.6	37	1.1	0.39	10	1*
AWM7	# 0.3	7.6	50	1.7	0.15	10	0.6*
	0.4	3.4	32	1.1	0.15	8.7	0.5
A1795	0.2	16	140	2	0.30	8.4	36
	# 0.3	2.9	62	1.1	0.15	5.4	12.5

Table 3.4: Enrichment models:column (1) Name of the object (2) Total iron excess; the hash indicates the model that was used to produce the plots in Fig. 3.1 and 3.2 (3) Half mass radius (4) k (5) Present-day SNIa rate (6) Source lifetime (For the definitions see the text)-(7) Effective diffusion coefficient: the models marked with the asterisk have an uncertainty due to the choice of the criterion to fix D of a factor $\%/ \times 2$, while for the other models the uncertainty is smaller.

Bibliography

[1] Allen S. W., Fabian A. C., 1994, MNRAS, 269, 409

[2] Allen S. W., Fabian A. C., Johnstone R. M., Arnaud K. A., Nulsen P. E. J., 2001, MNRAS, 322, 589

[3] Allen A. W., Dunn R. J. H., Fabian A. C., Taylor G. B., Reynolds C. S., 2006, MNRAS (astro-ph/0602549)

[4] Anders E., Grevesse N., 1989, Geochimica et Cosmochimica Acta, 53, 197

[5] Arnaud M., Rothenflug R., Boulade O., Vigroux L., Vangioni-Flam E., 1992, A&A, 254, 49

[6] Bîrzan L., Rafferty D. A., McNamara B. R., Wise M. W., Nulsen P. E. J., 2004, ApJ, 607, 800

[7] Bacon R., Monnet G., Simien F., 1985, A&A, 152, 315

[8] Beuing J.,Döbereiner, Böhringer H., Bender R., 1999, MNRAS, 302, 209

[9] Böhringer, H., Belsole, E., Kennea, J., et al., 2001, A&A, 365, L18

[10] Böhringer H., Matsushita K., Churazov E., Finoguenov A., Ikebe Y., 2004, A&A, 416, 21

[11] Briel U. G., Henry J. P., 1996, ApJ, 472, 131

[12] Bryan G. L., Norman M. L., 1998, ApJ, 495, 80

[13] Buote D. A., 2000, MNRAS, 311, 176

[14] Buote D. A., Lewis A. D., Brighenti F., Mathews W. G., 2003a, ApJ, 594, 741

[15] Buote D. A., Lewis A. D., Brighenti F., Mathews W. G., 2003b, ApJ, 595, 151

[16] Buote D. A., Brighenti F., Mathews W. G., 2004, ApJ, 607, L91

[17] Cappellaro E., Evans R., Turatto M., 1999, A&A, 351, 459

[18] Chandran B.D.G., 2005, ApJ, 632, 809

[19] Condon J. J. et al., 1998, AJ, 115, 1693

[20] Churazov E., Forman W., Jones C., Böhringer H., 2000, A&A, 356, 788

[21] Churazov E., Brüggen M., Kaiser C. R., Böhringer H., Forman W., 2001, ApJ, 554, 261

[22] Churazov E., Sunyaev R., Forman W., Böhringer H., 2002, MNRAS, 332, 729

[23] Churazov E.,Forman W., Jones C., Böhringer H., 2003, ApJ, 590, 225

[24] Churazov E., Forman W., Jones C., Sunyaev R., Böhringer H., 2004, MNRAS, 347, 29

[25] Ciotti L.,D'Ercole A., Pellegrini S., Renzini A., 1991, ApJ 376 380

[26] Crawford C. S., Hatch N. A., Fabian A. C., Sanders J. S., 2005, MNRAS, 363, 216

[27] David L. P., Jones C., Forman W., Daines S., 1994, ApJ, 428, 544

[28] De Grandi S., Ettori S., Longhetti M. Molendi S., 2004, A&A, 419, 7

[29] De Vaucouleurs G., De Vaucouleurs A., Corwin H. G., Buta R. J. Jr, Paturel G., Foqué P., 1991, Third Reference Catalogue of Bright Galaxies vol. II (Springer-Verlag)

[30] Dennis, T., Chandran, B., 2004, AAS, 36, 1592

[31] Dennis, T., Chandran, B., 2005, ApJ, 622, 205

[32] Di Matteo T., Johnstone R. M., Allen S. W., Fabian A. C., 2001, ApJ, 550, L19

[33] Domainko W. et al., 2006, A&A (astro-ph 0507605)

[34] Dunn R.J.H., Fabian A.C., 2004, MNRAS, 355, 862

[35] Dunn R. J. H., Fabian A. C., Taylor G. B., 2005, MNRAS, 364, 1343

[36] Ettori S., Fabian A. C., Allen S. W., Johnstone R. M., 2002, MNRAS, 331, 635

[37] Fabian A. C., Arnaud K. A., Bautz M. W., Tawara Y., 1994, ApJ, 436, L63

[38] Fabian A. C. et al., 2000, MNRAS, 318, L65

[39] Fabian A. C., Celotti A., Blundell K. M., Kassim N. E., Perley R. A., 2002, MNRAS, 331, 369

[40] Fabian A. C., Sanders J. S., Allen S. W., Crawford C. S., Iwasawa K., Johnstone R. M., Schmidt R. W., Taylor G. B., 2003a, MNRAS, 344, L43

[41] Fabian A. C. et al., 2003b, MNRAS, 344, L48

[42] Fabian A. C., Sanders J. S., Taylor G. B., Allen S. W., 2005, MNRAS, 360, L20

[43] Ferguson H. C., & Sandage A., 1990, AJ, 100, 1

[44] Finoguenov A., David L. P., Ponman T. J., 2000, ApJ, 544, 188

[45] Finoguenov A., Arnaud M., David L. P., 2001, ApJ, 555, 191

[46] Finoguenov A., Matsushita K., Böhringer H., Ikebe Y., Arnaud M., 2002, A&A, 381, 21

[15] Forman W. et al., 2005, ApJ, 635, 894

[48] Fukazawa Y., 1994, PASJ, 46, L55

[49] Furusho T., Yamasaki N.Y., Ohashi T., 2003, ApJ, 596, 181

[50] Gastaldello F., Molendi S., 2002, ApJ, 572, 160

[gil87] Gilfanov M. R., Sunyaev R.A., Churazov E., 1987, SvAL, 13, 3

[52] Graham J., Fabian A. C., Sanders J. S., Morris R. G., 2005, MNRAS (astro-ph/0602466)

[53] hat05 Hatch N. A., Crawford C. S., Johnstone R. M., Fabian A. C., 2005, MNRAS (astro-ph/0512331)

[54] Hernquist L., 1990, ApJ, 356, 359

[55] Ikebe Y. et al., 1999, ApJ, 525, 581

[56] Jerjen H., Dressler A., 1997, A&ASS, 124, 1

[57] Kaastra J. S. et al., 2004, A&A, 413, 415

[58] Kawaharada et al., 2003, PASJ, 55, 573

[59] Koranyi D. M., Geller M. J., 2002, AJ, 123, 100

[60] Laine S. et al., 2003, AJ, 125, 478

[61] Macchetto F. et al., 1997, ApJ, 489, 579

[62] Markevitch M., Forman W., Sarazin C. L., Vikhlinin A., 1998, ApJ, 503, 77

[63] Markevitch M., 2000, ApJ, 541, 542

[64] Matsushita K., Belsole E., Finoguenov A., Böhringer H., 2002, A&A, 386, 77

[65] Matsushita K., Finoguenov A., Böhringer H., 2003, A&A, 401, 443

[66] Molendi S. et al., 1998, ApJ, 499, 608

[67] Mushotzky, R. F., Loewenstein, M., 1997, ApJ, 481, L63

[68] Narayan R., Medvedev M. V., 2001, ApJ, 562, L129

[69] Neumann M. et al., 1994, A&ASS 106, 303

[70] Neumann D.M., Böhringer H., 1995, A&A, 301, 865

[71] Nevalainen J., Markevitch M. & Forman W., 2000, ApJ, 532, 694

[72] Oegerle W. R., Hill J. M., 1994, AJ, 107, 857

[73] Owen F. N., Hardee P. E., Cornwell T. J., 1989, ApJ, 340, 698

[74] Owen F. N., Eilek J. A., Kassim N E., 2000, ApJ, 543, 611

[75] O'Sullivan E., Vrtilek J. M., Kempner J. C., David L. P., Houck J. C., 2005, MNRAS, 357, 1134

[76] Peletier R. F., Davies R. L., Illingworth G. D., Davis L. E., Cawson M., 1990, AJ 100, 1091

[77] Pedlar A. et al. 1990, MNRAS, 246, 477

[78] Peres C. B. et al., 1998, MNRAS, 298, 416

78

[79] Peterson J. R., Kahn S. M., Paerels F. B. S., Kaastra J. S., Tamura T., Bleeker J. A. M., Ferrigno C., Jernigan J. G., 2003, ApJ, 590, 207

[80] Rebusco P., Churazov E., Böhringer H., Forman W., 2005, MNRAS, 359, 1041

[81] Renzini A., Ciotti L., D'Ercole A., Pellegrini S., 1993,ApJ, 419, 52

[82] Sanders J. S., Fabian A. C., 2002, MNRAS, 331, 273

[83] Sanderson A. J. R., Ponman T. J., Finoguenov A., Lloyd-Davies E. J., Markevitch M., 2003, MNRAS, 340, 989

[84] Sanders J. S., Fabian A. C., Allen S. W., Schmidt R. W., 2004, MNRAS, 349, 952

[85] Sanderson A. J. R., Ponman T. J., Finoguenov A., Lloyd-Davies E. J., Markevitch M., 2003, MNRAS, 340, 989

[86] Schmidt R. W., Fabian A. C., Sanders J. S., 2002, MNRAS, 337, 71

[87] Schombert J. M., 1987, ApJSS, 64, 643

[88] Schombert J. M., 1988, ApJ, 328, 475

[89] Schreier E. J., Gorenstein P., Feigelson E. D., 1982, ApJ, 261, 42

[90] Sparks W. B., Biretta J. A., Macchetto F., 1996, ApJ, 473, 254

[91] Sun M. et al., 2003, ApJ, 598, 250

[92] Sutherland R. S., Dopita M. A., 1993, ApJS, 88, 253

[93] Tamura T. et al., 2001, A&A, 365, L87

[94] Takahashi I., Kawaharada M., Makishima K., Ikebe Y., Tamura T., 2003, Proceedings of The Riddle of Cooling Flows in Galaxies and Clusters of Galaxies, Ed. Reiprich,Kempner&Soker

[95] Taylor G. B., Sanders J. S., Fabian A. C., Allen S. W., 2006, MNRAS, 365, 705

[96] Tozzi P.,Rosati P., Ettori S., Borgani S., Mainieri V., Norman C., 2003, ApJ, 593,705

[97] Vazza F., Tormen G., Cassano R., Brunetti G., Dolag K., 2006, accepted in MNRAS (astro-ph 0602247)

[98] Voigt L. M., Fabian A. C., 2004, MNRAS, 347, 1130

4

Metal mixing by buoyant bubbles in galaxy clusters

E.Roediger, M.Brüggen, P.Rebusco, H.Böhringer , & E.Churazov

Abstract

We studied the effect of bubble-induced motions on metallicity profiles in clusters of galaxies using a series of three-dimensional, hydrodynamic simulations (performed with the code FLASH). In particular, we have studied the dependence on the bubble size and position, the recurrence times of the bubbles, the way these bubbles are inflated and the underlying cluster profile. We find that in hydrostatic cluster models, the resulting metal distribution is very elongated along the direction of the bubbles. Anisotropies in the cluster or ambient motions are needed if the metal distribution is to be spherical. In order to parametrise the metal transport by bubbles, we compute effective diffusion coefficients. The diffusion coefficients inferred from our simple experiments lie at values of around $\sim 10^{29}$ cm^{2}s^{-1} at a radius of 10 kpc. The runs modeled on the Perseus cluster yield effective diffusion coefficients that agree very well with those inferred from X-ray observations.

4.1 Introduction

Currently, the most popular model that is invoked to explain the apparent stability of cool cores against a cooling catastrophe relies on heating by a central Active Galactic Nucleus (AGN). Radio-loud active galactic nuclei drive strong outflows in the form of jets that inflate bubbles or lobes. The lobes are filled with hot plasma, and can heat the cluster gas in a number of ways (e.g. Churazov et al. 2001, Brüggen et al. 2002, Brüggen & Kaiser 2002, Reynolds et al. 2002, Basson & Alexander 2003, Dalla Vecchia et al. 2004, Omma et al. 2004, Ruszkowski et al. 2004, Brüggen et al. 2005, Brighenti & Mathews 2006). High-resolution X-ray observations of cooling flow clusters with CHANDRA have revealed a multitude of X-ray holes on scales < 50 kpc, often coincident with patches of radio emission. In a recent compilation, Bîrzan et al. (2004) lists 18 well documented clusters which show X-ray cavities with radio emission.

Buoyantly rising bubbles induce subsonic motions in the cluster gas that can redistribute metals in the ICM (Brüggen 2002). Although this mode is likely to be very important, at least at redshifts $\leq$ 1, relatively little theoretical work has gone in establishing the importance of AGN-induced transport of metals in cluster centers (e.g. Omma et al. 2004).

The broad abundance peaks in clusters have been produced over a time span of several gigayears. If the peaks have been broadened by AGN, this process has taken a large number of activity cycles. In order to simulate the transport of metals by AGN-induced flows and to capture the hydrodynamical details important for the interaction between the AGN and the ICM, a fair resolution of the computational mesh is necessary. This prevents us from simulating the bubble transport over cosmological times. However, we can still study the efficiency of the metal transport by simulating a small number of AGN cycles and parametrise the transport efficiency. A convenient parametrisation that has been applied previously to observations (Rebusco et al. 2005) is based on a diffusion description. Even though we do not propose that the metal transport occurs via microscopic diffusion, transport processes like these may be described by a diffusion parameter. This allows a direct comparison to observations without having to simulate the entire life time of the cluster.

4.2 The model and the code

We model the hydrodynamical evolution of the ICM in a galaxy cluster. Initially, the ICM is set in hydrostatic equilibrium in a static cluster potential. We study two different cluster models. In the first, generic one, we take a

Table 4.1: ICM parameters for generic runs.

R_{ICM}	50 Kpc
ρ_{ICM_0}	$10^{-26}\ g\ cm^{-3}$
β	0.5
T_{ICM}	$4.7 \cdot 10^7$ K

Table 4.2: Central galaxy – metal injection parameters.

a	10 Kpc
$\dot{M}_{Metal_0}$	$952\ M_\odot\ Myr^{-1}$

constant ICM temperature and the pressure is set by assuming hydrostatic equilibrium. The density of the ICM follows a β-profile. Table 4.1 lists the ICM parameters.

In addition to the generic cluster model, we set up a cluster modeled on the brightest X-ray cluster A426 (Perseus) that has been studied extensively with CHANDRA and XMM-Newton. The electron density n_e and the temperature T_e profiles used in this case are the same as in Chapter 2.

We assume that a central cluster galaxy injects metals into the ICM with a rate proportional to its light distribution, which is modeled with a Hernquist profile :

$$\dot{\rho}_{metal} = \frac{\dot{M}_{Metal_0}}{2\pi} \frac{a}{r} \frac{1}{(r+a)^3}$$

Note that the injection rate could also be time-dependent. Rebusco et al. (2005) have used a time-dependent metal injection rate that accounts for the higher supernova rate in the past and the evolution of the stellar population (also see Renzini et al. 1993). However, we follow the evolution of the cluster for only about 1 Gyr. For typical cases studied in Rebusco et al. (2005), the metal injection rate does not change significantly over this time. Hence in our simulations we use a temporally constant metal injection rate. Table 4.2 lists the parameters for the metal injection.

We trace the distribution of the metals by injecting a tracer fluid into the ICM at a rate that is proportional to the light distribution of the central galaxy (for the details on the way the metals are traced throughout the simulation, see Roediger et al. 2006).

Finally, we model the AGN activity by inflating ambipolar pairs of underdense bubbles in the ICM that rise buoyantly and thus stir the ICM. In Subsection 4.2.1 we explain how the bubbles are generated.
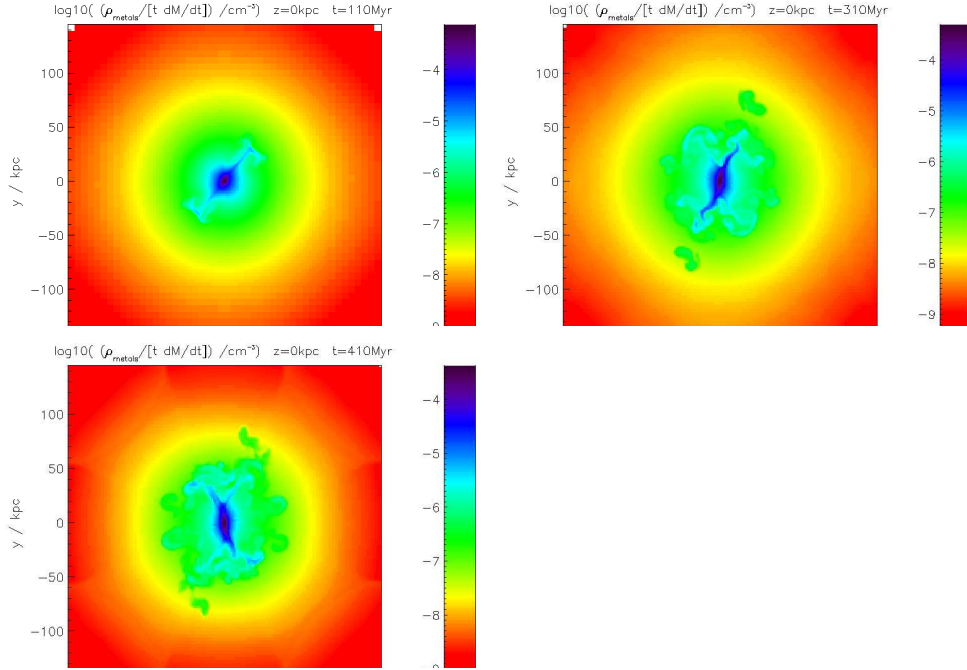
log10((ρ_{metals}/[t dM/dt]) /cm^{-3})   z=0kpc   t=110Myr

log10((ρ_{metals}/[t dM/dt]) /cm^{-3})   z=0kpc   t=310Myr

log10((ρ_{metals}/[t dM/dt]) /cm^{-3})   z=0kpc   t=410Myr

Figure 4.1: Slice through the computational box showing the local metal fraction at three different times (110, 310, 410 Myr). The simulation is based on Perseus cluster, with $r_{Bubble} = 10$ kpc, $\tau_{Bubble} = 50$ Myr, $n_{rot} = 4$ and evacuation method.

The simulations were performed by Elke Roediger and Marcus Brüggen with the FLASH code (Fryxell et al. 2000), a multidimensional adaptive mesh refinement code. The exact physics of viscosity and magnetic fields in clusters of galaxies is poorly constrained. FLASH solves the equations of inviscid hydrodynamics, without magnetic fields: the discretisation of the equations still leads to a numerical viscosity that stabilizes the bubbles.

4.2.1 Bubble generation

Bubbles in the ICM are thought to be inflated by a pair of ambipolar jets from an AGN in the central galaxy. In this simple picture, the jets inject energy into small volumina of the ICM at their terminal points. Thus, this region is in overpressure and expands until it reaches pressure equilibrium with the surrounding ICM. The result is a pair of underdense, hot bubbles.

In our simulations, we generate pairs of bubbles on opposite sides of the cluster centre. There are various ways in which one could produce these

bubbles and we have tested the following two methods:

- INFLATION: in the first method, we inflate the bubbles by injecting energy into two small spheres of radius r_{inj} with a constant rate over an interval of length τ_{inj}. The gas inside these spheres is heated and expands similar to a Sedov explosion in a few Myr to form a pair of bubbles. The inflation parameters are chosen such that the resulting bubbles show approximately a radius of r_{Bubble}. The expansion is much shorter than the rise of the generated bubbles. In addition to the bubbles, the explosion sets off shock waves that move through the ICM.

- EVACUATION: in the second method, we evacuate the bubble regions by removing gas while keeping them in pressure equilibrium with their surroundings. This evacuation method does not produce the shock waves generated by the inflation method (hence, it is computationally cheaper). We implement gas mass sinks inside two spheres of radius r_{Bubble}. Inside these regions, gas is removed with a certain rate $\dot{\rho}$ over a time τ_{Evac} (to prevent numerical problems). The evacuation method models the phase of the evolution after the radio-loud AGN has inflated a low-density bubble which has expanded to achieve pressure equilibrium with its surroundings (Brüggen & Kaiser 2001).

As found in previous studies, the bubbles start to rise buoyantly and fragment. While rising, they uplift the metals from the centre and distribute them in their wake. Quite quickly the bubble fragments into a torus. Associated with this torus is a vortical flow that causes gas to ascend through the axis of the torus. Along the axis of the torus, metals seem to be transported rather fast. However, this metal spreading seems to be restricted to a narrow region around this direction. Spreading along other directions seems negligible. The effect is that the metals are spread out significantly along the axis of the bubbles leading to a very elongated metal distribution. The bubbles do not continue to rise indefinitely and even after 1 Gyr they do not rise beyond 100 kpc from the centre. The fragments form a mushroom-shaped plume, not unlike the radio structures observed in M87, and this structure covers a larger azimuthal angle. There could be a certain radius where most metals are deposited.

Two effects can lead to a more isotropic mixing of metals: (i) ambient motions in the cluster that are triggered by galaxy motions and merger activity and (ii) a series of bubbles that are launched at changing locations in the cluster, for example by a precessing jet or by inhomogeneities of the accretion flow near the jet. Here we investigate the second scenario: for both methods,

we generate a pair of bubbles every τ_{Bubble}; for every bubble generation cycle, the position of the generated bubbles changes. For the next pair of bubbles, the axis that connected the previous bubbles is rotated around the y-axis. The angle of rotation is fixed by the demand that after n_{rot} cycles the bubbles are again inflated in the first position.

4.3 Results

The results of the simulations with the generic cluster model and with the parameters of the Perseus cluster can be summarized:

- Larger bubbles lead to mixing to larger radii. For realistic parameters ($r_{Bubble} \sim 10$ kpc) and in the absence of stabilizing forces, bubbles hardly move beyond distances of 150 kpc from the centre.

- We employed a recurrence time τ_{Bubble} of 50 and of 200 Myr: mixing scales roughly with the frequency of bubble generation, as one would expect (see Figure 4.2).

- The metal distribution is not sensitive to the way of how bubbles are inflated.

- In hydrostatic cluster models, the resulting metal distribution is very elongated along the direction of the bubbles. Anisotropies in the cluster and/or ambient motions are needed if the metal distribution is to be spherical (see Figure 4.1).

4.3.1 Estimate of the diffusion coefficient

In this section, we wish to parametrise the transport of metals by computing an effective diffusion constant. We will begin by defining a cumulative metal mass profile

$$M_{Metal}(R) = \int_{r<R} \rho_{Metal}(\mathbf{r})\mathrm{d}\mathbf{V} \qquad (4.1)$$

and the averaged metal density profile

$$\bar{\rho}_{Metal}(r) = \frac{1}{4\pi r^2}\frac{\partial M_{Metal}(r)}{\partial r}. \qquad (4.2)$$

On the basis of these quantities, we can estimate a diffusion constant that can be compared with Rebusco et al. (2005). We start from the spherically
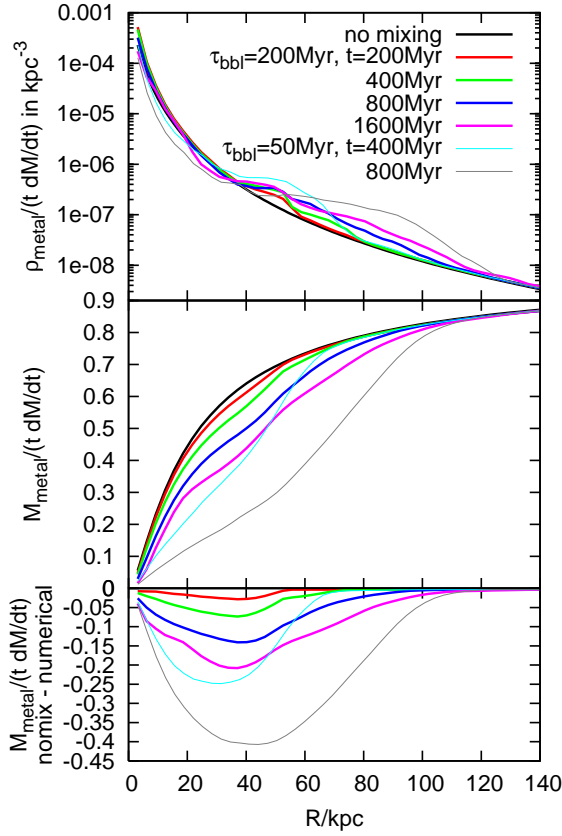
Figure 4.2: Evolution of normalized metal density profile (top panel) and normalized cumulative metal mass profile (metal mass inside r, middle panel) for the generic cluster model. The bottom panel shows the difference between mixing and no mixing. Comparison of two runs with different bubble evacuation timescale ($\tau_{Bubble} = 50$ Myr or 200 Myr). Different line styles and colors correspond to different times and runs, see the legend. The black line is the prediction of what should happen without any mixing.

symmetrical diffusion equation including the metal source term

$$\frac{\partial \bar{\rho}_{Metal}(r,t)}{\partial t} = \frac{\partial}{\partial r} D \frac{\partial}{\partial r} \bar{\rho}_{Metal}(r,t) + \dot{\rho}_{Metal}(r), \qquad (4.3)$$

where D is the diffusion constant, and $\dot{\rho}_{Metal}(r)$ is the metal source profile. Discretising this between the radii R_1 and R_2 (i.e. $\Delta R = R_2 - R_1$ and $\bar{R} = (R_1 + R_2)/2$) and timesteps t_1 and t_2 ($\Delta t = t_2 - t_1$ and $\bar{t} = (t_1 + t_2)/2$)
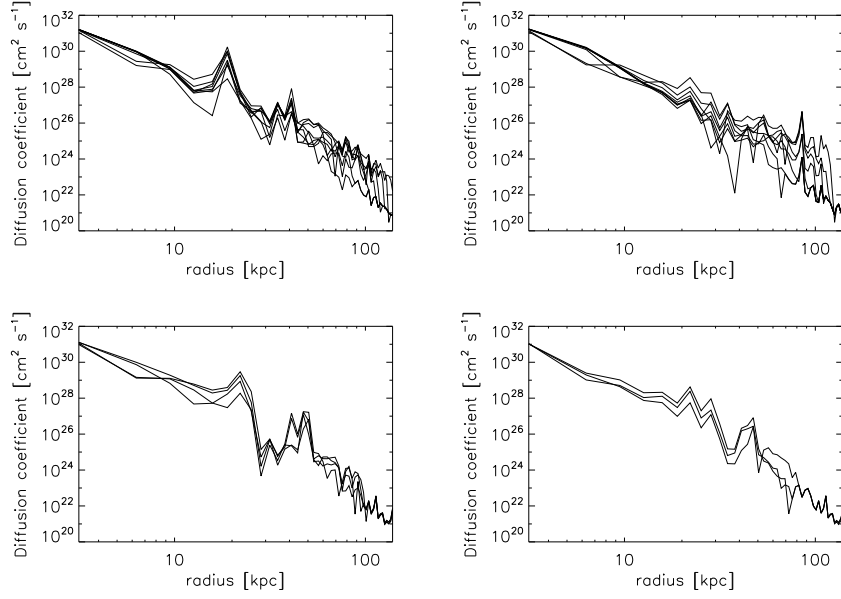
Figure 4.3: Top: effective diffusion coefficients for the runs with the general cluster model, EVACUATION (left) and INFLATION (right) methods. Bottom: diffusion coefficients for the runs with the Perseus cluster, $\tau_{Bubble} = 50$ Myr (left) and $\tau_{Bubble} = 200$ Myr (right). The different curves denote different times.

yields

$$
\frac{\bar{\rho}_{Metal}(\bar{R}, t_2) - \bar{\rho}_{Metal}(\bar{R}, t_1)}{\Delta t} = \dot{\rho}_{Metal}(\bar{R}) +
$$
$$
D(\bar{R}, \bar{t}) \; \frac{\frac{\partial}{\partial r}\bar{\rho}_{Metal}(R_2, \bar{t}) - \frac{\partial}{\partial r}\bar{\rho}_{Metal}(R_1, \bar{t})}{\Delta R}, \tag{4.4}
$$

where we have assumed that D varies only slowly with radius, i.e. $D(R_1, t) \approx D(R_2, t) \approx D(\bar{R}, t)$. Reordering yields

$$
D(\bar{R}, \bar{t}) =
$$
$$
\Delta R \; \frac{\bar{\rho}_{Metal}(\bar{R}, t_2) - \bar{\rho}_{Metal}(\bar{R}, t_1) - \dot{\rho}_{Metal}(\bar{R}) \, \Delta t}{\Delta t \; \left[\frac{\partial}{\partial r}\bar{\rho}_{Metal}(R_2, \bar{t}) - \frac{\partial}{\partial r}\bar{\rho}_{Metal}(R_1, \bar{t}) \right]} \tag{4.5}
$$

We have computed the radial profiles of the diffusion constants in Figure 4.3.

4.4 Discussion and conclusions

In our simulations, the dynamics of the ICM is entirely driven by underdense bubbles that are initially at rest and then start to rise by the action of buoyancy. This is clearly a simplified picture. In reality, these bubble are inflated by relativistic jets whose physics is still very poorly understood. Real AGN jets have a dynamics that can only be fully captured with special-relativistic MHD codes that need to resolve scales much below the scales resolved in our simulations.

However, bubbles such as those set up in our simulations are similar to the bubbles observed in galaxy clusters such as the Perseus cluster. The bubbles in Perseus and other clusters are nearly in pressure equilibrium with the ambient medium, they are nearly spherical and move subsonically through the ICM. Thus, we ignore the entire process that has led to the formation of these bubbles and focus solely on the buoyancy-driven motions of the bubbles.

If bubbles in a hydrostatic cluster are launched repeatedly at the same position, the resulting metal distribution becomes very aspherical and elongated along the axis of the bubble. If, however the bubbles are launched at changing positions, the metal distribution is somewhat isotropised. However, as is apparent e.g. from Fig. 4.1, even when we vary the bubble position within a cone of $\sim 30\,\mathrm{deg}$, the resulting metal distribution remains elongated and non-spherical. Thus, if the metal distribution should turn out to be spherical, this would necessitate additional motions caused for example by mergers or by stirring by galaxies in order to isotropise the metals.

In real clusters, the ICM is not in hydrostatic equilibrium and can show strong motions. Galaxies that fly through the cluster produce motions and turbulence. Merger activity can stir the ICM even more violently. These motions will all contribute to dispersing the metals throughout the ICM. Moreover, density anisotropies can cause the bubbles to move away from the axis of the AGN jet, as the bubbles follow the local density gradient. Indeed, in quite a few clusters, most famously in M87, the bubbles are widely dispersed through the cluster and do not trace the alleged axis of the AGN jet. Heinz et al. (2006) have performed three-dimensional adaptive-mesh simulations of jets situated at the centre of a cluster drawn from a cosmological simulation. These simulations show that cluster inhomogeneities and large-scale flows have a significant impact on the morphology of the bubbles.

The diffusion coefficients inferred from our simple experiments lie at values of around $\sim 10^{29}$ cm^{2}s^{-1} at a radius of 10 kpc. Right at the centre, they rise to

about $\sim 10^{31}$ cm^{2}s^{-1} and fall to about $\sim 10^{25}$ cm^{2}s^{-1} at a radius of 100 kpc. Modulo a factor of a few, the coefficients for all runs lie around these values. Differences are induced by the bubble sizes, the initial positions, the recurrence times and the pressure profile in the cluster. Interestingly, the runs modeled on the Perseus cluster yield effective diffusion coefficients that agree very well with those estimated by assuming a simple diffusion model (see Rebusco et al. 2005). As we do not take into account motions that may have been induced by mergers etc., the values for the diffusion coefficients constitute lower limits on the real values. Thus, we can conclude that AGN-induced motions are sufficient to explain the broad abundance peaks in clusters. It is also striking that the diffusion coefficients fall so steeply with the radial distance from the centre. Over two decades in radius they decrease by almost 10 orders of magnitude. Very approximately, they fall like r^{-5}. This strong radial dependence of the transport efficiency is, partially, a result of the three-dimensional nature of the bubble-induced motions, i.e. uplifted metals are diluted over the entire radial shell. A second effect is the decaying "lift" power of the bubbles as they rise. The bubbles accelerate only at the beginning of their ascent through the cluster. However, very quickly instabilities set in that slow down the bubble until it finally comes to a halt at about 100 kpc from the centre. The maximal lift power is attained when the bubbles are still intact and have their largest velocity. This occurs at radii of about 20 kpc - 30 kpc, and this coincides with peaks in the diffusion coefficient as can be seen from Fig. 4.3.

Finally, we may add that if hydrodynamic instabilities are suppressed by magnetic fields or viscous forces, for example, the bubbles would stay intact for longer and could rise to greater distances thus also enhancing the diffusion coefficients at larger radii.

Acknowledgments

Bibliography

[1] Basson J. F., Alexander P., 2003, MNRAS, 339, 353 339, 353

[2] Bîrzan L., Rafferty D. A., McNamara B. R., Wise M. W., Nulsen P. E. J., 2004, ApJ, 607, 800

[3] Brighenti F., Mathews W. G., 2006, ApJ, 643, 120 643, 120

[4] Brüggen M., 2002, ApJ, 571, L13

[5] Brüggen M., Kaiser C. R., 2001, MNRAS, 325, 676 325, 676

[6] Brüggen M., Kaiser C. R., 2002, Nature, 418, 301

[7] Brüggen M., Kaiser C. R., Churazov E., Enßlin T. A., 2002, MNRAS, 331, 545

[8] Brüggen M., Ruszkowski M., Hallman E., 2005, ApJ, 630, 740—

[9] Churazov E., Brüggen M., Kaiser C. R., Böhringer H., Forman W., 2001, ApJ, 554, 26

[10] Dalla Vecchia C., Bower R. G., Theuns T., Balogh M. L., Mazzotta P., Frenk C. S., 2004, MNRAS, pp 507–+

[11] Fryxell B., Olson K., Ricker P., Timmes F. X., Zingale M., Lamb D. Q., MacNeice P., Rosner R., Truran J. W., Tufo H., 2000, ApJS, 131, 273

[12] Heinz S., Brüggen M., Young A., Levesque E., 2006, MNRAS, 373, L65

[13] Omma H., Binney J., Bryan G., Slyz A., 2004, MNRAS, 348, 1105

[14] Rebusco P., Churazov E., Böhringer H., Forman W., 2005, MNRAS, 359, 1041

[15] Renzini A., Ciotti L., D'Ercole A., Pellegrini S., 1993, ApJ, 419, 52

[16] Reynolds C. S., Heinz S., Begelman M. C., 2002, MNRAS, 332, 271

[17] Roediger E., Brüggen M., Rebusco P., Böhringer H., Churazov E., 2007 MNRAS, in press (astro-ph/0611531)

[18] Ruszkowski M., Brüggen M., Begelman M. C., 2004, ApJ, 611, 158

5

Width of X-ray lines as a diagnostic of gas motions in cooling flows

P.Rebusco, E.Churazov, R.Sunyaev & W.Forman

Abstract

The dissipation of gas turbulent motions is one of the likely mechanisms for the intracluster medium (ICM) heating in the cores of clusters and groups of galaxies. We consider the impact of gas motions on the width of the most prominent X-ray emission lines. For heavy elements (like iron) the expected linewidth is much larger than for pure thermal broadening and it should be easily detected with the new generation of X-ray microcalorimeters. The radial dependence of the linewidth can be used to distinguish between various patterns of gas motions. For instance, isotropic turbulence (our baseline scenario) and pure radial gas motions (expected in scenarios where shocks/sound waves play a dominant role) lead to a markedly different radial dependence.

Keywords:turbulence - line:profiles - cooling flows-clusters:individual

5.1 Introduction

Clusters of galaxies are the largest gravitationally bound and nearly virialized systems in the Universe. High resolution X-ray surveys have revealed that the ICM (with temperatures in the range $\sim 2 - 10$ keV) is not fully relaxed. The substructures in the surface brightness and temperature are observed both on large scales and in the cluster cores indicating that the gas is not at rest. At the same time strong shocks are rarely observed (see Markevitch & Vikhlinin, 2007 for a review) suggesting that the cluster gas motions are predominantly subsonic. The shape of the emission lines as a source of information on the ICM velocity distribution has been discussed in detail in Sunyaev, Norman & Bryan (2003) and Inogamov & Sunyaev (2003). These papers mostly consider the gas motions induced by cluster mergers. In the present paper we focus on the linewidth as a diagnostic of gas motions in the cores of the galaxy clusters. In the cores of most clusters and many groups (e.g Stewart et al 1984, Nulsen et al 1984, Edge & Stewart 1991, Mulchaey et al 1993, Fabian 1994), the radiative cooling time of the gas is short compared to the age of the cluster and an external source of energy is needed if one tries to avoid catastrophic cooling (e.g. Matsushita et al. 2002, Peterson et al. 2003, Kaastra et al. 2004). The dissipation of turbulent gas motions is one of the plausible sources of the required energy (e.g. Pedlar et al. 1990, Churazov et al. 2002, Fabian et al. 2003a, Chandran 2005). These motions can have distinctive effects on the properties of the X-ray lines (e.g. Brüggen, Hoeft & Ruszkowski 2005). There are several indirect ways of probing the gas velocities, i) using the resonant scattering of the brightest emission lines (e.g. Gilfanov, Sunyaev & Churazov, 1987, Churazov et al., 2004); ii) considering the spreading of metals ejected by a central galaxy through the ICM (Rebusco et al., 2005,2006, Graham et al., 2006, Roediger et al., 2007); iii) using H_α emitting filaments as tracers of the gas motions (e.g. Fabian et al., 2003b, Hatch et al., 2006). In particular in Rebusco et al. (2005,2006) the characteristic spatial and velocity scales of the turbulent eddies were estimated assuming that the dissipation of turbulent motions can generate enough heat to prevent the gas from cooling and that the same motions provide moderate mixing of metals through the ICM. Using these estimates we calculated the expected width of the brightest X-ray lines for the brightest clusters (like A246 - Perseus).

The progress with X-ray calorimeters allows one to expect that an instrument with energy resolution of 1-4 eV will be soon operating in space. The Japanese-American X-ray satellite *Suzaku* was the first satellite that carried such a new type of micro-calorimeters. Unfortunately it failed after a day, having measured just a calibration line. The effective areas of the upcoming calorimeters ranges from few 100 up to few 10^4 cm^2 (see e.g.

(`http://www.rssd.esa.int/index.php?project=XEUS` , `http://constel`
`lation.gsfc.nasa.gov/index.html`), while the spatial resolution varies be-
tween few arcsec and few arcminutes. Even the instruments with the charac-
teristics in this modest range are fully sufficient to study the line broadening
associated with turbulent gas motions in the core of galaxy clusters.

The structure of the paper is the following. In section 5.2 we describe
the line broadening under different assumptions on the character of the gas
motions; in section 3 we consider the specific case of the Perseus cluster as an
example. Our findings are discussed and summarized in sections 4 and 5.
Throughout the paper when we mention turbulence, we mean all the non-
thermal gas motions. In particular, for the estimates in the Perseus cluster,
we refer to stochastic gas motions. We adopt a Hubble constant of $H_0 = 70$
km s^{-1} Mpc^{-1}, $\Omega_M = 0.3$ and $\Omega_\Lambda = 0.7$.

5.2 The impact of turbulence on the linewidth

There are several bright emission lines in the X-ray range, that are character-
istic of the ICM in galaxy clusters (Table 5.1). The He-like iron line at 6.7 keV
is the most prominent feature above a few keV: it is especially bright in the
high temperature ($T_e > 4$ keV) clusters. For the lower temperature clusters,
and in particular for the cooling flow regions, L lines of iron at $\sim$1 keV, lines
of Si, Mg and O can be substantially brighter than the 6.7 keV line. In Table
5.1 we list a sub-sample (incomplete) of these lines and provide an estimate
of their fluxes from the central 5' (radius) region of the Perseus cluster. All
the line parameters were taken from the ATOMDB data base (Smith et al.
2001a,b). Let us first assume that i) the cluster is spherically symmetric,
ii) the characteristic correlation length of the velocity field is much smaller
than the characteristic dimensions of the system and ii) at each location the
emission line profile can be approximated by a Gaussian:

$$p(\nu - \nu_0) = \frac{1}{\sqrt{2\pi}} \frac{1}{\sigma_\nu} \exp\left(-\frac{1}{2} \frac{(\nu - \nu_0)^2}{\sigma_\nu^2}\right), \tag{5.1}$$

where ν_0 and ν are the emitted and the observed frequencies respectively,
$\sigma_\nu = \sigma_\nu(R)$ is the width of the line, which is a function of the distance R from
the center of the cluster. The spectral surface brightness in a line at a given
projected distance (x) from the center of the cluster is given by the following
integral along the line of sight (l):

$$I(\nu, x) = \int_{-\infty}^{\infty} n_e^2 \, a \, \epsilon_{\nu_0} \, p(\nu - \nu_0) \, dl, \tag{5.2}$$

98

Ion	Z	u	l	E	ϵ_{peak}(phot cm^3 s^{-1})	T$_{peak}$	F($< 5'$)/10^{-3}
FeXXV	26	$1s2p$ $^1P_1$	$1s^2$ $^1S_0$	6.700	4.56×10^{-17}	5.42	1.25
FeXXIV	26	$1s^23p$ $^2P_{3/2}$	$1s^22s$ $^2S_{1/2}$	1.1675	9.92×10^{-17}	1.74	2.72
SiXIV	14	$2p$ $^2P_{3/2}$	$1s$ $^2S_{1/2}$	2.006	5.02×10^{-17}	< 1.50	1.38
MgXII	12	$2p$ $^2P_{3/2}$	$1s$ $^2S_{1/2}$	1.470	4.26×10^{-17}	< 1.50	1.17
OVIII	8	$2p$ $^2P_{3/2}$	$1s$ $^2S_{1/2}$	0.650	2.26×10^{-16}	< 1.50	6.21

Table 5.1: Emission lines: (1) ion, (2) atomic number Z, (3)-(4) respectively, upper and lower levels of the transition, (5) line energy in keV, (6) peak emissivity within the temperature range of interest $1.5 - 10$ keV, (7) temperature (in the range $1.5 - 10$ keV) at which the emissivity is the highest for a given line, (8) estimated flux (phot cm^{-2} s^{-1}) for the central $5'$ region of the Perseus cluster .

where $n_e = n_e(R)$ is the electron density, $a = a(R)$ the element abundance, $\epsilon_{\nu_0} = \epsilon_{\nu_0}(T_e(R))$ the plasma emissivity in a given line, which is a function of the plasma temperature $T_e(R)$. In the above expression $R = \sqrt{x^2 + l^2}$. The line broadening is decomposed into two components

$$\sigma_\nu^2 = \sigma_{thermal}^2 + \sigma_{turb}^2, \tag{5.3}$$

where

$$\sigma_{thermal} = \nu_0 \frac{\sqrt{\frac{kT_e}{Am_p}}}{c}$$
$$\sigma_{turb} = \nu_0 \frac{v_\parallel}{c}, \tag{5.4}$$

where k is the Boltzmann constant, m_p the proton mass, A the atomic weight of the element, c the speed of light and $v_\parallel$ the line of sight component of the turbulent velocity. E.g. for an isotropic turbulence $v_\parallel^2 = v_{turb}^2/3$, where v_{turb}^2 is 3-dimensional turbulent velocity scale. A comparison of thermal and turbulent broadenings in a 4 keV plasma is given in Table 5.2. Note that even for the iron line at 6.7 keV the natural width of the line due to radiative decay is only ~0.2 eV (and it is much lower for the other transitions in Table 5.2). We therefore neglect the natural width of all the lines throughout this paper.

As it is obvious from equation 5.4 the heaviest elements are the best probes of gas motions, since for them the turbulent broadening can significantly dominate over the thermal broadening. Indeed the ratio of the e.g. iron thermal velocity to the proton thermal velocity is small ($\sim (m_p/Am_p)^{1/2} = 0.13$). Thus even for small velocities the turbulent broadening will exceed the thermal broadening (Table 5.2). For an instrument with a given spectral resolution the energy of the line also plays an important role, since the width of the line simply scales with the line energy. This makes the iron 6.7 keV line the best probe of the turbulent ICM, as long as the instrument has a substantial effective area at 6-7 keV.

The above assumption of the line shape due to turbulent motions is of course only an approximation (see Inogamov & Sunyaev 2003 for a discussion). However it is fully sufficient to assess the detectability of the turbulent broadening. In fully developed turbulence a full range of scales is produced through an energy cascade (e.g. Richardson 1922, Tennekes & Lumley 1972, Lesieur 1997, Mathieu 2000, Davidson 2004), which is characterized by large scale energy-containing motions and a small dissipation scale. In our simplified treatment we assume that the v_{turb} entering all our equations can be obtained from the kinetic energy of the turbulent motions: $\epsilon_K = \rho \frac{v_{turb}^2}{2}$, where ρ is the gas density. Since the integration of equation 5.2 may result in a line shape different from a pure Gaussian we use below an "effective" full width

Ion, E(keV)	v_{turb}(km/s)	FWHM$_{thermal}$(eV)	FWHM$_{turb}$(eV)	$\frac{FWHM_{total}}{FWHM_{thermal}}$
FeXXV, 6.700	100	4.35	3.04	1.22
	300	4.35	9.12	2.30
	900	4.35	27.35	6.31
FeXXIV, 1.170	100	0.76	0.53	1.22
	300	0.76	1.59	2.32
	900	0.76	4.78	6.36
SiXIV, 2.006	100	1.84	0.91	1.12
	300	1.84	2.73	1.79
	900	1.84	8.19	4.55
MgXII, 1.470	100	1.46	0.67	1.10
	300	1.46	2.00	1.70
	900	1.46	6.00	4.23
OVIII, 0.650	100	0.79	0.29	1.07
	300	0.79	0.88	1.50
	900	0.79	2.65	3.50

Table 5.2: Thermal and turbulent broadening in a 4 keV plasma: (1) line energy in keV, (2) turbulent velocity in km/s, (3) FWHM due to pure thermal broadening, (4) FWHM due to isotropic turbulent broadening alone, (5) ratio of the total FHWM to the pure thermal broadening.

half maximum (eFWHM), which is defined as the interval of energies centered at the line energy and containing 76% of the line flux.

5.2.1 Isotropic, radial and tangential motions

While there is indirect evidence that the gas in the cluster centers is involved in some sort of motion, neither the characteristic velocity scale nor the characteristic patterns of the hot gas motions have been directly measured. One can identify two major sources of turbulent gas motions in the cores: cluster mergers and the action of a central active galactic nucleus (AGN). Each process may produce a velocity field different in intensity and directionality. Let us consider the extreme cases of isotropic, pure radial or pure tangential velocity fields as illustrated in Figure 5.2. If one fixes the total kinetic energy in the motions, then the line of sight component of the velocity can be written
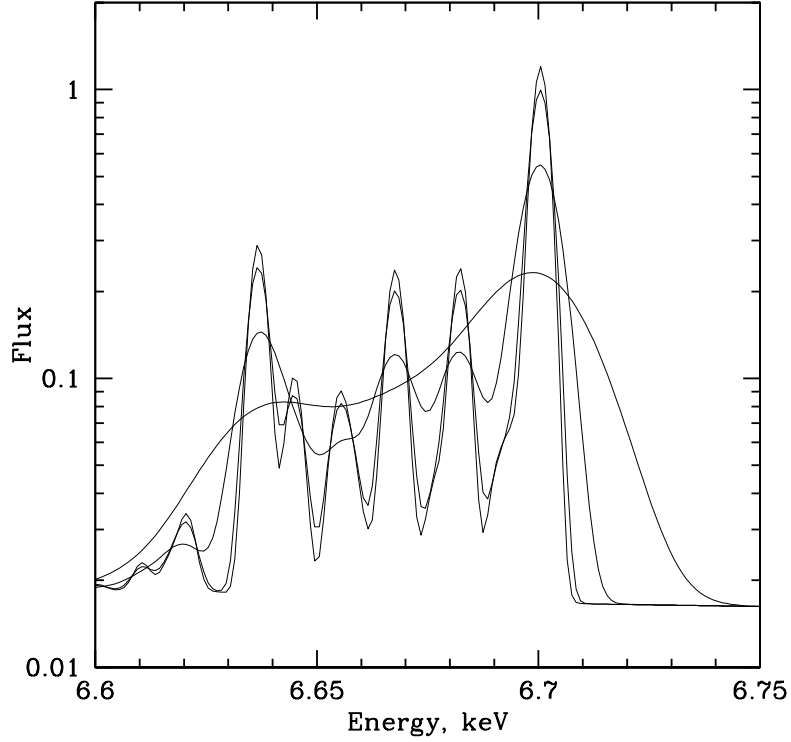
Figure 5.1: 6.7 keV line complex for a $T = 4$ keV plasma. The spectra correspond to the thermal broadening and turbulent broadenings with $v_{turb}=0$, 100, 300 and 900 km/s. For comparison the sound speed in a 4 keV plasma is $\sim$1000 km/s.

as:

$$
v_{\parallel}^2 = \begin{cases} \frac{v_{turb}^2}{3} & \text{isotropic,} \\ v_{turb}^2 \frac{l^2}{R^2} & \text{radial,} \\ \frac{v_{turb}^2}{2} \frac{x^2}{R^2} & \text{tangential.} \end{cases} \tag{5.5}
$$

The first case (isotropic gas motions) can occur for a wide variety of driving mechanisms, ranging from mergers to the motions caused by rising buoyant bubbles of relativistic plasma or to convection driven by a mixture of thermal plasma and cosmic rays (Chandran 2005). Pure radial gas motions would naturally appear if energy generated by a central AGN goes into weak shocks and sound waves (e.g. Forman et al. 2005, 2006, Fabian et al. 2006) which
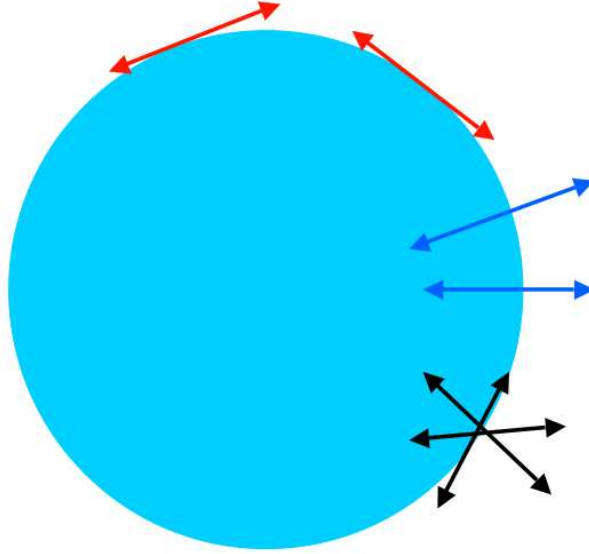
102

Figure 5.2: Sketch of isotropic, radial and tangential motions.

propagate through the ICM almost radially from the central source. The case of pure tangential motions seems to be less natural and it is included mostly for completeness. We note however that in the stratified atmosphere of clusters the characteristic frequencies of the turbulent motions can be smaller than the Brunt-Väisälä frequency:

$$N^2 = g \left(\frac{1}{\gamma} \frac{1}{p} \frac{dP}{dr} - \frac{1}{\rho} \frac{d\rho}{dr} \right), \tag{5.6}$$

where g is the gravitational acceleration due to the dark matter potential, ρ is the gas density, P is its pressure and $\gamma = 5/3$ is the adiabatic index. In Figure 5.3 we plot the Brunt-Väisälä frequency, evaluated for the Perseus cluster, and compare it with the characteristic frequency of turbulent motions v_{turb}/l for $v_{turb} = 100$km s^{-1} and $l = 20$ kpc. Clearly turbulent motions can excite gravity waves in cluster cores (e.g. Churazov et al., 2001, 2002, Omma et al., 2004) and these waves can transport the energy from a localized patch of turbulent ICM. Such a process is well known in atmospheric science and oceanography and it may lead to the formation of non-propagating pancake-shaped vortices (e.g. Riley & Lelong 2000). For any non-monotonic shape of the Brunt-Väisälä frequency N excited gravity waves with a frequency ω will be trapped in a spherical layer set by the condition $\omega = N$ (see also Balbus &
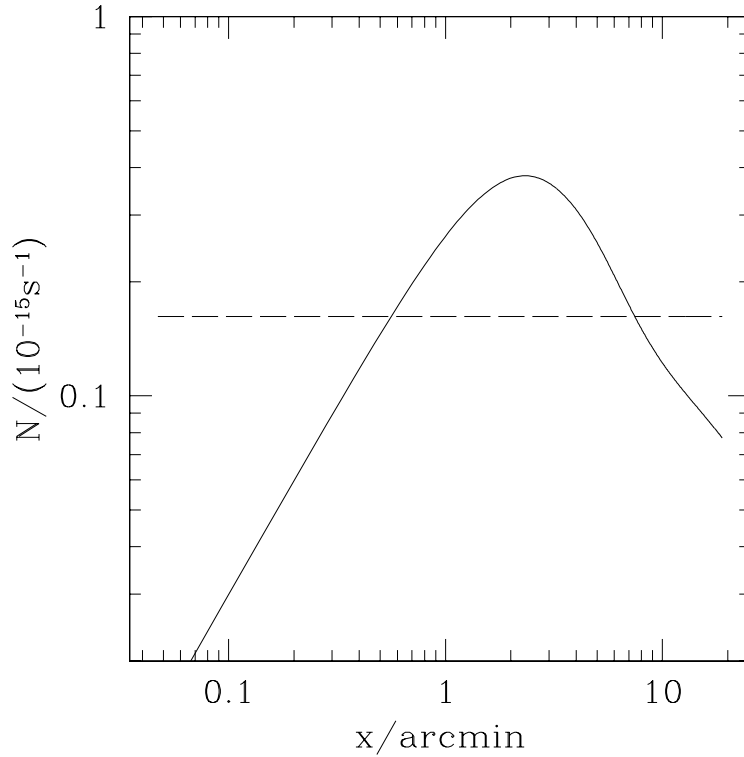
Figure 5.3: Brunt-Väisälä frequency N (solid line) for the Perseus cluster in comparison with the characteristic frequency of turbulent motions v_{turb}/l for $v_{turb} = 100$km s^{-1} and $l = 20$ kpc (dashed line).

Soker 1990 and Lufkin et al. 1995 for a discussion of trapped gravity waves). Thus in clusters the energy of excited waves does not escape to infinity, but it remains in the core region. Nevertheless one can image that patches of predominantly 2-dimensional (tangential) vortices can be created with this mechanism.

We now calculate (Figure 5.4) the expected width of the iron 6.7 keV line for each of the three limiting cases given in equation 5.5 for a model cluster with the density parameterized by a simple β model: $n_e = n_e(0) \left[1 + (r/r_c)^2 \right]^{-3/2\beta}$, where r_c is the core radius of the cluster and $\beta = 0.3, 0.5, 0.9$. The gas temperature and the abundance of iron are assumed to be constant. The velocity v_{turb} is fixed to 300 km s^{-1}. The thermal broadening (first term in equation 5.3) is omitted in the calculation of the linewidth, but the level of thermal broadening for a 6 keV plasma is shown for comparison (dashed line). The three plots in Figure 5.4 correspond to $\beta = 0.3, 0.5, 0.9$ from left

to right, respectively. As expected, from equation 5.5 the isotropic turbulence produces a linewidth independent of the projected distance from the cluster center. Pure radial gas motions would result in a line whose width is peaked towards the center of the cluster, while pure tangential motions produce the broadest line outside the cluster core. For $x \gg r_c$ the curve approaches asymptotic values (different for each velocity pattern), that are functions of β only. For large β the cluster is more "compact" and the gradients of the width of the line with the radius become stronger, while for low β the change of the linewidth is more gradual.

5.2.2 Radially dependent velocity amplitude

It is quite plausible that the characteristic velocity scale of the turbulent motions vary with the distance from the cluster center.
For instance, if the gas motions are driven by the outflows of a central AGN, then their amplitude will likely decrease for large radii, since the energy would be spread over larger masses of gas and it would be partly dissipated at smaller radii. Note moreover that, for example, the characteristic amplitude of sound waves propagating through a declining density profile decreases as $v \propto \left(\rho\, R^2 \right)^{-1/2}$. E.g. for $\rho(R) \propto 1/R$ the velocity $v \propto (R)^{-1/2}$. If furthermore dissipation is taking place then the amplitude will decline more quickly. For rising buoyant bubbles of relativistic plasma the terminal velocity scales as $v \propto v_K \sqrt{r_b/R}$ (e.g. Churazov et al., 2001), where v_K is the Keplerian velocity at a given radius R and r_b is the characteristic size of the bubble. Adiabatic expansion of the bubble leads to a slow change of the bubble size $r_b \propto P^{-1/4}$ (assuming that the adiabatic index of the medium inside the bubble is 4/3). Thus the characteristic bubble velocity is $v \propto v_K R^{-1/2} P^{-1/8}$ - a decreasing function of the radius for plausible $v_K(R)$ and $P(R)$. If the bubble breaks down into smaller bubbles, then the terminal velocity will decrease even further with the radius. Alternatively, if the turbulence is driven by shocks from minor mergers then it is possible that the velocity amplitude will instead decline towards the center, where the gas density and the thermal gas pressure are the highest. E.g. for a plane sound wave propagating into a region of increasing density the characteristic velocity $v \propto \rho^{-1/2}$, i.e. $v \propto R^{1/2}$ if $\rho \propto 1/R$. Here we have ignored both the possible reflection of the sound waves by a steep density gradient (important for long wavelength perturbation) and the focusing of sound waves due to decreasing sound speed towards the center (Pringle, 1989). In reality the effect of mergers on the cluster core is much more complicated and the above estimate can at best be considered as indicative.

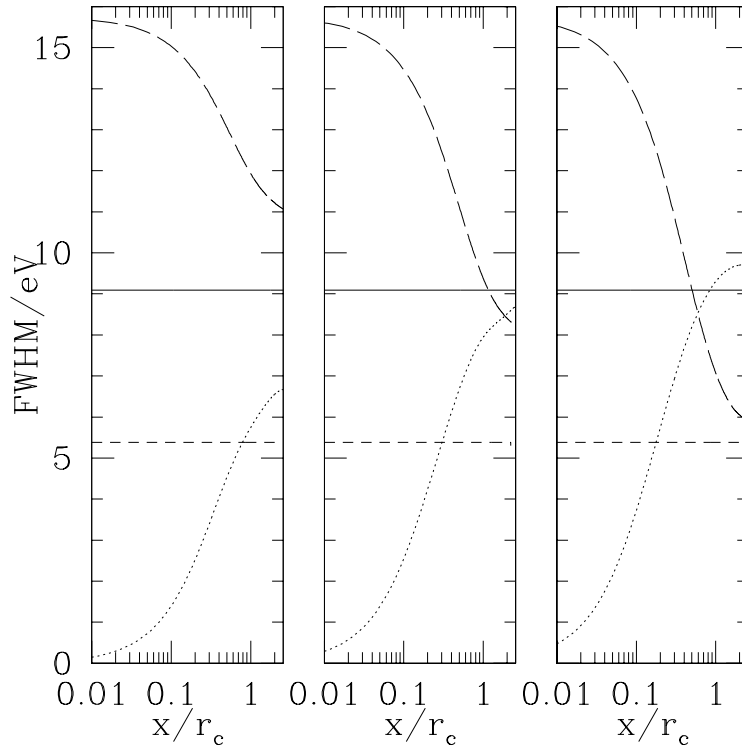For illustration we model two possibilities (decreasing or increasing turbu-

Figure 5.4: Linewidth as a function of the projected radius, for isotropic (solid), tangential (dotted) and radial (long-dashed) turbulence. The profile is obtained by integrating equation 5.2, as explained in section 5.2. In the three panels the gas density profile is different: from left to right $\beta = 0.3, 0.5, 0.9$. The thermal broadening is neglected, but its magnitude in a plasma at 6 keV is shown for reference (short-dashed line).

lence) by considering $v(R) = v_0 \left(\frac{R}{r_c}\right)^{\alpha}$, with $\alpha = \pm 1$ and $v_0 = 200$ km/s. We further assume that when $v(R) > 1000$ km/s, the velocity saturates at 1000 km/s. The resulting linewidth profiles are shown in Figure 5.5. Clearly the radial dependence of the velocity amplitude can strongly affect the dependence of the linewidth on the projected distance.

5.3 An example: the Perseus Cluster

We now calculate the expected width of the 6.7 keV line by using the Perseus cluster as an example.

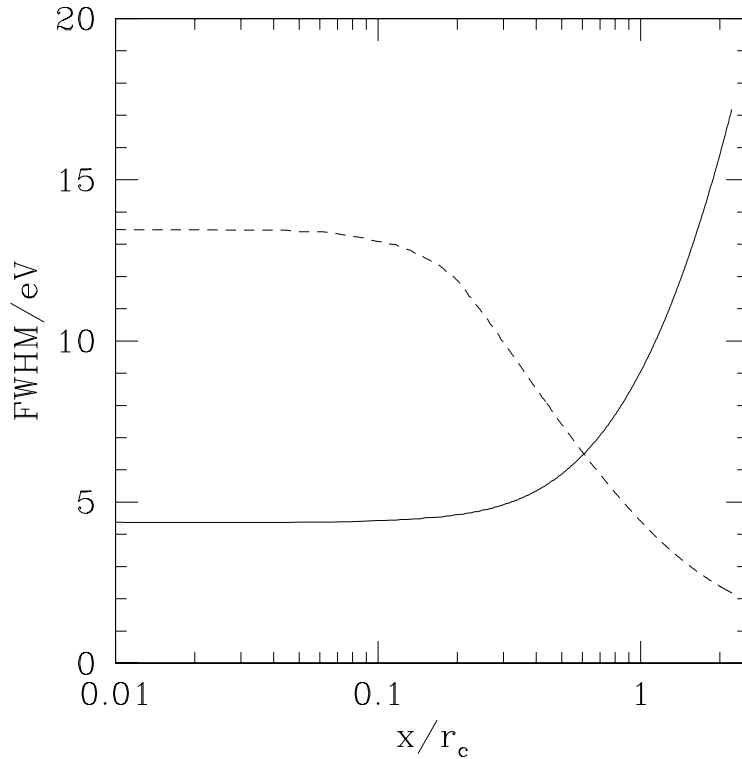Perseus (A 426) is the brightest nearby X-ray cluster and it is one of the best-

Figure 5.5: Linewidth as a function of the projected radius, for isotropic turbulence when the velocity scale follows the law $v(R) = v_0 \left(\frac{R}{r_c} \right)^\alpha$, with $\alpha = \pm 1$. In each case the velocity scale was assumed to saturate at 1000 km/s. The solid line is for turbulent velocity increasing with radius, the dashed line for turbulent velocity declining with radius. For clarity the thermal broadening is neglected.

studied cool core clusters, together with M87 and Centaurus. It hosts in its core a luminous elliptical galaxy NGC 1275, containing a bright radio source (3C 84). In the core region a complex substructure is seen in temperature, surface brightness and optical light distributions, including holes in the X-ray images due to bubbles of relativistic plasma (Böhringer et al., 1993, Fabian et al. 2000), quasi-spherical ripples (Fabian et al. 2003a) and optical Hα filaments (Fabian et al. 2003b, Hatch et al. 2005).

In our estimates of the expected linewidth in Perseus we assume that the gas cooling losses are compensated by the dissipation of the turbulent motions at all radii. This is of course a strong and not fully justified assumption, but it provides clear predictions if the turbulent heating is indeed important in
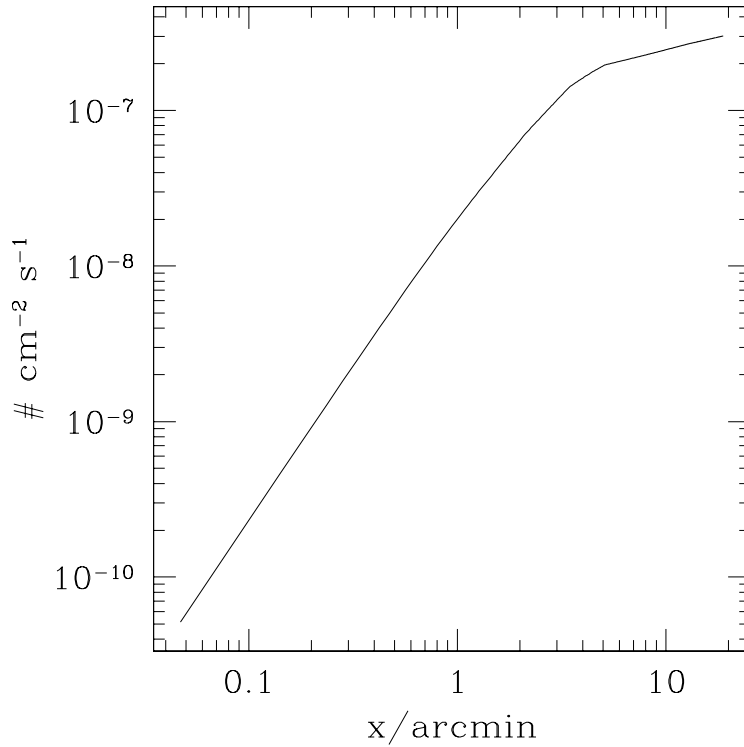
Figure 5.6: The estimated total flux in the 6.7 keV line (in phot/s/cm^2) coming from a circle enclosed in a given projected radius from the Perseus cluster.

cluster cores. Thus one can write:

$$C \; \rho \; v_{turb}^3/l \approx n_e^2 \Lambda(T), \tag{5.7}$$

where $\Lambda(T)$ is the gas cooling function and C is a dimensionless constant of the order of unity (see e.g. Dennis & Chandran, 2005), which depends on the character of the turbulent motions. Since the electron density and temperature are known from observations (e.g. Churazov et al., 2003) one can estimate v_{turb}^3/l from equation 5.7. As the linewidth depends explicitly on v_{turb} one has to determine (or assume) some constraints on l. For instance, Rebusco et al. (2005, 2006) and Graham et al. (2006) considered the turbulent spreading through the ICM of metals produced by the brightest cluster galaxy. Treating this process in a diffusion approximation one can estimate the effective diffusion coefficient D. In the Perseus cluster $D \sim 2 \; 10^{29}$ cm^2/s (Rebusco et al., 2006). One can then cast D in the form $D = C' \; v_{turb} \; l$, where

C' is a dimensionless constant of the order of unity (see Dennis & Chandran 2005 for a compilation of values of C and C'). Combining equation 5.7 (at some radius) and the expression for the diffusion coefficient, one gets both v_{turb} and l. In Perseus the characteristic values were found to be $l \sim 20$ kpc and $v_{turb} \sim 400$ km/s (Rebusco et al. 2006). If we adopt $v_{turb} = 410$ km/s as the characteristic velocity of turbulent motions at every radius in Perseus then, depending on the directionality of the turbulence (see section 5.2.1), the expected width of the 6.7 keV line in Perseus should be in the range 10-20 eV. Of course the above values of l and v_{turb} are only order of magnitude estimates. From equation 5.7 it is clear that $v_{turb} \propto (n_e \ l \ \Lambda(T))^{1/3}$. If $l = $ const then $v_{turb} \propto n_e^{1/3} \ R^{-1/3}$ (when $n_e \propto 1/R$). In Figure 5.8 we calculate the linewidth for several illustrative cases: three solid lines with different thickness correspond to $l = 2, 20, 200$ kpc (at all radii). This spread of two orders of magnitude in l results in a factor of 3 change of the linewidth. If we follow the arguments of Dennis & Chandran (2005) and set $l \sim \alpha R$, where $\alpha = 0.3$, then $v_{turb} \approx$ const when $n_e \propto 1/R$. The corresponding curve is shown in Figure 5.8 by the dashed line.

5.4 Linewidth versus shift of the line centroid

All the results obtained in the previous sections are based on the assumption that the characteristic size of the turbulent eddies l is much smaller than the characteristic length of the line of sight. In practice there are at least two complementary ways of getting information on the turbulent gas motions with microcalorimeters. One can i) use the variations of the line centroid with the position and/or ii) the width/shape of the line. The latter method is applicable to large regions of the cluster (e.g. the whole cooling flow region), but accurate measurements of the linewidth require many line photons. The centroid variations can be measured very accurately, but this probe works the best only if the characteristic size of the eddies is not too small. Indeed, in practice one observes the spectrum coming from a selected region of the cluster with characteristic sizes X (in projection) and L (along the line of sight). If $X \gg l$ and $L \gg l$ then $N = X^2 L / l^3$ independent eddies are seen by the instrument at the same time. Assuming that each eddy produces a centroid shift of the order of v_{turb}, then the observed centroid shift will be $\sim v_{turb}/\sqrt{N} \propto X^{-1} L^{-1/2}$. Increasing X would increase the number of line photons the instrument detects during observations, but this would simultaneously decrease the amplitude of the centroid shift. Obviously these two effects cancel each other and increasing X beyond the characteristic eddy size l does not improve the detectability of the centroid variations. Making X smaller
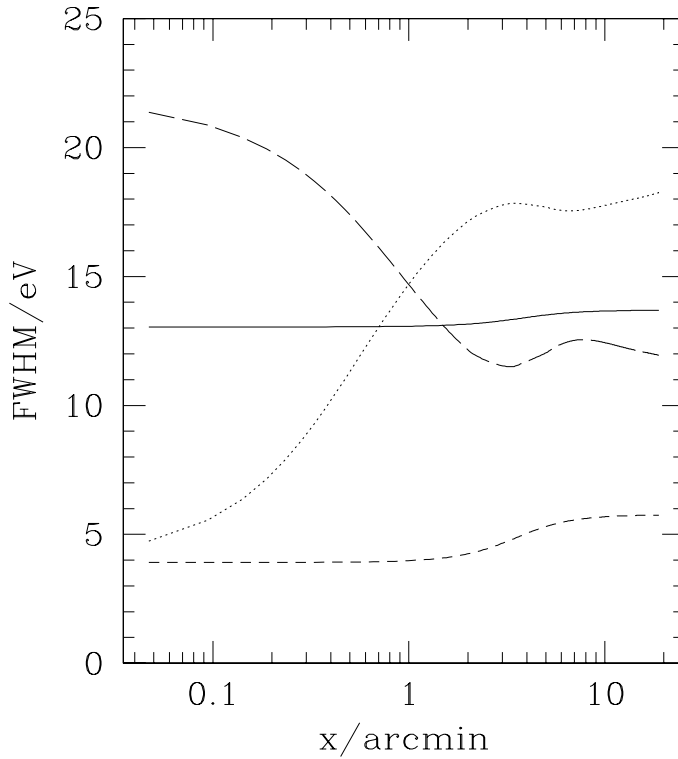
109

Figure 5.7: 6.7 keV linewidth in the Perseus cluster for isotropic, radial and tangential motions. $v_{turb} = 410$ km/s was adopted. The thermal broadening was included in calculation of the linewidth.

than l would just make the number of line photons smaller: the amplitude of the centroid variation should not vary much. Of course studying the centroid variations on spatial scales larger and smaller than l will be a very useful test of the distribution of characteristic eddie sizes, but for the principal detection of the gas turbulent motions, the choice of $X \approx l$ is obviously the optimal one. Thus the question of prime importance is whether the instrument has an effective area large enough to collect photons from a region with size $X \sim l$ (e.g. sufficient to detect the centroid variations). Of course, averaging along the line of sight remains an unavoidable effect independent of the choice of the region size. In Figure 5.9 we plot the effective length L of the region along the line of sight which provides 75% of the total surface brightness in the 6.7 keV line, at a given projected distance from the center of the Perseus cluster. It is clear from this figure that in the core of the Perseus cluster L is of the order of 130 kpc and it increases linearly outside the core. A non-monotonic behavior
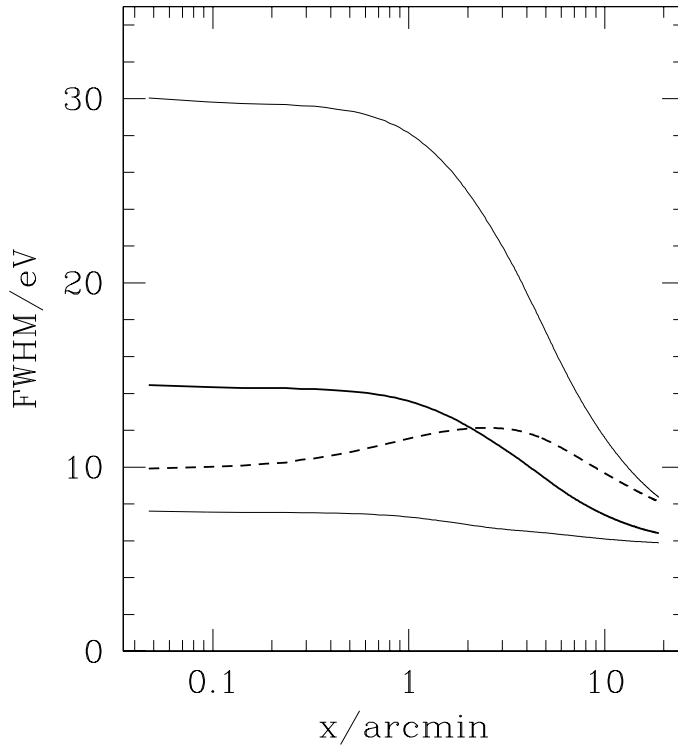
Figure 5.8: Expected radial dependence of the 6.7 keV linewidth in the Perseus cluster for several illustrative cases. For all curves we assume a balance between gas cooling losses and turbulent heating at each radius according to eq.5.7. The solid lines correspond to $l = 2, 20, 200$ kpc, independently of the radius. The dashed line corresponds to the $l = 0.3R$.

of the curve at 20-30 kpc from the center is caused by the complicated iron abundance profile (see e.g. Schmidt et al. 2002, Churazov et al. 2003). Thus, even for the optimal size of the observed region, the typical amplitude of the centroid variations will be $v_{turb}/\sqrt{L/l}$. E.g. adopting for estimates $v_{turb} \sim 400$ km/s and $l \sim 20$ kpc (Rebusco et al., 2006) one can expect in the Perseus cluster centroid variations of the order of 170 km/s on spatial scales of arcminutes. Such a shift in velocity corresponds to $\sim$3.57 eV shift in energy for the 6.7 keV line.

On the other hand the detection of the line broadening has no limitation from the point of view of the region size and the whole cooling flow region can be probed at once. However the number of photons required to detect the turbulent line broadening on top of the thermal broadening is larger.
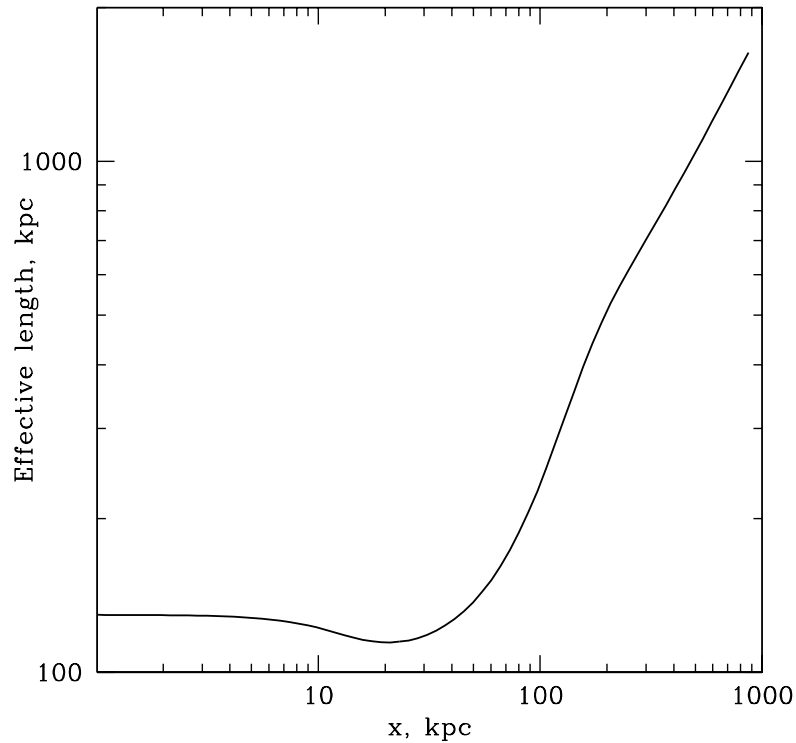
Figure 5.9: Effective length of the region along the line of sight which provides 75% of the total surface brightness in the 6.7 keV line at a given projected distance from the center of the Perseus cluster. The "wiggle" around 20-30 kpc is due to the complicate structure in the radial abundance profile (e.g. Schmidt et al. 2002, Churazov et al. 2003).

5.5 Conclusions

The dissipation of turbulent gas motions driven by AGN activity is a plausible source of heat for the cooling gas in cluster cores. In this case, we show that the expected width of the iron 6.7 keV line is well above the thermal broadening for most plausible values of turbulent velocities. In our fiducial model of the Perseus cluster, the 6.7 keV linewidth is larger than 10 eV. The radial dependence of the linewidth can be a useful probe of the "directionality" (isotropic, radial, tangential) of the dominant gas motions, although it might be difficult to distinguish the "directionality" from the radial dependence of

the velocity amplitude itself.

Acknowledgments

Bibliography

[1] Balbus S.A., Soker N. 1990, ApJ, 357, 353

[2] Böhringer H., Voges W., Fabian A.C., Edge A.C., Neumann D.M. 1993, MNRAS, 264, L25

[3] Brüggen M., Hoeft M., Ruszkowski M. 2005, ApJ, 628, 153

[4] Chandran B.D.G. 2005, ApJ, 632, 809

[5] Churazov E., Brüggen M., Kaiser C.R., Böringer H., Forman W. 2001, ApJ, 554, 261

[6] Churazov E., Sunyaev R.A., Forman W., Böringer H. 2002, MNRAS, 332, 729

[Churazov et al. 2003] Churazov E.,Forman W., Jones C., Böringer H. 2003, ApJ, 590, 225

[Churazov et al. 2004] Churazov E.,Forman W., Jones C., Sunyaev R., Böringer H. 2004, MNRAS,347, 29

[7] Davidson P.A. 2004, *Turbulence*, Oxford Univ. Press (New York)

[8] Dennis T., Chandran B. 2005, ApJ, 622, 205

[9] Edge A.C., Stewart G.C. 1991, MNRAS, 252, 414

[10] Fabian A.C. 1994, ARA&A, 32, 277

[11] Fabian A. C. et al., 2000, MNRAS, 318, L65

[12] Fabian A. C., Sanders J.S., Allen S.W., Crawford C.S., Iwasawa K., Johnstone R.M., Schmidt R.W. 2003a, MNRAS, 344, L43

[13] Fabian A.C. et al. 2003b, MNRAS, 344, L48

[14] Fabian A.C., Sanders J.S., Taylor G.B., Allen S.W., Crawford C.S., Johnstone R.M., Iwasawa K. 2006, MNRAS, 366, 417

[15] Forman W. et al. 2005, ApJ, 635, 894

[16] Forman W. et al. 2006, astro-ph/0604583

[gil87] Gilfanov M.R., Sunyaev R.A., Churazov E. 1987, SvAL, 13, 233

[17] Graham J., Fabian A. C., Sanders J. S., Morris R. G., 2006, MNRAS, 368, 1369

[18] Hatch N.A., Crawford C.S., Johnstone R.M., Fabian A.C. 2006, MNRAS, 367, 433

[19] Inogamov N.A., Sunyaev R.A. 2003, Astron. Lett., 29,12

[20] Kaastra J.S. et al. 2004,A&A, 413, 415

[21] Lesieur M. 1997, *Turbulence in Fluids*, Reidel Ed. (Dordrecht)

[22] Lufkin E.A., Balbus S.A., Hawley J.F. 1995, ApJ, 446, 529

[23] Markevitch M., Vikhlinin A. 2007

[24] Mathieu J. 2000, *An introduction to turbulent flow*, Cambridge Univ. Press (Cambridge)

[25] Matsumoto H., Koyama K., Awaki H., Tomida H., Tsuru T., Mushotzky R., Hatsukade I., 1996, PASJ, 48, 201

[26] Matsushita K., Belsole E., Finoguenov A., Böhringer H. 2002, A&A, 386, 77

[27] Mulchaey J.S., Davis D.S., Mushotzky R.F., Burstein D. 1993, ApJ, 404, L9

[28] Nulsen P.E.J., Stewart G.C., Fabian A.C. 1984, MNRAS, 208, 185

[29] Omma H., Binney J., Bryan G., Slyz A. 2004, MNRAS, 348, 1105

[30] Pedlar A. et al. 1990, MNRAS, 246, 477

[31] Peterson J.R., Kahn S.M., Paerels F.B.S., Kaastra J.S., Tamura T., Bleeker J.A.M., Ferrigno C., Jernigan J.G. 2003, ApJ, 590, 207

[32] Pringle J.E. 1989, MNRAS, 239, 479

[33] Rebusco P., Churazov E., Böhringer H., Forman W., 2005, MNRAS, 359, 1041

116

[34] Rebusco P., Churazov E., Böhringer H., Forman W., 2006, MNRAS, 372, 1840

[35] Richardson, L.F. 1922, Weather Prediction by Numerical Processes, Cambridge Univ. Press

[36] Riley J.J., Lelong M. 2000, Annu.Rev.Fluid Mech., 32, 613

[37] Roediger E., Brüggen M., Rebusco P., Böhringer H., Churazov E. 2007, MNRAS in press (astro-ph/0611531)

[38] Schmidt R.W., Fabian A.C., Sanders J.S. 2002, MNRAS, 337, 71

[39] Smith R.K., Brickhouse N.S., Liedahl D.A., Raymond J.C. 2001a, ApJ, 556, L91

[40] Smith R.K., Brickhouse N.S., Liedahl D.A., Raymond J.C. 2001b, Spectroscopic Challenges of Photoionized Plasmas, ASP Conference Series Vol. 247, 159. Ed. G.Ferland&D. Wolf Savin

[41] Stewart G.C., Fabian A.C., Jones C., Forman W. 1984, ApJ, 285, 1

[42] Sunyaev R.A., Norman M.L., Bryan G.L. 2003, AstL, 29, 783

[43] Tennekes H., Lumley J.L. 1972, *A first course in turbulence*, MIT Press (Cambridge)

6

Conclusions

This section summarizes the major outcomes of this PhD project.

The semi-analytical work presented here deals with the feedback from supermassive black holes on the hot (2-10 keV) gas in galaxy clusters. In particular we aimed at finding observational tests which could provide constrains on the characteristics of the gas turbulent motions. We focused on the central regions of the rich and relaxed clusters that are often called "cooling flow" regions. We wanted to investigate i) the characteristic velocities and spatial scales of the gas motions ii) what is the role of supermassive black holes in creating these motions and iii) what impact these motions have on the properties of the gas.

The gas in the centers of rich clusters is so dense that the radiative cooling time is orders of magnitude shorter than the age of the cluster. However most of the recent observations show that the gas does not cool below X-ray temperatures, strongly suggesting that there is a source of energy which compensates the gas cooling losses. The activity of a central supermassive black hole is a plausible candidate for such energy source. In a simple scenario (broadly supported by recent observations) the black hole releases the energy in form of relativistic plasma (jets and outflows), which mechanically interacts with the thermal gas, generating turbulent motions and sound waves. Finding the characteristics of the gas motions is an important step in these studies. Ideally one would like to map the velocity field of the gas directly,

or at least to measure the broadening of the emission lines to quantify the characteristic amplitude of the gas motions. Unfortunately it is not possible with the currently operating X-ray observatories. It is therefore necessary to consider indirect methods to measure the turbulence in cluster cores.

The hot gas in clusters is enriched by heavy elements to the level of 30-50% of the Solar photospheric abundance. The observed abundance profiles are peaked at the centre of the cluster and this central excess of heavy elements is believed to come from the stars of the brightest cluster galaxy. However the observed abundance profiles are much broader than the light profiles of the central galaxies. We suggested that the turbulent gas motions are responsible for mixing of heavy elements through the large masses of gas in the cluster core. Assuming that a diffusion approximation can be used to describe this process, we found that for a typical object from our sample of nearby clusters and groups the effective diffusion coefficients of the order of $D \sim 10^{29}$ cm^2 s^{-1}. To the first approximation the value of the diffusion coefficient can be used to determine the product of the characteristic velocities v and spatial l scales of the turbulent gas motions, i.e. $D \propto vl$.

We then assumed that the dissipation of the same turbulent motions offsets the gas cooling losses. The gas cooling losses are known from observations and we therefore were able to get constraints on another combination of v and l, namely the energy dissipation rate $\propto v^3/l$. Using two "observables" (the effective diffusion coefficient and the effective dissipation rate) we therefore were able to measure v and l for each cluster. We found that the spatial scales of few tens of kpc and characteristic velocities of order few hundreds km/s are required in a typical cluster. These parameters agree well with the observed sizes of radio bubbles inflated in the hot gas by a central active galactic nuclei (AGN) and with the expected velocities of their motions. This agreement strongly suggests that indeed the AGN/ICM interactions have a strong impact on the gas in the cluster cores.

These conclusions are also supported by numerical simulations: indeed the effective diffusion coefficient inferred from hydrodynamical simulations of AGN-induced buoyant bubbles in galaxy clusters agree well with our semi-analytical estimates.

Having derived the characteristic velocity amplitudes and spatial scales of the gas motions we then revisited the prospects for direct measurements of the gas velocities with near-future planned X-ray observatories. With characteristic velocities of the motions in the ICM being of the order of few hundreds

km/s (as it seems from our analysis of the abundance profiles and from numerical simulations), the turbulent broadening of the line would dominate over the thermal broadening. We derived a number of observational tests to study the character of the turbulent motions (e.g. to verify if the turbulence is isotropic) and to distinguish between various alternative models, that are assuming different mechanisms of the gas heating.

The findings of the present work can be summarized as follows:

- in a typical cluster with a cool core an effective diffusion coefficient of the order of $D \sim 10^{29} \mathrm{cm}^2 \mathrm{~s}^{-1}$ is needed to match the observed shallow iron abundance profiles;

- stochastic gas motions with spatial scales of few tens of kpc and characteristic velocities of order few hundreds km/s provide the right diffusion and their dissipation balances the gas cooling losses;

- these parameters agree with models where outflows driven by a central supermassive black hole stir the gas in the cluster core and they are consistent with numerical simulations;

- a more direct probe of such gas motions will be possible in the near-future, by measuring the linewidth of the heavy elements emission lines with the upcoming generation of X-ray calorimeters.

APPENDIX

Adopted Units of Physical Quantities

This Appendix summarizes different physical parameters that we encounter and some units that are adopted usually in Astrophysics. The numbers are approximate and they are intended to give an idea of the range.

Age of the Universe ~ 14 Gyr $\sim 4.4 \times 10^{17}$ s
Mass of the Sun $1 M_\odot = 1.99 \times 10^{30}$ kg
Parsec 1pc$= 3.08 \times 10^{16}$ m
Hubble constant $H_0 = 70$ km s^{-1} Mpc^{-1}
Proton mass $1\, m_p = 1.67 \times 10^{-27}$ kg
Solar blue luminosity $1\, L_\odot^B = 6 \times 10^{25}$ J s^{-1}
Solar iron metallicity $Z_\odot = 4.68 \times 10^{-5}$

Curriculum Vitae

Paola Rebusco   **Born**: February 2, 1981 in Brescia, Italy
Via Gasparo 126   **Citizenship**: italian
25087 Saló(BS), Italy   **E-mail**:pao@mpa-garching.mpg.de

Education

- **Universitá degli Studi di Trieste** — Trieste, Italy
  Graduated in Theoretical Physics with distinction (110/110) — 11 November 2003
  Thesis: QPOs in nearly geodesic orbits in strong gravity

- **E. Fermi Scientific Liceo** — Saló, Italy
  Graduated with distinction (100/100) — 1994-1999

Additional

- **International Max Planck Research School** — München, Germany
  PhD student in Astrophysics — 2003-2006

- **Pelham Memorial High School** — Pelham, NY(USA)
  One full semester — 1998
  Sarah Lawrence College — NY(USA)
  Summer writing workshop, one week — 1998
  V. Montiglio High School — Santiago, Chile
  One full semester — 1997

Languages: **Italian** native, **English** fluent: Toefl=270/300, **Spanish** fluent, **French** good, **German** learning, **Polish** learning

Computer skills: Microsoft Office, Fortran77, C, VHDL, Mathematica

Working experience:
    ***Teacher at the Munich International School** — Starnberg, Germany
    ***Teaching assistant at the Physics Department** — Müenchen, Germany
    Ludwig Maximillian University — Summer semester 2005
    ***Guide and children education** — Trieste, Italy
    Immaginario Scientifico Museum — 2002-2003
    ***Bar-women, waitress and cook** — Saló, Italy
    Gato Gordo Bar — 2001-2002

Activities: Traveling, tae-kwon-do (blue belt), playing piano and violin, sewing, sailing, basketball, full contact, cooking, baby-sitting, Argentinean tango